

**NUMERICAL STUDY OF COMBUSTION FOR A
4-STROKE GASOLINE ENGINE USING
TURBULENT FLAME SPEED CLOSURE
MODEL**



MOHD FADZIL BIN ABDUL RAHIM

**MASTER OF ENGINEERING (AUTOMOTIVE)
UNIVERSITI MALAYSIA PAHANG**

UNIVERSITI MALAYSIA PAHANG

DECLARATION OF THESIS

Author's full name : Mohd Fadzil Bin Abdul Rahim
Date of birth : 19/04/1980
Title : Numerical Study of Combustion for a 4-stroke
Gasoline Engine using Turbulent Flame Speed
Closure Model
Academic Session : Semester 2 2008/2009

I declared that this thesis is classified as:

CONFIDENTIAL (Contains confidential information under the Official Secret Act 1972)

RESTRICTED (Contains restricted information as specified by the organization where research was done)

OPEN ACCESS I agree that my thesis to be publish as online open access (full text)

I acknowledged that Universiti Malaysia Pahang reserves the right as follows:

1. The thesis is the property of Universiti Malaysia Pahang
2. The Library of Universiti Malaysia Pahang has the right to make copies for the purpose of research only
3. The Library has the right to make copies of the thesis for academic exchange

UMP

Certified by:

SIGNATURE

800419 – 06 – 5125
NEW IC NO./ PASSPORT NO

Date: 15 JUNE 2009

SIGNATURE OF SUPERVISOR

PROF. DR. ROSLI ABU BAKAR
NAME OF SUPERVISOR

Date: 15 JUNE 2009

**UNIVERSITI MALAYSIA PAHANG
CENTER FOR GRADUATE STUDIES**

We certify that the thesis entitled“Numerical Study of Combustion for a.....
...4-stroke Gasoline Engine using Turbulent Flame Speed Closure Model” is written by
...Mohd Fadzil Bin Abdul Rahim... . We have examined the final copy of this thesis and
in our opinion; it is fully adequate, in terms of scope and quality for the award of the
degree of Master of Engineering in ...Automotive... . We herewith recommend that it be
accepted in fulfilment of the requirements for the degree of Master of Engineering
specializing in ...Automotive... .

Committee of Final Examination:

1. Dr. Ahmad Syahrizan Sulaiman
Faculty of Mechanical Engineering,
Universiti Malaysia Pahang.

2. Dr. Mohd Zulkifly Abdullah
Associate Professor,
School of Aerospace Engineering.
Universiti Sains Malaysia.

UMP

NUMERICAL STUDY OF COMBUSTION FOR A 4-STROKE GASOLINE ENGINE
USING TURBULENT FLAME SPEED CLOSURE MODEL

The logo of the University of Malaysia Pahang (UMP) is a shield-shaped emblem. It features a central white vertical stripe. The left side of the shield is light blue, and the right side is light purple. At the top center, there is a yellow diamond shape. A stylized, multi-colored ring (purple, green, blue) encircles the diamond. The name 'MOHD FADZIL BIN ABDUL RAHIM' is printed in black capital letters across the middle of the shield.

MOHD FADZIL BIN ABDUL RAHIM

Thesis submitted in fulfilment of the requirements for the award of the degree of
Master of Engineering (Automotive).

UMP
Faculty of Mechanical Engineering
UNIVERSITI MALAYSIA PAHANG

JUNE 2009

SUPERVISOR'S DECLARATION

We hereby declare that we have checked this thesis and in our opinion this thesis is adequate in terms of scope and quality for the award of the degree of Master of Engineering in Automotive.

Signature

Name of Supervisor : DR. ROSLI ABU BAKAR

Position : PROFESSOR

Date : 15 JUNE 2009

Signature

Name of Co-supervisor: DR. MD. MUSTAFIZUR RAHMAN

Position : SENIOR LECTURER

Date : 15 JUNE 2009

The logo of Universiti Malaysia Perlis (UMP) is a large, downward-pointing triangle. It is divided into four quadrants by a vertical and a horizontal line. The top-left quadrant is light blue, the top-right is light purple, the bottom-left is light purple, and the bottom-right is light blue. In the center of the triangle, the letters 'UMP' are written in a bold, white, sans-serif font.

UMP

STUDENT'S DECLARATION

I hereby declare that the work in this thesis is my own except for quotations and summaries which have been duly acknowledged. The thesis has not been accepted for any degree and is not concurrently submitted in candidate of any other degree.

Signature

Name

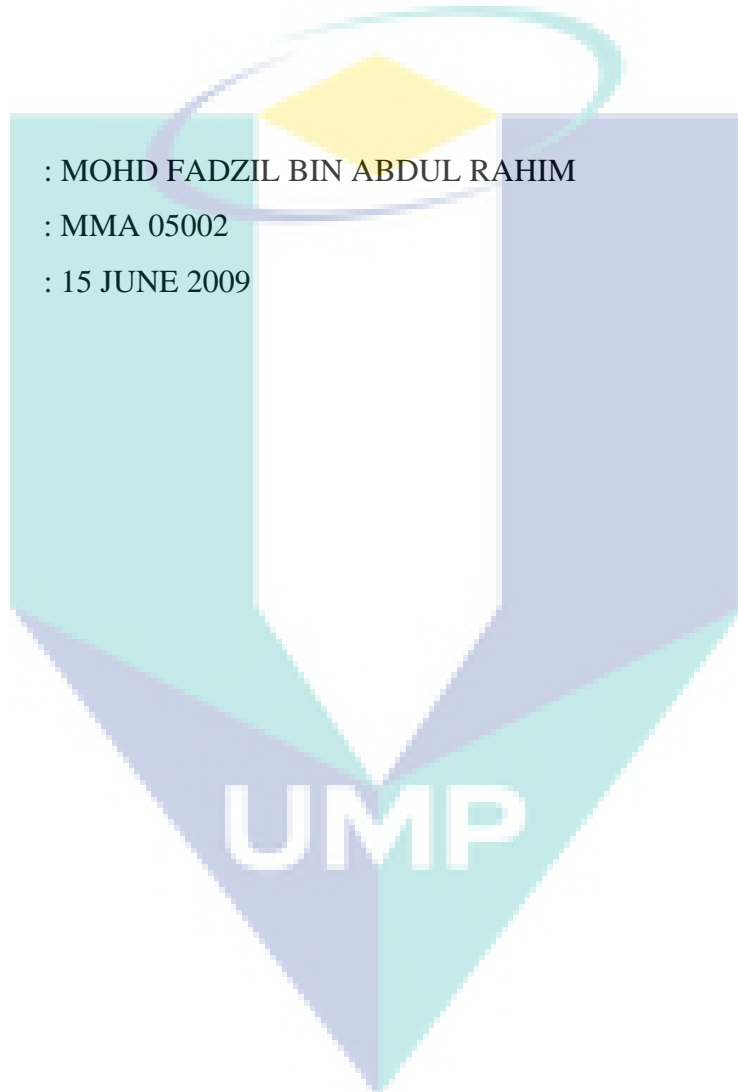
: MOHD FADZIL BIN ABDUL RAHIM

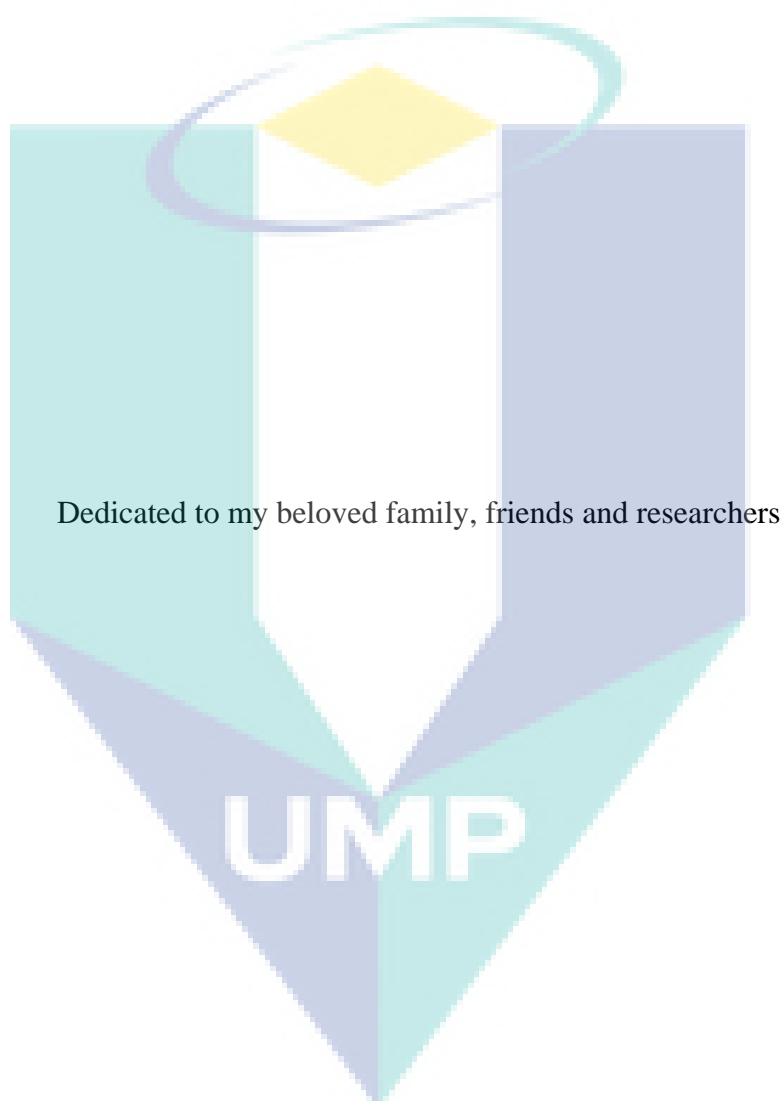
ID Number

: MMA 05002

Date

: 15 JUNE 2009





Dedicated to my beloved family, friends and researchers

ACKNOWLEDGEMENTS

In the name of Allah, the Most Benevolent and the Most Merciful. Every sincere appreciation and gratitude is only to God. Only by His Kindness and Guidance that this thesis is finally realized. It is ardently desired that this little effort be accepted by Him to be of some service to the cause of humanity. I would like to express my thanks to my supervisor, Professor Dr. Rosli Abu Bakar and Dr. Md. Mustafizur Rahman for their confidence, supportiveness and invaluable opinion for me throughout all the stages of this study. I would also like to express very special thanks to Mr. Awang b. Idris, Mr. Ismail Ali, Mr. Mohd Aminuddin, Mr. Faizul, Mr. Idzwanrosli, Mr. Nik Mohd Izual, Mr. Mohd Fairusham, Mr. Wong Hong Mun, Dr. Ahmad Syahrizan and Dr. Wan Azhar of Universiti Malaysia Pahang (UMP). Special thanks to Professor Ir. Dr. Azhar Dato' Abdul Aziz, Dr. Zulkarnain Ab Latif, Dr. Mazlan Wahid and Mr Mohsin Sies of Universiti Teknologi Malaysia (UTM). Also special thanks to Associate Professor Dr. Mohd. Zulkifly Abdullah and Professor Dr. Horizon Walker Gitano-Briggs of Universiti Sains Malaysia (USM). In addition, special thanks to all members of Automotive Excellence Center (AEC) of UMP and associates of Faculty of Mechanical Engineering of UMP for their supports and co-operations throughout the study. I would also like to express my sincere gratitude to Universiti Malaysia Pahang for sponsored the scholarship for this master study. Finally, I would like to acknowledge my sincere indebtedness and gratitude to my wife and son, parents, and all family members for their love, and sacrifice throughout my life. I cannot find appropriate words that could properly describe my appreciation for their devotion, support and faith in my ability to attain my goals and apologies for all the unintended and regretful ignorance.

The logo of Universiti Malaysia Pahang (UMP) is a large, stylized letter 'V' shape. The left side of the 'V' is light blue, the right side is light green, and the bottom point is a darker blue. The letters 'UMP' are written in white, bold, sans-serif font across the center of the 'V'.

ABSTRACT

This thesis deals with the numerical study of turbulent premixed combustion of 4-stroke spark ignition (SI) engine using Turbulence Flame Speed Closure (TFSC) model developed by Zimont. The key objective of the modelling is to assess the applicability of TFSC model for SI engine combustion. The study was also conducted with purpose to assess the influential factors that affect the TFSC model's prediction. The assessment is primarily based on cylinder pressure data and supported by mass fraction burned, visualization of flame propagation, and turbulent flame speed. Recent progress of TFSC modelling demonstrates that the model tends to diverge at high turbulence which associated with high engine speed. This study consists of experimental engine testing to gather experimental data as means of validation and inputs to the numerical engine model and computational fluid dynamic (CFD) modelling of SI combustion on the baseline engine design. Consecutive tests on Mitsubishi Magma 4G15 engine has been carried out at wide-open throttle from 1500 to 4000 revolution per minute (rpm) of engine speed. Where as the condition at wide-open throttle of 2000 rpm is selected as a baseline condition for the initial simulation purpose. The engine model is tested for combustion simulation using the Zimont combustion model coupled with $k - \varepsilon$ turbulence model with standard wall function, and the ignition model developed by Lipatnikov. Preliminary results indicate that the model prediction of peak cylinder pressure was strongly dependent on number of iteration per time step. Thus, iteration number has been studied further in order to reveal the crucial modelling factor. Five different cases have been run using 20, 100, 500, 1000 and 1500 number of iterations per time steps. The acquired results show that the acceptable peak cylinder pressure are obtained when the numerical model's iteration are larger than 1000. The best prediction has been obtained by using 1500 iteration per time step. A large discrepancy is noticed due to the consideration of mixture properties. This clearly an evidence of the importance of appropriate iteration number for transient engine combustion modelling. Further simulation at high engine speed up to 4000 rpm is recommended to be tested in the next stage of the study.

ABSTRAK

Tesis ini merangkumi kajian berangka pembakaran pra-campuran gelora bagi enjin 4-lejang pencucuhan bunga api dengan menggunakan Model Lengkapan Halaju Nyalaan Gelora oleh Zimont. Objektif utama kajian adalah untuk pengujian kesesuaian model ini bagi permodelan pembakaran enjin pencucuhan bunga api. Kajian juga adalah bertujuan untuk menilai faktor-faktor yang mempengaruhi ketepatan pengiraan model. Penilaian ini secara asasnya adalah berasaskan data tekanan silinder dan dibantu oleh pecahan jisim terbakar, pemerhatian perebakan nyalaan, dan halaju nyalaan gelora. Perkembangan terkini kajian terhadap model ini menunjukkan bahawa ketepatan model semakin berkurangan pada takat gelora tinggi yang terhasil pada halaju enjin tinggi. Kajian ini terbahagi kepada pengujian enjin secara eksperimen bagi mendapatkan data sebenar sebagai kaedah validasi dan masukan kepada model berangka enjin dan juga permodelan pembakaran pencucuhan bunga api secara Dinamik Aliran Berkomputer bagi rekabentuk asas enjin. Beberapa rentetan pengujian ke atas enjin Mitsubishi Magma 4G15 telah dijalankan pada ujian pendikitan penuh pada halaju enjin 1500 ke 4000 pusingan per minit (ppm). Sementara itu, keadaan pendikitan penuh pada halaju 2000 ppm telah dipilih sebagai keadaan asas untuk kajian permodelan permulaan. Model berangka enjin telah diuji untuk proses pembakaran dengan menggunakan model pembakaran Zimont bersama-sama model gelora $k - \varepsilon$ dengan fungsi dinding piawai dan model pencucuhan Lipatnikov. Keputusan awal telah menunjukkan bahawa pengiraan model ke atas tekanan puncak silinder adalah sangat bergantung kepada bilangan lelaran bagi setiap sela masa. Oleh itu, kesan bilangan lelaran setiap sela masa telah dikaji dengan lebih mendalam bagi menjelaskan faktor permodelan yang amat penting ini. Lima kes berbeza dengan bilangan lelaran 20, 100, 500, 1000 dan 1500 setiap sela masa telah diuji. Keputusan menunjukkan hanya model dengan bilangan lelaran melebihi nilai 1000 memberikan nilai tekanan puncak silinder yang boleh diterima. Pengiraan terbaik telah diperolehi dengan menggunakan 1500 bilangan lelaran bagi setiap sela masa. Perbezaan ketara yang wujud akibat masukan ciri-ciri campuran juga telah dikesan. Ini menunjukkan kepentingan bilangan lelaran bagi setiap sela masa bagi pemodelan pembakaran enjin secara tak mantap. Permodelan pada halaju enjin tinggi seperti 4000 ppm adalah dicadangkan untuk kajian pada peringkat yang seterusnya.

TABLE OF CONTENTS

	Page
SUPERVISOR’S DECLARATION	ii
STUDENT’S DECLARATION	iii
DEDICATION	iv
ACKNOWLEDGEMENTS	v
ABSTRACT	vi
ABSTRAK	vii
TABLE OF CONTENTS	viii
LIST OF TABLES	xi
LIST OF FIGURES	xii
LIST OF SYMBOLS	xiv
LIST OF ABBREVIATIONS	xix
CHAPTER 1 INTRODUCTION	
1.1 Background of the Study	1
1.2 Problem Statement	2
1.3 Objectives of the Study	3
1.4 Scopes of the Study	3
1.5 Flow Chart of the Study	4
1.6 Organization of Thesis	5
CHAPTER 2 LITERATURE REVIEW	
2.1 Introduction	6
2.2 Spark Ignition Engine Process	6
2.2.1 Physics of Spark Ignition Engine Process	6
2.2.2 Turbulent Flame Structure and Flame Speed	8
2.3 Cylinder Pressure based Combustion Analysis	9
2.4 Combustion Modelling using CFD	10
2.4.1 Computational Domain	11
2.4.2 Turbulence Modelling and Near Wall-Turbulence	12

2.4.3	Spark Ignition Modelling	14
2.4.4	Heat Transfer Modelling	15
2.4.5	Reaction Rate Modelling	15
2.5	Applications of TFSC Model for SI Engine Modelling	18
2.5.1	Convergence Study on TFSC modelling	22
2.6	Summary	23

CHAPTER 3 EXPERIMENTAL SETUP AND NUMERICAL MODELLING

3.1	Introduction	24
3.2	Engine Test-rig	24
3.2.1	Baseline Engine Specification	27
3.3	Important Parameters and Measurement Method	28
3.3.1	Cylinder Pressure	28
3.3.2	Air and Fuel Consumption	28
3.3.3	Engine Speed	30
3.3.4	Ignition Timing	30
3.3.5	Engine Torque	30
3.3.6	Engine Testing Procedure	31
3.4	Numerical Modelling Approach	32
3.4.1	Computational Domain	32
3.4.2	Grid Generation	32
3.4.3	Governing Equations for CFD Modelling	38
3.4.4	Turbulent $k - \varepsilon$ Model	39
3.5	Zimont's TFSC Model	40
3.5.1	TFSC Model Equation	41
3.5.2	Turbulent Flame Speed Model	43
3.5.3	Mean Reaction Rate Term	43
3.5.4	Model's Approach for Calculation of Cylinder Pressure	45
3.5.5	Modification Suggested for SI Engine Combustion	45
3.6	Heat Transfer Model	48
3.7	Ignition Model	49
3.8	Input Data for Numerical Analysis	49
3.8.1	Premixed Mixture Properties	50
3.8.2	Boundary and Initial Conditions	51
3.9	Simulated Problems	53
3.9.1	Technical Specification of Workstation	54

3.10	Summary	55
------	---------	----

CHAPTER 4 RESULTS AND DISCUSSION

4.1	Introduction	56
4.2	Experimental Test-Rig Results	56
4.2.1	Engine Torque	57
4.2.2	Fuel Air Equivalence Ratio and Ignition Timing	58
4.2.3	Cylinder Pressure	60
4.2.4	Mass Fraction Burned	62
4.2.5	Engine Performance Parameters	66
4.3	Numerical Combustion Results	71
4.3.1	Grid Sensitivity Analysis	71
4.3.2	Preliminary Result of the Baseline Model	73
4.3.3	Effect of Iteration Number Study	75
4.4	Summary	94

CHAPTER 5 CONCLUSION AND RECOMMENDATIONS

5.1	Conclusion	96
5.2	Recommendations for Future Work	97

REFERENCES

98

APPENDICES

A	ATE-60 Hydraulic Dynamometer Specification And Performance Curve From Manufacturer Data Sheet	102
B	Specification and Technical Data of Spark Plug Type Pressure Transducer (Type 6117 b)	104
C	Measurement System for Determination of Engine Speed	106
D	Load Measurement System and Details Specification of Load Cell	107
E	General Procedure of Engine Testing	109
F	List of Formula for Engine Parameters Calculation	112

LIST OF TABLES

Table No.	Title	Page
3.1	Mitsubishi Magma 4G15 engine specifications	27
3.2	Events definition from -360° to 360° CA	36
3.3	Input for pre-mixed mixture material properties at 2000 rpm	51
3.4	Boundary conditions at 2000 rpm	52
3.5	Initial conditions at 2000 rpm	52
3.6	Convergence limits for the solved equation	54
3.7	Problems setup for the case study	54
3.8	Technical specification of computers used for numerical study	55
4.1	Measured maximum peak pressure and timing of the peak pressure at different engine speed for wide-open throttle condition	62
4.2	Measured flame development angle, rapid burning angle and overall burn rate angle at different engine speed	64
4.3	Timing of overall burn rate angle and actual combustion period at different engine speed	65
4.4	Grid element size and corresponding element density	72
4.5	Effect of iteration number per time step on total computing time	76
4.6	Peak pressure predicted for cases 1 to 5	78
4.7	Peak Pressure timing predicted for cases 1 to 5	78
4.8	Burn rate angle predicted for cases 1 to 5	82
4.9	Timing of overall burn-rate angle predicted for cases 1 to 5	82

LIST OF FIGURES

Figure No.	Title	Page
1.1	Flow chart of the overall procedure of the study	4
2.1	Vital requirement for premixed turbulent combustion modelling of spark ignition engine	11
2.2	Comparison of predicted and measured combustion pressure at (a) 2000 rpm, WOT (b) 6000 rpm, WOT and (c) 2000 rpm, 2.8 bar, stratified.	20
3.1	Schematic diagram of the engine test-rig	25
3.2	Overview of hydraulic dynamometer engine test-rig	26
3.3	(a) Engine cooling system and (b) Dynamometer water supply system	26
3.4	Comparisons of measured orifice flow meter measurement and Super Flow 1020 measurement	29
3.5	Comparison of measured and theoretical torque for dynamometer's load cell	31
3.6	(a) Structural domain and (b) model with complete grid of the baseline engine	33
3.7	Cross sectional view of grid details (a) Exhaust valve closing in progress (b) Intake valve at maximum lift (c) Overview of mesh elements selection	34
3.8	Computational domain associated with the event definition (a) during all valve opened (b) after exhaust valve closed and exhaust manifold deactivation and (c) during all valve closed	37
4.1	Measured engine torque at different engine speed for wide-open throttle condition	57
4.2	Equivalence ratio at different engine speed for wide-open throttle condition	59
4.3	Spark ignition timing before top centre at different engine speed for wide-open throttle condition	60
4.4	Measured cylinder pressure at different engine speed for wide-open throttle condition	61

4.5	Characterization of combustion process based on mass fraction burned curve.	63
4.6	Mass fraction burned curve at different engine speed for wide-open throttle condition	64
4.7	Indicated and brake power at different engine speed for wide-open throttle condition	67
4.8	Indicated and brake mean effective pressure at different engine speed for wide-open throttle condition	68
4.9	Indicated and brake specific fuel consumption at different engine speed for wide-open throttle condition	69
4.10	Mechanical efficiency at different engine speed for wide-open throttle condition.	70
4.11	Brake thermal efficiency at different engine speed for wide-open throttle condition	71
4.12	The effect of mesh density on simulated cylinder pressure at top dead centre	73
4.13	Comparison between measured and simulated cylinder pressure for the baseline model	74
4.14	Comparison between measured and simulated mass fraction burned for the baseline model	74
4.15	Comparison of measured and simulated cylinder pressure for each simulated cases	77
4.16	Comparison of the measured and simulated mass fraction burned for each simulated cases	82
4.17	Isometric view of flame propagation in term of progress variable contour	86
4.18	Visualization of instantaneous flame propagation in term of progress variable contour of each simulated cases at two different timing after the ignition	87
4.19	Relationship between turbulent flame speed and cylinder pressure	90
4.20	Turbulent flame speed prediction of cases 1 to 5	91

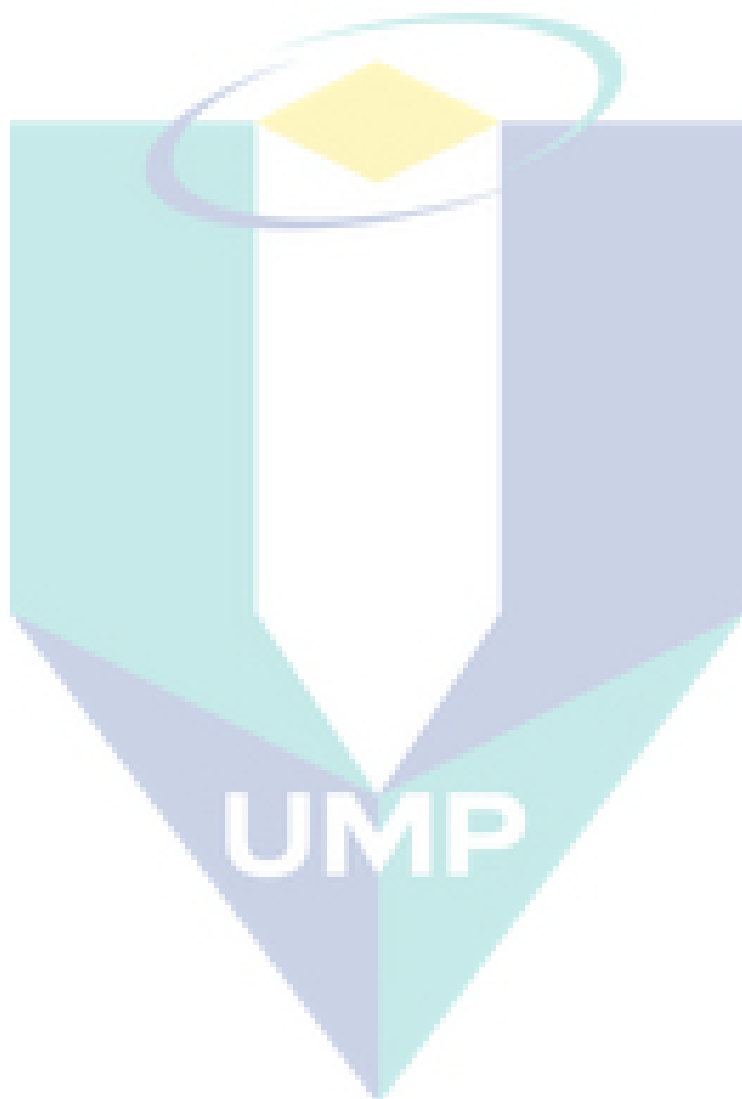
LIST OF SYMBOLS

A	TFSC model constant
A/F	air to fuel ratio
\tilde{c}	Progress variable
C_d	Discharge co-efficient
$C_{\varepsilon 1}$	Model constant for ε equation
$C_{\varepsilon 2}$	Model constant for ε equation
C_{μ}	Model constant for of μ_T equation
c_p	Specific heat
C_{st}	Mass- stoichiometric co-efficient
$d_{oxy / fuel}$	Ratio of air to fuel molecular diffusivity
$erfc$	Error function
F_i	Total body forces in i direction
F/A	Fuel to air ratio
g	Gravitational acceleration
g_{cr}	Critical rate of strain
G	Stretching factor
H_{comb}	Heat of combustion for burning 1 kg of fuel
h	Height
h_t	Total enthalpy
h_k	Enthalpy for species k
I	Turbulent intensity

J_j^h	Laminar enthalpy diffusion flux
J_j^k	Laminar species diffusion flux
k	Turbulent kinetic energy
k_{th}	Laminar thermal conductivity
k_T	Turbulent or effective thermal conductivity
l_T	Turbulent or integral length scale
\dot{m}	Mass flow rate
MW	Mixture molecular weight
n	Number of species
N	Engine speed
N_c	Number of cylinders
n_R	Number of crank revolution at each power stroke per cycle
P	Local gauge pressure
p_{op}	Operating pressure
p_{unb}	Unburned mixture pressure
p_{ref}	Reference pressure (ambient condition)
Pr	Prandtl number
Q	Volumetric flow rate
R	Standard universal gas constant
S_c	Normalized averaged rate of product formation
Sc_T	Turbulent Schmidt number
Sc_k	Schmidt number for species k
Sc_{kt}	Turbulence Schmidt number for the species k .

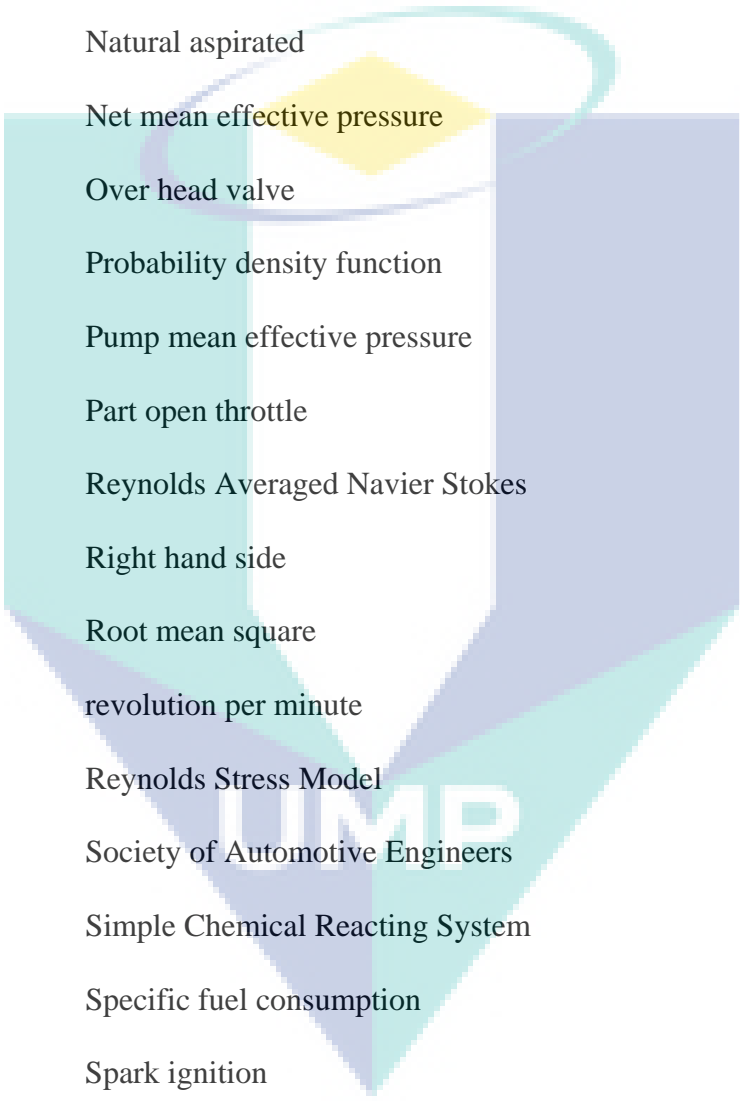
$S_{h,chem}$	Heat gains due to chemical reaction
S_L	Laminar flame speed
$S_{L,0}$	Baseline laminar flame speed
S_T	Turbulent flame speed
t	Time
t'	Effective diffusion time
t_{ig}	Timing of ignition
t_{id}	Period of timing after ignition
T	Temperature
T_e	Engine torque
T_{eff}	Effective temperature
T_{unb}	Unburned mixture temperature
T_{ref}	Reference Temperature
\tilde{u}_j	Velocity component in x, y and z direction
u'	Root-mean square velocity
\bar{v}	Velocity vector
V_{ref}	Volume for the reference quantity
Y_{fuel}	Unburned fuel mass fraction in mixture
Y_k	Mass fraction of product species, k
$Y_{k,eq}$	Equilibrium mass fraction of product species, k
α_L	Laminar thermal diffusivity

α_{fuel}	Thermal diffusivity of fuel
α_{oxy}	Molecular diffusivity of oxygen
α_k	Molecular diffusivity coefficient of species k
α_{ref}	Reference laminar thermal diffusivity
α_T	Effective or turbulent diffusivity
δ_{ij}	Kronecker delta symbol
ε	Turbulent dissipation rate
ε_{cr}	Turbulent dissipation rate at critical rate of strain
λ_0	Stoichiometric ratio of unburned mixture composition
λ_{lp}	Stoichiometric ratio of leading point composition
μ_T	Turbulent molecular viscosity
μ_L	Laminar molecular viscosity
μ_{ref}	Reference viscosity
ρ	Density
ρ_u	Unburned mixture density
$\bar{\rho}$	Averaged density
σ_ε	Standard deviation of distribution of ε
σ_k	Turbulent Prandtl or Schmidt number for k
τ_T	Turbulent time scale
τ_c	Chemical time scale
τ_{ij}	Viscous stress tensor of ij surface
ϕ	Fuel –air equivalence ratio

$\dot{\omega}_k$ Mass reaction rate of species k 

LIST OF ABBREVIATIONS

AKTIM	Arc and Kernel Tracking Ignition Model
ATDC	After top dead centre
ABDC	After bottom dead centre
BDC	Bottom dead centre
BBDC	Before bottom dead centre
BMEP	Brake mean effective pressure
BML	Bray-Moss-Libby
BP	Brake power
BTDC	Before top dead centre
BTE	Brake thermal efficiency
CA	Crank angle
CFD	Computational fluid dynamic
CFM	Coherent flame model
CNG	Compress Natural Gas
DAQ	Data acquisition
DISI	Direct ignition spark ignition
DNS	Direct numerical simulation
DOHC	Double over head cam
EGR	Exhaust gas recirculation
FMEP	Friction mean effective pressure
ICE	Internal combustion engine
IMEP	Indicated mean effective pressure
IP	Indicated power



LDV	Laser Doppler Velocimetry
LES	Large eddy simulation
LHS	Left hand side
ME	Mechanical efficiency
MEP	Mean effective pressure
NA	Natural aspirated
NMEP	Net mean effective pressure
OHV	Over head valve
PDF	Probability density function
PMEP	Pump mean effective pressure
POT	Part open throttle
RANS	Reynolds Averaged Navier Stokes
RHS	Right hand side
RMS	Root mean square
rpm	revolution per minute
RSM	Reynolds Stress Model
SAE	Society of Automotive Engineers
SCRS	Simple Chemical Reacting System
SFC	Specific fuel consumption
SI	Spark ignition
<i>STP</i>	Standard Temperature and Pressure
TDC	top dead centre
TFSC	Turbulent flame speed closure
WOT	Wide open throttle

CHAPTER 1

INTRODUCTION

1.1 Background

Spark ignition (SI) engine is one of the most favourable power train for passenger vehicle. The SI engine is converting the chemical energy of fuel into useful mechanical work which is primarily used for transportation purpose. However, application of the device is restricted by the limited fossil fuel resources, stringent emission requirement and low thermal efficiency (Delhaye and Cousyn, 1996). In fact the core constraint that controls the SI engine performance is the combustion process inside the engine cylinder. State of art methods for engine combustion analysis is based on the laser diagnostic tools with optical window (Drake and Haworth, 2007). But, all the related methods are relatively expensive and required huge financial allocation. Another promising tool in getting the insight information of the process is using multi-dimensional computational fluid dynamic (CFD) modelling approach.

CFD modelling of spark ignition combustion process are based on the solution of the fluid dynamic governing equations which are comprise of mass, momentum, energy and species conservation equation (Versteeg and Malasekera, 1995). Additional equation for turbulence, heat transfer, spark ignition and reaction rate are also required to capture all the associated combustion phenomena (Gosman, 1999). The main issue in SI engine combustion is the definition of the reaction rate terms. The effort devoted to the study of reaction rate modelling has produced a numbers of different reaction models by considering the chemical, thermodynamic and fluid dynamic aspect of the process. However, there is still no model can be regarded as universal for SI engine combustion (Merker et al., 2006).

Among the developed reaction model for spark ignition engine combustion, one of the most potential is the Turbulent Flame-Speed Closure (TFSC) model developed by Zimont (Lipatnikov and Chomiak, 2000). However, the model is less accurate at high turbulence which associated with high engine speed. In addition it must be tested for a wide range of engine operating condition. Furthermore, in previous study of the model, there is no source that state an appropriate number of iteration per time steps that will lead to a converge solution. Therefore, the model has been adopted in current study of turbulent premixed SI engine combustion in order to test its robustness for engine performance prediction. It is also intended to extend the model's application for carburetted four stroke gasoline engine running at wide open throttle condition from low to high engine speed. Hence, major influential factor and modification of the model for SI engine combustion are needed to be clarified.

1.2 Problem Statement

The study is carried out with purpose to analyze the feasibility of the TFSC model to predict the turbulent premixed SI engine combustion process using CFD method. This includes determining the factors that dominantly diverge the model's prediction from the actual combustion process as well as the modification required for turbulent premixed SI engine combustion application. Specifically, this study needs to determine an appropriate number of iteration per time step which will guarantee converge and accurate prediction. This is vital for reliable prediction of the actual process since the model is originally developed for gas turbine (GT) combustion. Previous research of Lipatnikov and Chomiak (2000) also indicated that the model's prediction tends to diverge at high turbulence. Thus further analysis at high engine speed which associated with high turbulence is required to identify the problem and improve the model.

1.3 Objectives of the Study

1. To study the combustion process in terms of cylinder pressure using TFSC combustion model on Mitsubishi Magma 4G15 engine at wide open throttle operation.
2. To assess the influential factors that affect the prediction accuracy of the TFSC model specially related to the number of iteration and its effect on convergence.

1.4 Scopes of the Study

The combustion simulation is carried out with purpose to test the feasibility of the TFSC combustion for turbulent premixed combustion SI engine modelling. Input for the simulated model are calculated based on the specified thermo-chemical properties method, $k - \varepsilon$ model with standard wall function for turbulence, energy equation for convective heat transfer, and Lipatnikov ignition model (Fluent, 2005). For this stage of study, simulation has been carried out at engine speed of 2000 rpm only. The baseline engine condition is associated with moderate turbulence which is assumed to be appropriate for this initial study as demonstrated by previous researcher. Major outcome of the simulation is the cylinder pressure data which is vital for engine performance prediction. The model's influential factor and modification for SI engine application are then clarified. Prior to all simulation work, a successive engine test is conducted to collect appropriate data of engine conditions such as i) the rate of air consumption, ii) the rate of fuel consumption, iii) cylinder pressure iv) ignition timing v) engine speed and vi) engine torque. The main interest parameter is the cylinder pressure. The cylinder pressure is used to validate the model prediction of combustion process. All the work is based on the carburetted gasoline engine, type Mitsubishi Magma 4G15, 12 valve, 1.5 litre engine with pent-roof combustion chamber. The engine is coupled to a hydraulic dynamometer equipped with customized cooling system for both the engine and hydraulic dynamometer. The test-rig is developed by using in-house facilities.

1.5 Flow Chart of the Study

The flow chart of the overall procedure of the study is shown in Figure 1.1:

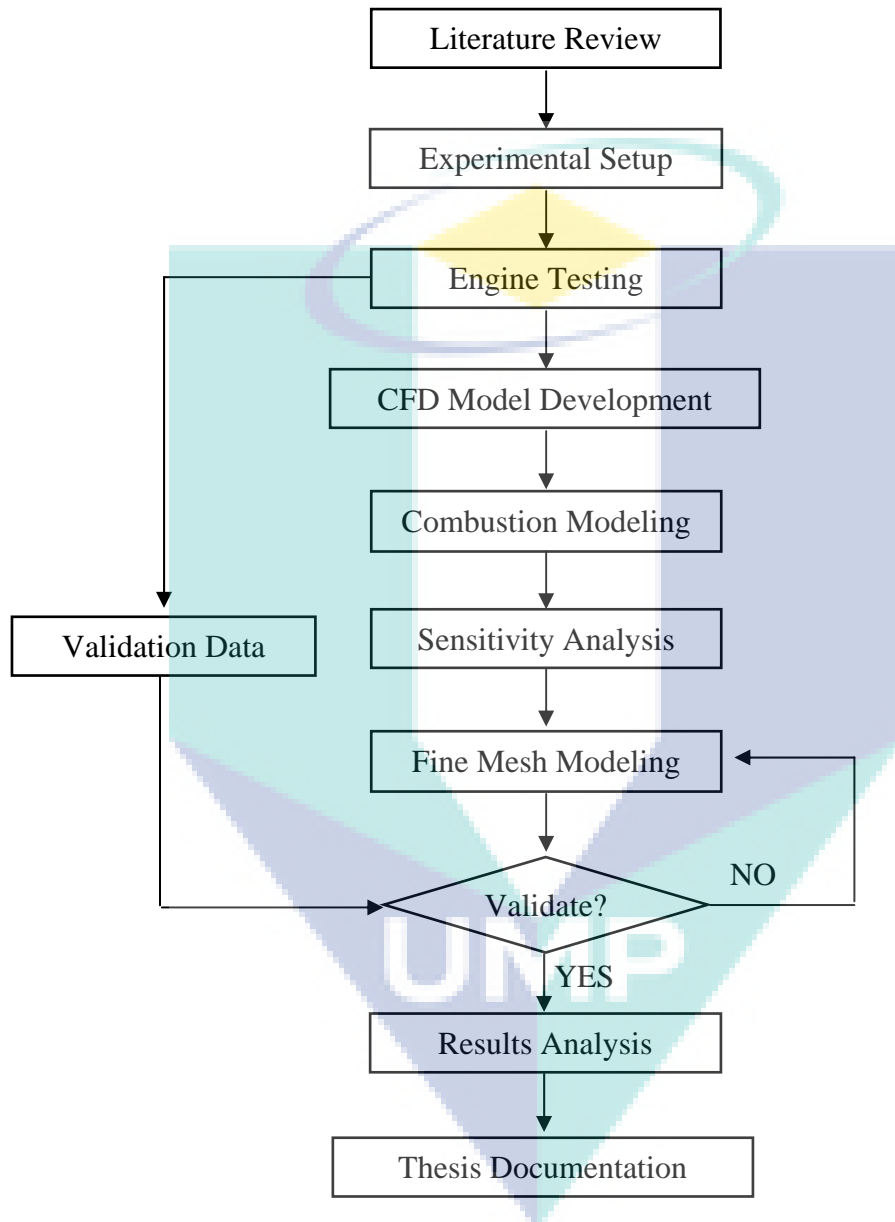
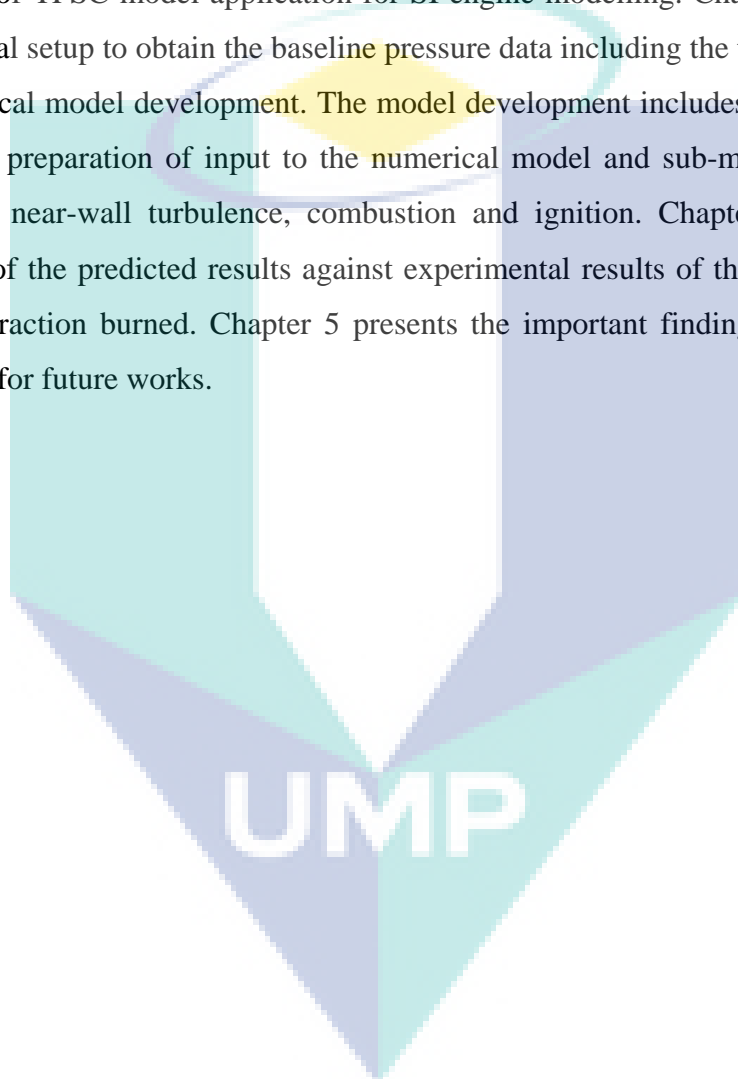


Figure 1.1: Flow chart of the overall procedure of the study

1.6 Organization of Thesis

This thesis is divided into four chapters excluding the introduction which is composed to present the series of logical thoughts. Chapter 2 gives critical study on premixed engine combustion in practice, experimental method for cylinder pressure measurement and its importance, aspect of numerical analysis of combustion and details discussion of TFSC model application for SI engine modelling. Chapter 3 presents the experimental setup to obtain the baseline pressure data including the test-rig description, and numerical model development. The model development includes details of the grid generation, preparation of input to the numerical model and sub-model employed for turbulence, near-wall turbulence, combustion and ignition. Chapter 4 addresses the validation of the predicted results against experimental results of the cylinder pressure and mass fraction burned. Chapter 5 presents the important finding of the study and suggestion for future works.



CHAPTER 2

LITERATURE REVIEW

2.1 Introduction

This chapter presents previous studies and recent progress in SI engine modelling that formed the framework of current study. The literature are coarsely composed of four distinguished subjects, which are (i) SI engine combustion process, (ii) cylinder pressure measurement and its importance, (iii) an overview of progress in SI engine combustion modelling and finally (iv) a review of Turbulent Flame Speed Closure (TFSC) model and its previous application of SI engine combustion modelling.

2.2 Spark Ignition Engine Process

Most of current models employed for SI engine are developed based on physical observation of actual SI engine combustion processes. Thus, the knowledge and understanding of the physics of the real process become important in the model development as well as to understand the mathematical formulation developed for such models (Heywood, 1994). The SI engine process into three distinctive stages (i) the ignition and flame development (ii) turbulent flame propagation and (iii) the flame termination or flame-wall interaction (Pulkrabek, 1997).

2.2.1 Physics of Spark Ignition Engine Process

The first stage of the combustion, the ignition and flame development is associated with burning of 5-10 % of the cylinder mixture. Based on Heywood (1994), the spark creates high temperature kernel between the spark plug electrodes of order 1

mm in size and ignite the mixture in vicinity of the spark plug gap. A nearly spherical laminar flame form and propagates in the outward direction at a rapid time scale of order of $300 \mu\text{sec}$. The process is nearly laminar in nature at least at low to intermediate engine speed. There is only a very small pressure and temperature rise during this period due to low mixture burned and consequently low energy released (Pulkrabek, 1997).

The next stage, turbulent propagation flame is usually associated with 90-95% mass fraction burned. The reaction sheet flame propagating outward in an approximately spherical manner. The thin reaction sheet flame is wrinkled by the turbulence motion at scale smaller than the flame radius. Comparable and larger scales of turbulence than the flame radius only distorted and convected the overall flame shape. The smallest turbulence scales is usually larger than the laminar flame thickness and resulted with undisturbed reaction sheet structure. Turbulent Reynolds number is in order of 100-1000 while Damkohler number is in order 100 (Heywood, 1994). Thus, turbulent premixed SI engine combustion is normally in the wrinkled laminar flamelet regime of premixed turbulent combustion. In the regime, turbulent flame consists of pockets of unburned reactants and fully burned products separated from each other by thin wrinkled and stretched laminar flames. In the regime, the reaction is treated as fast chemistry compared to the flow field time scales and single reaction progress variable can be used to describe the combustion process (Amstrong and Bray, 1992).

The effect of turbulence enhanced the flame propagation speed and the value is about 10 times faster than laminar flame front propagation in which the flame moving in stationary air-fuel mixture (Pulkrabek, 1997). There are two mechanisms induced by turbulence, including the wrinkling and stretching effects on the flame. The wrinkling effect increases the burning rate by increasing the surface of thin reaction sheet within the turbulent flame zone, which is also called the flame brush. While the stretching effects, which is produced by the wrinkling primarily, slowing down the burning rate by slowing the molecular diffusive process within the reaction sheet (Heywood, 1994).

The flame termination is the period where the flame front has reached the extreme corner of the combustion chamber near the wall and associated with the

burning of the rest of the mixture (Pulkrabek, 1997). At this time, the end gases only fulfilled a few percent of chamber volume due to the expanded burned gas and reacts in a very small volume closest to the wall. It reacts at a very reduce rate. The wall act as the heat sink to the energy being release by the flame front and dampen the turbulence mass motion of the gas mixture. These consequently reduced the rate of reaction and the flame speed (Pulkrabek, 1997).

The mean reaction rate of the cylinder mixture is mostly governed by the three most important factors, (i) the structure or the geometry of the flame front, which is highly influenced by the geometrical confinement of the flame. (ii) The unburned mixture composition and state, which related with thermo-chemical properties and finally (iii) the turbulence flame speed, which govern the rate at which the flame front propagates across the combustion chamber (Heywood, 1994).

2.2.2 Turbulent Flame Structure and Flame Speed

The Section 2.2.1 was described the physics of the spark-ignition combustion process. It is observed from various experimental studies and has become directive knowledge in the progress of SI combustion modelling. The three most important factors that influence the burning rate of the cylinder mixture have become the centred of study for almost engine combustion modelling. However, the most basic requirement for almost engine combustion models generally can be divided into two most distinctive components (i) the flame structure model and (ii) the flame speed model (Heywood, 1994).

The flame structure model provides an approximation to the actual turbulent-wrinkled reaction-sheet flame geometry. Most SI engine flames are spherical in nature. This model also considers the convective-diffusive effect of cylinder mixture bulk-flow. The ignition model, which simulates the flame kernel initiation, usually considered as part of the flame structure model. The flame structure model requires input of flame speed to control the propagation rate of the flame reaction sheet. These parameters are the key parameters that are solved through turbulent flame speed based models. Most of

the current flame speed models also include the effects of flame wrinkling and stretching in the reaction rate terms (Heywood, 1994).

2.3 Cylinder Pressure based Combustion Analysis

Cylinder pressure is one of the most established methods of analyzing engine combustion. Measurement of cylinder pressure is completed using pressure transducer. It measures instantaneous averaged cylinder pressure inside combustion chamber. Pressure indicator diagram is utilised in the early day of engine research, dated back to James Watt and Nicolas Otto, in early 1880 (Amann, 1985). Measured cylinder pressure, coupled with measured instantaneous cylinder volume and engine crank angle degree (CAD) are primarily used to plot the utmost important engine diagram, the pressure-crank angle (p-t) and pressure-volume (p-V) diagram which can be further used to evaluate engine performance (Randolph, 1994). Combustion analysis based on cylinder pressure has been widely studied and correlated with other engine parameters. The p-t diagram is useful for determining the mean effective pressure, derivation of mass fraction burned curve and instantaneous cylinder temperature. The mass fraction burned curve is used primarily for distinguish each stage of SI engine combustion process (Heywood, 1988).

Douglas et al. (1997) have investigated proper techniques of cylinder pressure measurement and methods of analysis for determination of mass fraction burned curve and cylinder temperature. The p-V diagram is used to determine the indicated quantity of work and power. These describe the actual work and power produce inside the engine cylinder. The method of analysis, validity and associated precaution steps in determining the indicated work, power and mean effective pressure (MEP) of a racing engine has also been addressed (Randolph, 1994). Additionally, log p-V diagram is useful for studying the pumping effect of an engine. The combustion pressures are also used to analyze engine knock, cyclic variation and misfire-detection.

The latest transducer technologies are mostly based on piezoelectric principle (Walter et al., 2004) and fibre-optic transducer (Roth et al., 2002). The piezoelectric type transducer is state of art technology for the measurement. The fibre optic type is

the newly designed spark plug. It is evidently has the advantageous of being lower-cost, longer life span and more suitable for system monitoring, but the newly developed system is not fully tested for a wide range of engine operation. In addition, Roth et al. (2002) has investigated that fibre-optic pressure transducer tend to be effected larger by the thermal shock effect after long-hour operation. However, current measurement method is still exposed to a few undesired drawbacks including the method is restricted to un-cooled miniature pressure sensors with low sensitivity, the sensor element is exposed to an extraordinarily high thermal load, proximity to high ignition voltage carries the risk of electromagnetic interference, positioning between the valve seats means they are subject to heavy vibration, and incorporating the pressure sensor into the spark-plug results in more complex design (Walter et al., 2004).

2.4 Combustion Modelling using CFD

Numerical combustion analysis of spark ignition engine using multi-dimensional or computational fluid dynamics modelling has reached the age of maturity in its growth. By overall, the advent of computing power, model's capabilities, validation, and solution algorithm have allowed the CFD modelling to provide sufficient predictive capability for engine performance prediction. The multidimensional models are demonstrate the most useful in examining problems characterized by the need of detailed spatial and temporal information of gas velocity, temperature, pressure, as well as cylinder composition and complex interactions of many phenomena simultaneously (Heywood, 1980).

CFD methodology in combustion problem is based on the solution of mass, momentum, energy and species conservation equations in either two or three-dimensional domain (Heywood, 1980). Details of the CFD formulation and solution techniques can be found in Ferziger and Peric (2002) as well as Versteeg and Malasekera (1995). For specific application of IC engine process, a more comprehensive model is required to consider turbulence, chemical reaction, ignition, heat transfer and boundary layer process near the wall (Gosman, 1999). However, state of art approach implies that each phenomenon is tackle by using different sub-models simultaneously. It was also showed that the geometrical description played a major role

in determining for solution accuracy. Figure 2.1 presents all the important consideration that needed to be considered in each SI engine simulation.

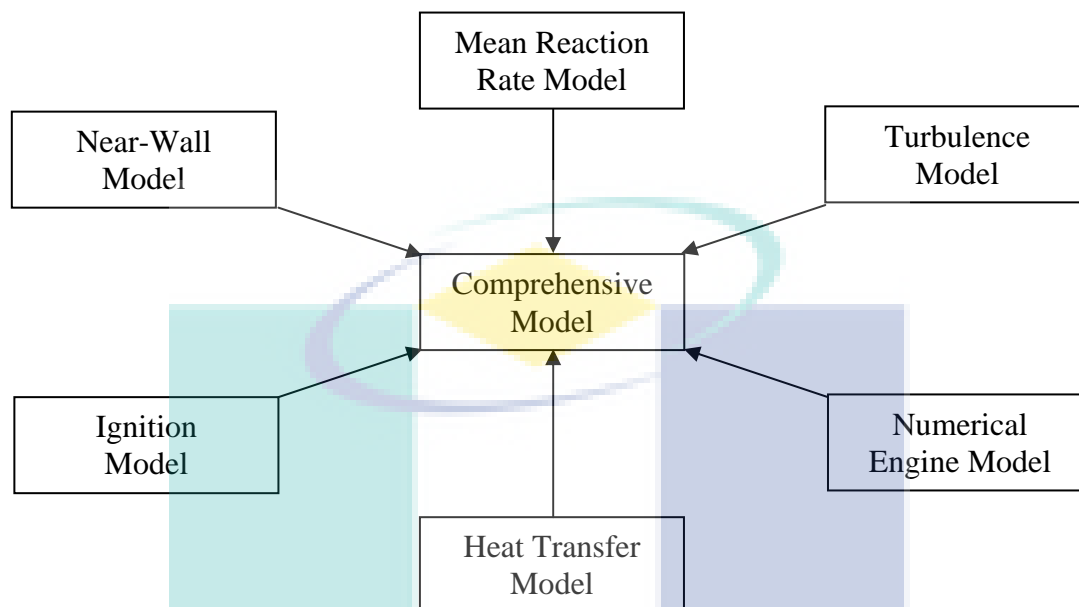


Figure 2.1: Vital requirement for premixed turbulent combustion modelling of SI engine

2.4.1 Computational Domain

Computational domain is referring to the geometrical description of the baseline engine used for turbulent combustion modelling. It includes details of the engine geometrical design with moving parts of valve and piston, and numerical grids. All information assembled the engine computational domain. Full cycle simulation generally required all information of engine geometrical features. During early attempt of turbulent flow and combustion modelling of IC engine, the model employed is a relatively simple shape, with coarse grid, limited to two-dimensional cases, and often steady in nature (Heywood, 1980). However, an attempt to solve a transient cold flow in-cylinder processes with detail feature has been demonstrated by Gosman et al. (1980).

The advent of meshing technologies of moving and deforming grid and computing power has enabled the transient solutions in-cylinder process with relatively

complex geometry and enabled a more realistic transient solution of 3-dimensional in-cylinder problem as evidenced from Gosman (1985) and Nishiwaki (1985). However, until 1985, all the works are mostly limited to cold-flow study and yet no progress has been achieved for full cycle simulation of flow and combustion simultaneously. Full-cycle CFD analysis of flow and combustion are then reported by Delhay and Cousyn (1996). This approach has a very significant advantage because the flow at valve boundary is solved automatically by CFD solver. Consequently, it provides initial condition for combustion modelling. However, this clearly required longer computing time.

Nevertheless, in certain circumstances of engine's combustion study, when the focus of the study is on the combustion process only, or due to the limiting computing power, one might limit the computation range into combustion period only. This approach has also been proven very useful and sufficient by previous study of Zhao et al. (1993) and Matthews et al. (1996). Computation of combustion process is carried in the period of the combustion process only, from the start of ignition until all the mass fraction of the cylinder is fully burned. Thus, no detail inclusion of engine geometrical features except the combustion chamber is required. This consequently reduced computing time. However, this required experimental data of cylinder flow field provided at the instance of ignition.

2.4.2 Turbulence Modelling and Near Wall-Turbulence

Most engineering flow problems are turbulence in nature. The solution of turbulence flow can be realized using a complete solution of Navier-Stokes equations through the so-called Direct Numerical Simulation (DNS). These equations are founded more than century ago independently by Louis Marie Henry Navier and Sir George Gabriel Stokes (Cengel and Cimbala, 2006). However, there is still no effort has been devoted to the three-dimensional engine's turbulent combustion modelling using the previous approach. This is because the full solution of Navier-Stokes equations for turbulence flow is truly expensive and its associated references for engine application are hardly found. Major alternative lies in the usage of Large Eddy Simulation and full

field modelling especially based on Reynolds averaging procedure (Drake and Haworth, 2007).

Recent progress has demonstrated the debut effort for the application of LES for the engine's turbulent combustion (Richard et al., 2007). However, its application for variety of engine's complex problem still taking years for establishment and surely the utmost important requirement is computing power. This is because the LES modelling required that all the large scale eddies be fully solved while the small scale eddies is still modelled using sub-grid scale model. In addition, it only applies for 3-dimensional domain (Ferziger and Peric, 2002). Thus, full field modelling based on Reynolds Averaged Navier-Stokes (RANS) equation has become the most preferred option for almost engine combustion study. Using this approach, details turbulence eddies are not solved, but rather focused on modelling the effect of turbulence (Ferziger and Peric, 2002).

Among RANS based models for turbulent flow are one equation Spallart-Allmaras model, two equations $k-\varepsilon$ model, two equations $k-\omega$ model and Reynolds-Stress Model (RSM). Spallart-Allmaras turbulent model is one-equation model typically used for solving external flow or aerodynamic problems. Two equations $k-\omega$ model is rarely employed for engine combustion study, while application of RSM on multi-dimensional engine study is quite expensive in computation time. This is because the model solved every component of the Reynolds stresses. Two equations $k-\varepsilon$ model is the most established and the most widely validated mathematical model for turbulence (Versteeg and Malasekera, 1995). In fact, it is the most widely used model for engine flow and combustion modelling as found in many literatures.

For internal or wall-bounded flow, any CFD model is required to have a fine mesh adjacent to the wall. This is important to capture the associated viscous effects near the wall. However, limited computing power restricts the usage of too fine mesh at the wall. Thus, a modelling approach is required to bridge the core flow to the wall. Previous studies of engine flow and combustion have demonstrated the usage of the wall function to model the near-wall turbulence coupled with existing turbulence models. Such analyses have resulted with sufficiently good agreement between model's

prediction and experimental results as studied by Delhay and Cousyn (1996) and Delhay and Duverger (1998). The wall-function approaches are proven useful since it reduce the number of element adjacent to the wall. The wall function approach is popular because it is economical, robust, and reasonably accurate (Fluent, 2005).

2.4.3 Spark Ignition Modelling

The most important requirement of the ignition model is the spark is able to deposit a sufficient energy to heat up the cylinder mixture and initiate the combustion (Yasar, 2001). However, details of the spark ignition process are regularly unknown. There are two type of spark ignition model that have been developed which are the one-dimensional model that only consider the energy parameter and the multi-dimensional model which consider geometrical description of spark plug gap (Duclos and Colin, 2001). The one-dimensional model is addressed by Heywood (1994) who described that the nature of kernel initiation is simplified by considering only the initial and final spark-generated flame kernel size and its associated energy distribution along kernel development. Based on the same approach, Lipatnikov and Chomiak (2002) have employed an ignition model put forward by Zimont for SI engine application. The model can consider a fixed and time varying spark size with moderate energy input. It also incorporates an effective diffusion time for the spark energy diffusion.

A more complicated but realistic model is the Arc and Kernel Tracking Ignition Model (AKTIM), which has been suggested by Duclos and Colin (2001). This model is purposely developed to describe the flame kernel expansion during SI engine combustion. This model consists of four different sub-models, which proposed to simulate the stages of the ignition process. These sub-models account for the spark plug electrical circuit, the associated energy breakdown, the structure of the flame kernel, and the geometry of the spark plug gap respectively. However, this model requires a relatively complex computational domain especially the geometrical description of the spark plug gap. This consequently will difficult the meshing procedure.

2.4.4 Heat Transfer Modelling

Engine heat transfer involved all three modes of heat transfer including the heat conduction from the inner wall to the outer wall of coolant or lubricant passage, the heat convection from the heated gases to the wall and the radiation of gases in the period of combustion (Pulkarabek, 1997). However, in previous studies of engine combustion using multi-dimensional modelling, many researchers have isolated the multiple mechanism of heat transfer involved into simpler cases, for example, radiation process since it is only significant in a very short period. In addition, additional model equations are required to solve the radiation effects, thus result with increase the computing power.

Simultaneous solution of all modes of heat transfer process is hardly found, as separate calculations of the both problems tend to be more efficient and less time-consuming as demonstrated by Peters et al. (2001) and Mugele et al. (2001). Therefore, in most combustion analysis, researchers are always solved the convective process, which can be executed by solving a single energy equation. This equation, coupled with turbulence models and standard wall-function is sufficient to enable the solution of the wall heat flux in conditions where the wall temperature is provided and vice versa with relatively good agreement with experimental results (Pinchon, 1990). In addition, the development of more precise and comprehensive heat transfer model is hampered by the difficulties associated with the experimental data collection of heat transferred (Gosman, 1999).

2.4.5 Reaction Rate Modelling

The key issue in premixed turbulent combustion modelling of SI engine is the chemical reaction modelling. Heywood (1994) has stated that a combustion model must have at least two types of components: Firstly, the flame structure model, which describes the flame geometry and secondly the flame speed model that governs the rate of the flame propagation. Veynante and Vervisch (2002) has addressed that the reaction rate model must be based on the known quantity resolved from the earlier approach for turbulence, ignition and heat transfer to reduce the complexity of model's formulation.

Current models that are appropriate for the solutions of turbulent premixed combustion of SI engine are mostly based on the RANS approach. The available combustion models for turbulent premixed engine combustion are: (i) Flame Fractal Model (Heywood, 1994) (ii) Coherent Flame model (Delhay and Cousyn, 1996) (iii) Turbulent Flame Speed Closure (TFSC) model (Lipatnikov et al, 1998) (iv) Bray-Moss-Libby model (Veynante and Vervisch, 2002), (v) Finite Rate Model (Fluent Inc., 2005) and (vi) G-field Equation Model (Ewalds and Peters, 2007).

Finite rate model solved the original species conservation equation. One species equation is required for every single species. In actual engine combustion, it involved multiple reactants and product where at least several hundred species and several thousands of reaction must be considered for hydrocarbon reaction. This is greatly effect the computing time. In, addition, the reaction mechanism is needed to be pre-determined as part of the model inputs. If a problem regards more than two reaction mechanism, the expression for the reaction rate becomes stiff and special stiffness solver is required (Veynante and Vervisch, 2002). Another crucial factor is the reaction rate term is based on Arrhenius laws of reaction (Fluent Inc., 2005). The reaction rate is non-linear, and the mean reaction rate cannot be simply averaged and express in terms of species mean mass fraction, mean temperature or mean density as mathematically proven by Veynante and Vervisch (2002).

The other models of (i)-(iv) and (vi) are mostly based on the solution of single equation for a conserved scalar, which is more efficient for multi-dimensional modelling. In premixed combustion, the conserved scalar approach defines a reactive scalar, the so-called progress variable which can be further defined in terms of species mass fraction or temperature etc. (Turns, 2000). Multiple reactants and products can be treated as a single component mixture, which can be either unburned or burnt only. This approach is called as the Simple Chemical Reacting System (SCRS) (Versteeg and Malasekera, 1995). In addition, all these models are developed based on the geometrical description of the flame rather than inclusion of details aspect of chemical kinetic. They include at least the description of the flame structure and turbulence flame speed (Heywood, 1994).

In terms of reaction rate, the TFSC model and G-equations model are based on turbulent flame speed closure as found in Lipatnikov et al. (1998), and Ewalds and Peters (2007) respectively. While the flame surface density models is closed based on the rate of consumption of the flame surface area, which is obtained from analysis of strained effect on the flame surface (Delhaye and Cousyn, 1996). For these models, the underlying effect of chemical kinetics are treated using the laminar flame speed and it has become one of the most important input to the model (Veynante and Vervisch, 2002). Therefore, expression for the laminar flame speed must be based on rigorous empirical analysis. In addition, it usually must consider the effect of varying mixture distribution, the pressure and temperature fluctuations and the existence of residual gases Wallesten et al. (2002).

Models of (i)-(iv) and (vi) are mostly based on the flamelets assumption. In the origin of the flamelets concept, turbulent flame can be view as an ensemble of locally stretched laminar flames, called flamelets. This thin layer of flamelets is separating the burned and unburned state of the cylinder mixture. The turbulence and chemistry influence each other through these mechanism: (1) the flamelet introduces heat expansion and flow acceleration across the flame front, which changes the turbulent flow fields on both side of flame front; (2) on the other hand, the turbulent eddies convect and distort the flame front, but are not able to disturb the structure of flamelets. In this way, the calculation of turbulence and chemistry are decoupled. In brief, the flamelet concept is build upon an assumption that turbulence cannot disturb the structure of laminar flames.

Models of (i)-(iv) and (vi) are initially developed to consider the turbulent flame propagation stage. Therefore, all the models need special treatment of the ignition phases and this has lead to the inclusion of external ignition model. In addition, different turbulence model is required to capture the turbulence. The most widely used model for that purpose is the two equations $k - \varepsilon$ model as reported by Veynante and Vervisch (2002). Almost all the mathematical models aforementioned are assume that the reactants are in gaseous state. This implies that the previous models are capable modelling the gaseous reaction only, which is not absolutely true in practice. The fuel

droplets are somehow incompletely vaporized during the intake and compression process, thus create inhomogeneous region (Merker et al., 2006).

From the aspect of simplicity, the TFSC model and the G-equation model (Ewalds and Peters, 2007) are considered the simplest model compared to the other model (Heywood, 1994). The TFSC model is the most widely model embedded in commercial CFD code as FLUENT, STAR-CD and AVL FIRE. This is because the model is mathematically simpler and required low-cost computing power. In addition, it was shown that the model is well predict the combustion of expanding spherical flames under numerous condition of various mixtures composition, pressure, root mean square (RMS) turbulence velocities, length scales, flame ball radius, open or closed flows, and decaying or stationary turbulence (Lipatnikov and Chomiak, 2003).

2.5 Applications of TFSC Model for SI Engine Modelling

The applications of the TFSC model for realistic spark-ignition engine combustion have been first reported by Lipatnikov et al. (1998). The model has been validated against numerous experimental data from various groups of researchers investigated on the expanding spherical turbulent flames from a simple and well-defined problem in combustion bomb. However, it was found that the model predictions is mostly suits for prediction at moderate turbulence. The model validation at low and high turbulence is still hampered by discrepancies and lack of experimental data. The study was extended to simulate realistic engine combustion process and two modifications have been suggested to account for (i) the burning acceleration due to the mixture compression inside the cylinder (ii) the effect of mixture in-homogeneity through the laminar flame speed expressions. The model is tested for a port fuel injected 4-valve 4-stroke gasoline engine at 1800 rpm. The results of burned fuel mass fraction of simulated model has been compared to the experimental data and showed good agreement (Lipatnikov et al., 1998).

Wallesten et al. (1998) had then extended the previous work of Lipatnikov by employed the TFSC models for the same engine configuration and same engine speed. In this study, the effect of different ignition timing and mean effective pressure on the

burned fuel mass fraction curve have been considered. In the next stage, Lipatnikov and Chomiak (2000) had conducted a series of theoretical study using numerous turbulent premixed combustion models on the effects of pressure on turbulent flame speed and non-stationary nature of turbulent flame development. The results are compared with various experimental data of simple and well-defined problem. Important conclusions drawn out by Lipatnikov and Chomiak (2000) was that there are five most promising models suitable for SI engine modelling which are (i) the TFSC model (ii) the coherent flame model (iii) the thickened flamelet approach (G-equation) model (iv) the pair exchange model (v) the fractal model.

In the next progress, Wallesten et al. (2002) had further employed the model to study the combustion process in a direct injected 4-valve 4-stroke gasoline engine at 2000 and 6000 rpm, with different injection timing. The modified model accounts for the dependency of pressure, temperature, equivalence ratio and residual gases onto the thermal diffusivity and laminar flame speed. The study has been extended to include the prediction of NO_x and soot formation in conjunction of combustion simulation. This have been accomplished by using NO_x and soot models of Extended Zeldovich model and Kennedy-Hiroyasu-Magnussen model respectively. Important findings from the study are the model is also applicable to the stratified charge or partially premixed combustion of DI-SI engine, the model is shows that the simulation of high engine speed combustion (at 6000 rpm) is over predicted the combustion pressure , in which the model's constant has been reduced till 15% to fit the experimental results. The results of the measured and simulated cylinder pressure are presented in Figure 2.2. Comparison of the simulated and measured results had been executed via cylinder pressure, thus indicated that cylinder pressure is a viable parameters to study spark ignition engine combustion.

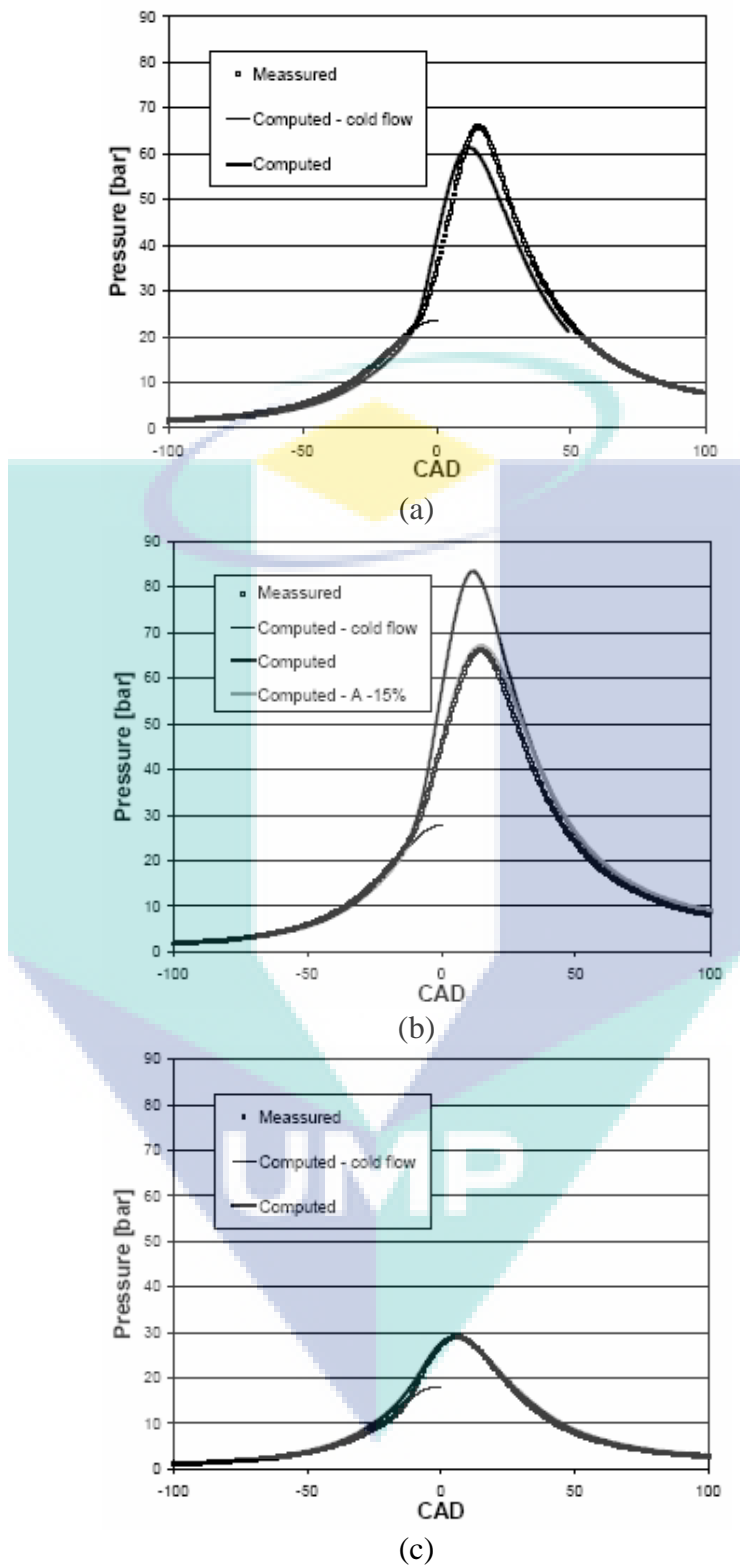


Figure 2.2: Comparison of predicted and measured combustion pressure at (a) 2000 rpm, WOT (b) 6000 rpm, WOT and (c) 2000 rpm, 2.8 bar, stratified.

Source: Wallesten et al., (2002)

Lipatnikov and Chomiak (2003) have reported a few utmost important issues that must be resolved by any combustion model to correctly predict the SI engine combustion. By comparing numerous experimental and numerical results, they concluded major source of discrepancies of current model is due to fact that most models could not correctly predict the transient growth of turbulent flame thickness according to the diffusion law. It was also suggested that different time scales is introduced to capture the turbulent flame speed development and turbulent flame thickness. As indicated by experimental results, turbulent flame speed is controlled by small-scale eddies which is corresponding to a minor scale. While the growth of laminar flame thickness is controlled by a large-eddies and thus controlled by a larger time scale.

The next issue, a combustion model is required to consider the laminar flame kernel growth and its transition to turbulence in a correct manner. The third issue is that the model is required to consider the effect of elevated pressure and temperature inside the engine cylinder. This is due to recent findings shows that the increment of turbulent flame speed at elevated pressure and temperature (Lipatnikov and Chomiak, 2003). Finally, the models for SI engine combustion require more validation at wide engine operating condition. With the updated of existing experimental data, Lipatnikov and Chomiak (2003) have extended the validation of the model to the condition of weak turbulence. It was found out that the modified equation of TFSC model predicted an acceptable flame structure of spherical propagating flame but overestimates the flame speed at weak turbulence and underestimates the turbulence flame-speed thickness.

From the modelling effort reported so far, the TFSC model has been used to predict the combustion process in realistic engine model and in simple well-defined combustion problem of spherically-propagates flame front. The latter approach is usually carried out in a combustion bomb (Bradley et al., 2003) which sometimes includes the fan-stirred flow to generate turbulence, and/or moving boundary to include the effect of compression. As suggested by Lipatnikov and Chomiak (2003) this method is more appropriate to study the cause-effect relationship of turbulent combustion parameters at a more fundamental level.

2.5.1 Convergence Study on TFSC modelling

The key factor determining the solutions accuracy in computational fluid dynamics modelling or other comparable numerical methods is convergence (Fluent, 2005). The solution is said to be converged when the values of any variables at any points tends to approximating exact solution as the grid spacing and element size is reduce to zero (Versteeg and Malasekera, 1995). Turbulence combustion modeling is considered as one of the most complex problem and required a huge amount of computing power for a converge solution. This is due to the addition of complex engine geometry and the existence of multiple intrinsic phenomena during the combustion process (Gosman, 1999). Primarily for a turbulent combustion modeling, in order to accelerate convergence, reliable initial guesses for the turbulence kinetic energy, k and turbulence dissipation rate, ε are required. However, from the aspect of numerical methods, a converged solution can only be obtain by providing a sufficient number of iteration in any specific time step before the next time step's calculation begin. In addition, the best possible result in a transient calculation can only be obtained by achieving convergence at each time step (Fluent, 2005).

Tatschl et al. (1994) have employed a pdf combustion model to solve a flow and combustion in a 4-valve spark ignition engine. Well agreed results of measured and simulated mass fraction have been obtained. A computational time step size equivalent to 1/10 degree crank angle has been used in the study but no exact figure of the iteration number at each time step has been provided. In the next stage, Wallesten et al. (1998) have studied the time step size dependency of combustion prediction by using TFSC combustion model on a 4-valve pentroof combustion chamber of a SI engine and concluded that the time step size has no significant effect on the prediction of mass fraction burned with the exception of increased computing time when the time step size is reduced. However, from the same study, Wallesten et al. also did not suggest any appropriate number of iteration for each time step to assure convergence. Other studies of Lipatnikov et al. (1998), Lipatnikov and Chomiak (2000), Wallesten et al. (2002) and Lipatnikov and Chomiak (2003) on TFSC application for turbulent combustion SI engine modelling have revealed a few issues related to TFSC for engine's turbulence

combustion modeling as discussed in Section 2.5. However, all the studies have also provided inadequate information about convergence.

2.6 Summary of Literature

This chapter dedicated the literature findings relevant to this study. Primarily, reviews have been made on the nature of actual spark-ignition engine combustion and the needs of current combustion model. Then portion of the focus is given onto the cylinder pressure based combustion analysis and its importance. At the latter stage, some subjects that form the framework and scopes for current study have been assessed. The assessment comprised of the definition of computational domain, turbulence modelling, spark ignition modelling, heat transfer modelling and finally the reaction rate modelling. The reaction rate modelling which is the centred of combustion modelling is elaborated in more detail. The descriptions have stressed out some state-of-art approaches that mostly employed in previous study. The application of TFSC model of Zimont is then discussed. The extensions of works on TFSC modelling for turbulent SI engine's combustion have been pointed out. As a major influential factor in any CFD modelling, convergence related study are also reviewed. It was found out that there is no specific guidance in terms of appropriate number of iterations per time step in transient calculation for a converged solution has been provided in previous study.

The logo for UMP (Université de Moncton) is a large, stylized 'U' shape composed of four overlapping triangles in shades of teal and blue. The letters 'UMP' are printed in white, bold, sans-serif font across the center of the 'U' shape.

UMP

CHAPTER 3

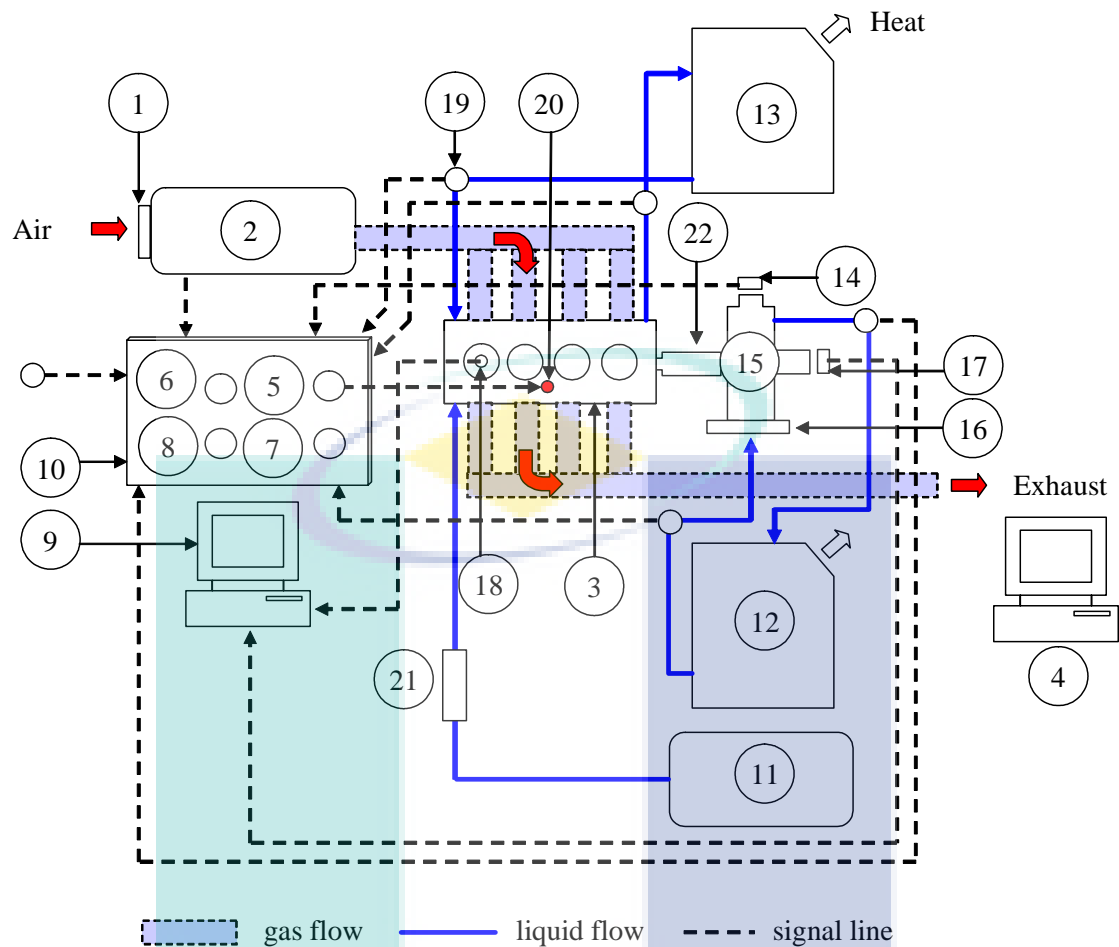
EXPERIMENTAL SETUP AND NUMERICAL MODELLING

3.1 Introduction

This chapter is dedicated to the description of major experimental setups and numerical modelling techniques. Experimental setup describes the experimental engine test-rig, important parameters and measurement techniques including the cylinder pressure, rate of air and fuel consumption, engine speed, ignition timing and engine torque. Numerical modelling technique describes the approach CFD on reactive flow simulation. These include the domain definition, grid generation, governing equations of CFD, turbulence modelling, reaction rate modelling using TFSC model of Zimont, heat transfer modelling and ignition modelling. Input data for numerical analysis are also described. Initial and boundary condition as well as the limitation of the numerical study also presented in this chapter.

3.2 Engine Test-Rig

The experimental engine test-rig is developed based on the ATE-60 hydraulic dynamometer that has a maximum power of 170-brake horsepower. The hydraulic dynamometer is coupled to a 4-stroke multi-cylinder SI engine. Figure 3.1 presents a schematic of the hydraulic dynamometer engine test-rig and details indication of its main components and connection. The rig has been built using in-house facilities and tested for a wide range of speed and load.

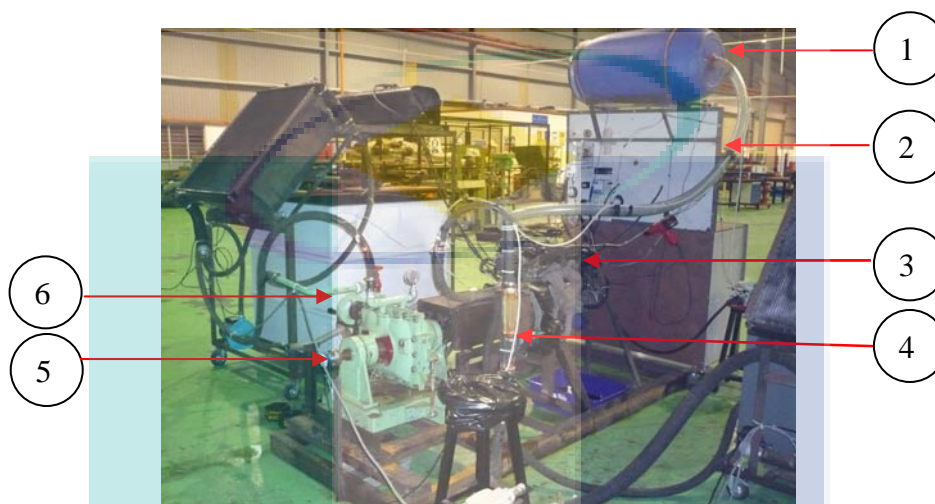


1.	Orifice plate meter	12.	Dynamometer water supply
2.	Surge tank	13.	Engine cooling system
3.	Tested engine	14.	Load sensor
4.	Emission analyzer	15.	Hydraulic dynamometer
5.	Throttle controller	16.	Dynamometer controller
6.	Pressure manometer	17.	Crank angle encoder
7.	Load indicator	18.	Pressure Transducer
8.	Temperature scanner	19.	Temperature sensor
9.	Combustion analyzer	20.	Throttle body
10.	Instrumentation panel	21.	Fuel flow meter
11.	Fuel supply tank	22.	Engine-dynamometer coupling

Figure 3.1: Schematic of the engine test-rig

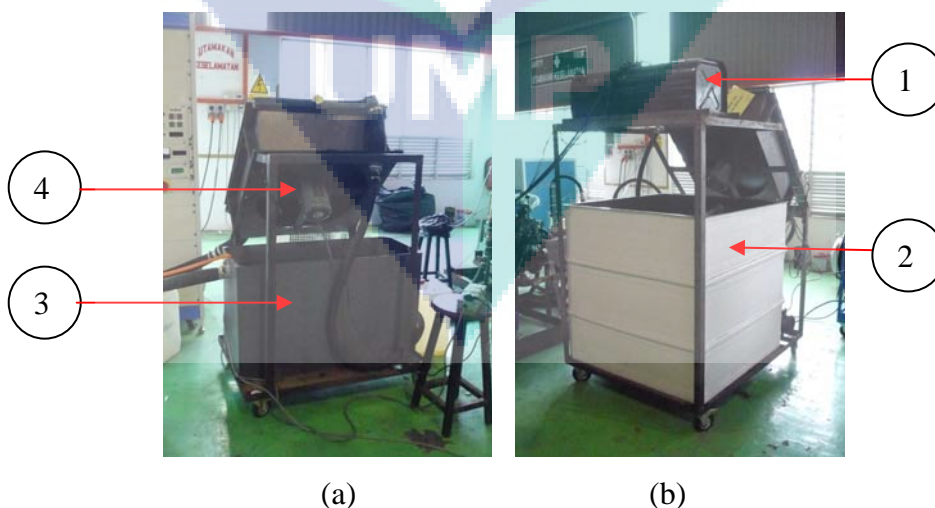
In order to fulfil an optimum operation, a sufficient supply of water is fed to the dynamometer and the engine. The dynamometer water supply is pressurized in the range of 1.0-1.75 bar for operations ranging from 1000 to 5000 rpm. In order to supply the water as well as to release the heat generated by the dynamometer operation, a customized cooling system that consist a heat exchanger, cooling fan and special water

reservoir are connected with the outlet water pipeline. As for the engine, sufficient flow rate of water is required to cool down the engine especially when running at full power. Mass flow rate of water in the range of 4 to 15 litres per minute is supplied accordingly appropriate with engine speed and load. Appendix A presents the dynamometer manufacturer data-sheet.



1.	Surge tank	2.	Instrumentations panel
3.	Tested engine	4.	Cooling water flow meter
5.	Crank angle encoder	6.	Hydraulic dynamometer

Figure 3.2: Overview of hydraulic dynamometer engine test-rig



1.	Fuel tank	2.	Water tank for the dynamometer
3.	Water tank for the engine	4.	Radiator's fan

Figure 3.3: (a) Engine cooling system and (b) Dynamometer water supply system

Figure 3.2 presents the overview of the hydraulic dynamometer engine test-rig and indicates all the major components of the rig. Figure 3.3 presents the customized cooling system for the engine and hydraulic dynamometer.

3.2.1 Baseline Engine Specification

The 4-cylinder in-line Mitsubishi Magma (4G15) 1.5 litre engine is selected for the baseline engine. The engine specification is remaining unchanged except for the cooling system where it has been modified to incorporate external and portable characteristics. The coolant temperature is controlled manually based on instantaneous cooling water outlet temperature. The temperature is measured using adapted thermocouple and temperature scanner. The original intake system is naturally aspirated and the mixture formation system is carburetted in designed. Table 3.1 listed the details of the engine specifications.

Table 3.1: Mitsubishi Magma 4G15 engine specifications

Parameter	Size and Feature
Valve train type	In-line OHV, SOHC
Number of cylinders and valves	4 cylinders with 3 valves per cylinder (two intake valves and one exhaust valve)
Combustion chamber type	Pent-Roof type
Total displacement (cm ³)	1,488
Cylinder bore (mm)	75.5
Piston stroke (mm)	82.0
Compression ratio	9.2
Intake valves open/close	15° BTDC/63° ABDC
Exhaust valve open/close	57° BBDC/ 13° ATDC
Lubrication system	Pressure load, full – flow filtration
Oil pump type	Trochoid type
Cooling system	Water – cooled forced circulation – crankshaft driven water pump
Water pump type	Centrifugal impeller type
Maximum output	66 kW@6000 rpm
Maximum Torque	124 Nm@3000 rpm

3.3 Important Parameters and Measurement Method

The following sub-sections present the method of measurement of important engine operating variables. The engine operating variables are (i) cylinder pressure, (ii) the rate of air and fuel consumption, (iii) engine speed, (iv) ignition timing and (v) engine torque.

3.3.1 Cylinder Pressure

Measurement of combustion process is accomplished using the combustion pressure sensor of Kistler™ (Type 6117) which is a spark plug type pressure transducer. The design allowed the sensor to be inserted in the spark plug body with adapter for dual-functional operation which are to supply spark discharge and to measure the cylinder pressure (Walter et al., 2004). The combustion pressure sensor is integrated with DEWE-CA 5000, a computerized based combustion analyzer, completed with data acquisition system. Measurement of the combustion pressure is executed only in cylinder number one, which is set as the reference cylinder. During the measurement, cylinder pressure data is taken as ensemble-averaged over 200 consecutive cycles. The effect of cylinder to cylinder variation is out of the scope of current study and assumed to be negligible. Details specification of the spark plug type sensor and the calibration certificate is given in Appendix B.

3.3.2 Air and Fuel Consumption

Measurement of air consumption is completed using conventional differential-pressure measurement method with square edge orifice method. The size of the orifice is 100.0 mm diameter (Plint and Martyr, 1999). Pressure drop across the orifice meter is measured using u-tube pressure manometer. This is connected with rubber tube to the tapping on the surge tank about a distance, which is equal to a half of the tank diameter after the orifice plate location. The manometer employed a coolant liquid for better visibility with an average density of 721 kg/m^3 .

A surge tank was located in the intake system to dampen the flow pulsation created by the reciprocal motion of the piston and the crankshaft inside the engine. A simple calibration procedure was conducted with the usage of a flow bench, named Super-Flow S-1020. The objective of the calibration is to compare the mass flow rate across the orifice plate meter. The input for the calibration based on the estimated airflow of the engine for a speed range of 1500 rpm to 6000 rpm. Calibration results are presented by Figure 3.4. It shows that the orifice meter measurement gives a good agreement with the Superflow results. The maximum deviation was recorded 3.52 % for tested flow conditions.

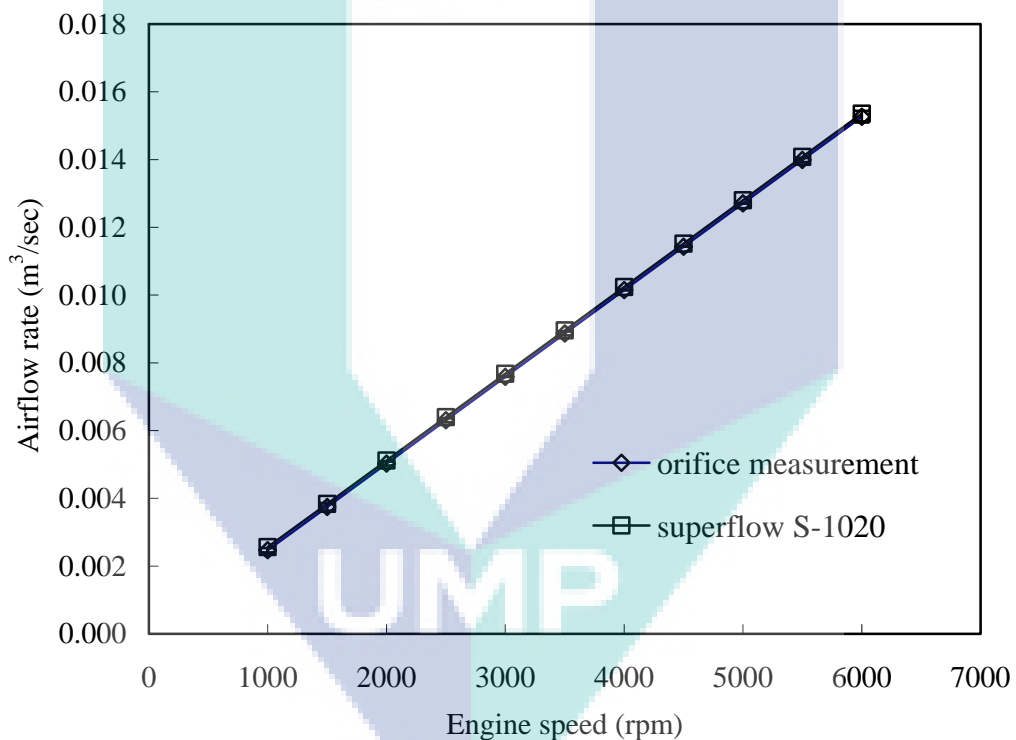


Figure 3.4: Comparisons of measured orifice flow meter measurement and Super Flow 1020 measurement

Fuel flow measurement was conducted to determine the rate of fuel consumption at specified engine condition. Fuel flow measurement is accomplished using gravimetric method, where the consumption time of specific volume of fuel in bulb glass tube was recorded manually. The bulb glass tube contains calibrated bulb volumes of 50 ml. Calibration of the double bulb glass tube was carried out by measuring the bulb glass volume using calibrated volumetric apparatus. Determination of the fuel density was

carried out for Petronas Primax 3 (RON 97) gasoline fuel. The averaged density of the fuel is 768.27 kg/m^3 .

3.3.3 Engine Speed

Engine speed was measured using crank angle encoder of Kistler (Type 2613B). Engine speed is an important parameter because of it includes time or crank angle as one of the variable that characterize engine combustion process. The overall system for speed measurement includes the crank angle encoder, the signal conditional and combustion analyzer. The signal from the crank angle encoder was send to the combustion analyzer for recording and display. The maximum allowable speed for the system is 20 000 rpm. Details specification of the crank angle encoder is presented in Appendix C.

3.3.4 Ignition Timing

Measurement of ignition timing was carried out using a stroboscope based measurement tools called Strobotester (Model DG83-D) product. This is a standard tool of ignition timing measurement for automotive laboratory. The measurement of ignition timing is important to determine the advanced ignition timing of the engine, which characterised the start of combustion. In addition, the ignition timing is one of the important inputs for the CFD engine model.

3.3.5 Engine Torque

The value of brake power was calculated based on the value of engine torque. Measurement of engine torque was carried out using a load cell attached to the dynamometer's arm. The load cell is a S-type load cell (Model 60001). Details specification of the load cell is given in Appendix D. Calibration of the load sensor is carried out by employing a known load quantity to the load cell and compared the given reading of the load cell to the theoretical value. Figure 3.5 presents comparison of measured and theoretical torque for dynamometer's load cell. Based on in-house calibration, the load cell gives a maximum deviation of 2.33%.

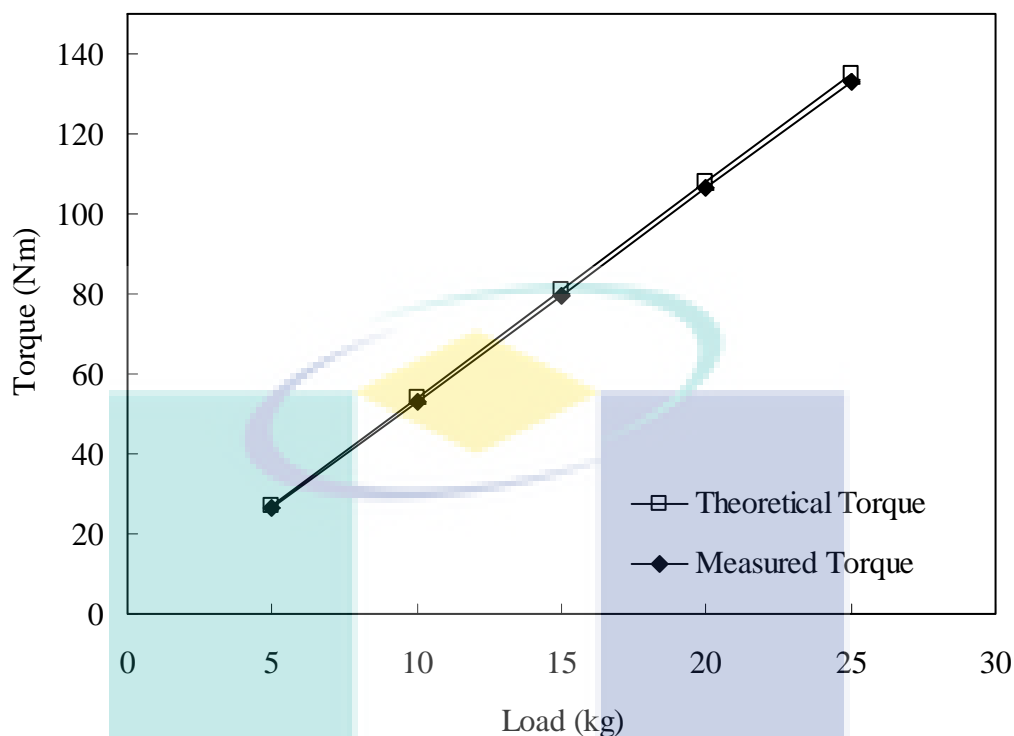


Figure 3.5: Comparison of measured and theoretical torque for dynamometer's load cell

3.3.6 Engine Testing Procedure

The data collection procedure is using the 'position-speed mode' test sequence (Plint and Martyr, 1999). The throttle opening, engine speed and engine torque are considered as independent variables. The throttle opening is controlled to achieve 100% opening. The engine speed is set independent to satisfy the selected engine speed condition. The dynamometer load is then imposed to achieve the highest possible engine torque in that condition. Hence, other variables such as cylinder pressure, the rate of air and fuel consumption, and the ignition timing are considered as dependent variables. The data collection is carried out from 1500 rpm to 4000 rpm with speed interval of 500 rpm. Appendix E presents brief steps associated with the data collection procedure. Subsequently, Appendix F presents the list of formulas used to calculate engine performance parameters.

3.4 Numerical Modelling Approach

CFD modelling of turbulent premixed SI engine combustion is carried out by considering all the factors that have been stated in Chapter 2. The approach for computational domain definition, grid generation, governing equation of CFD and turbulence modelling are elaborated in the following sub-sections.

3.4.1 Computational Domain

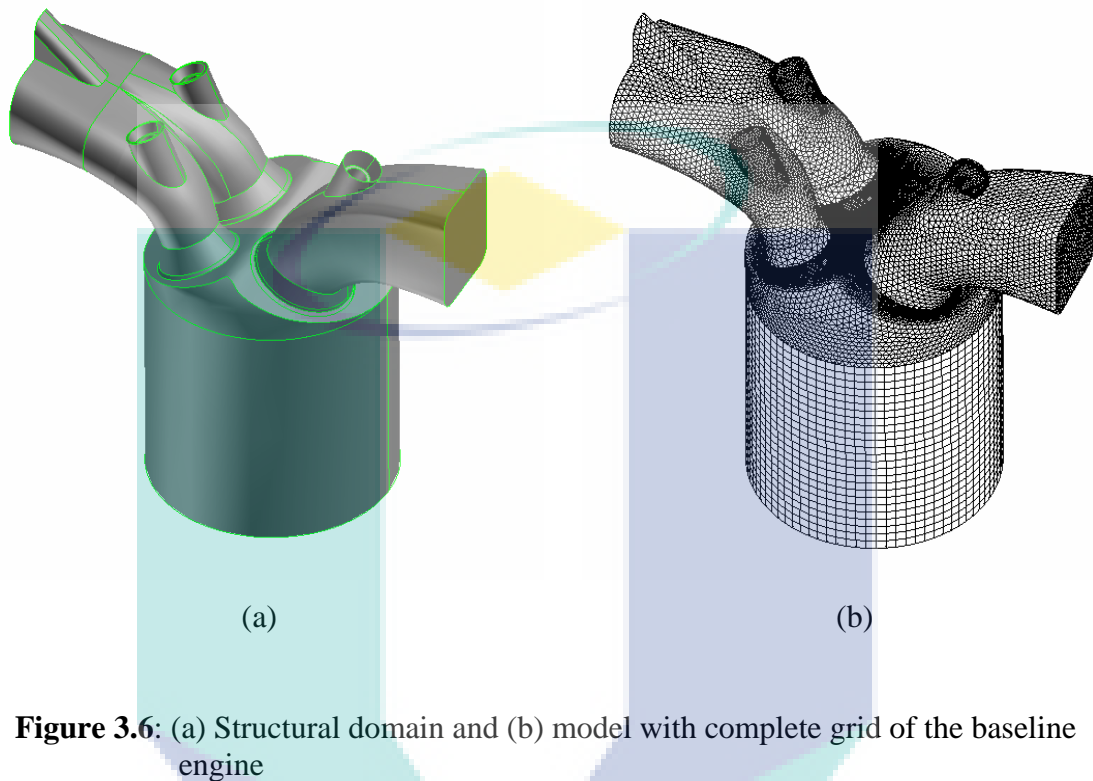
The domain for the numerical calculation is selected from the inlet of the intake until the outlet of the exhaust manifold. This embrace the intake valves, the exhaust valve and the combustion chamber. The engine has two intake valves and one exhaust valve per cylinder. The combustion chamber is pent roof in design with flat piston face. As demonstrated by previous researcher (Delhaye and Cousyn, 1996; Mugele et al., 2001), the addition of the intake and exhaust manifold for full cycle simulation are vital for the solution of the in-cylinder flow-field during induction and compression.

In term of the domain size, it is praiseworthy to impose symmetrical boundary. However, for the baseline engine, the approach is invalid due to the actual geometry, which has two intake valves, and one exhaust valve with each valve is different in size. Furthermore, the spark plug position is located at the side of the combustion chamber. Only the reference cylinder is modelled by assuming that cylinder-to-cylinder variation is negligible. In addition, the measured cylinder pressure is taken from the same reference cylinder.

3.4.2 Grid Generation

The grid generation process is the most time consuming stage during the study. Major tasks are to generate grids for each decomposed domain and to set up the moving boundary as well as deforming mesh event in order to resemblance the actual engine motion. The dynamic mesh simulation of the engine is accomplished by the optimal usage of the commercial software (Fluent, 2005). The domain is decomposed into several regions, which can be divided as the (i) intake and exhaust manifold volume (ii)

intake and exhaust valve volume (iii) combustion chamber volume and (iv) deforming cylinder volume. Structural and computational model with grids are shown in Figure 3.6 (a) and (b) respectively.



The layering hexahedral mesh is used to define the deforming cylinder volume and valve volume. The flat piston face and the valve's upper and lower faces are selected as the moving boundary. As the volume expands, the moving faces are move in isotropic direction and the hexahedral meshes are layered adjacent to the moving boundary automatically by the solver to represent the expanding volume. Moreover, when the volume is reduced, the layered hexahedral mesh adjacent to the moving boundary is removed.

For the pentroof chamber volume, special approaches of spring smoothing and remeshing are employed to the tetrahedral mesh. The volume is constructed to fulfilled small displacement of moving faces adjacent to the deforming cylinder volume. The displacement is about 0.12% of engine stroke. This is purposely done to avoid the collision of the valve and the flat piston faces. The unstructured meshes are

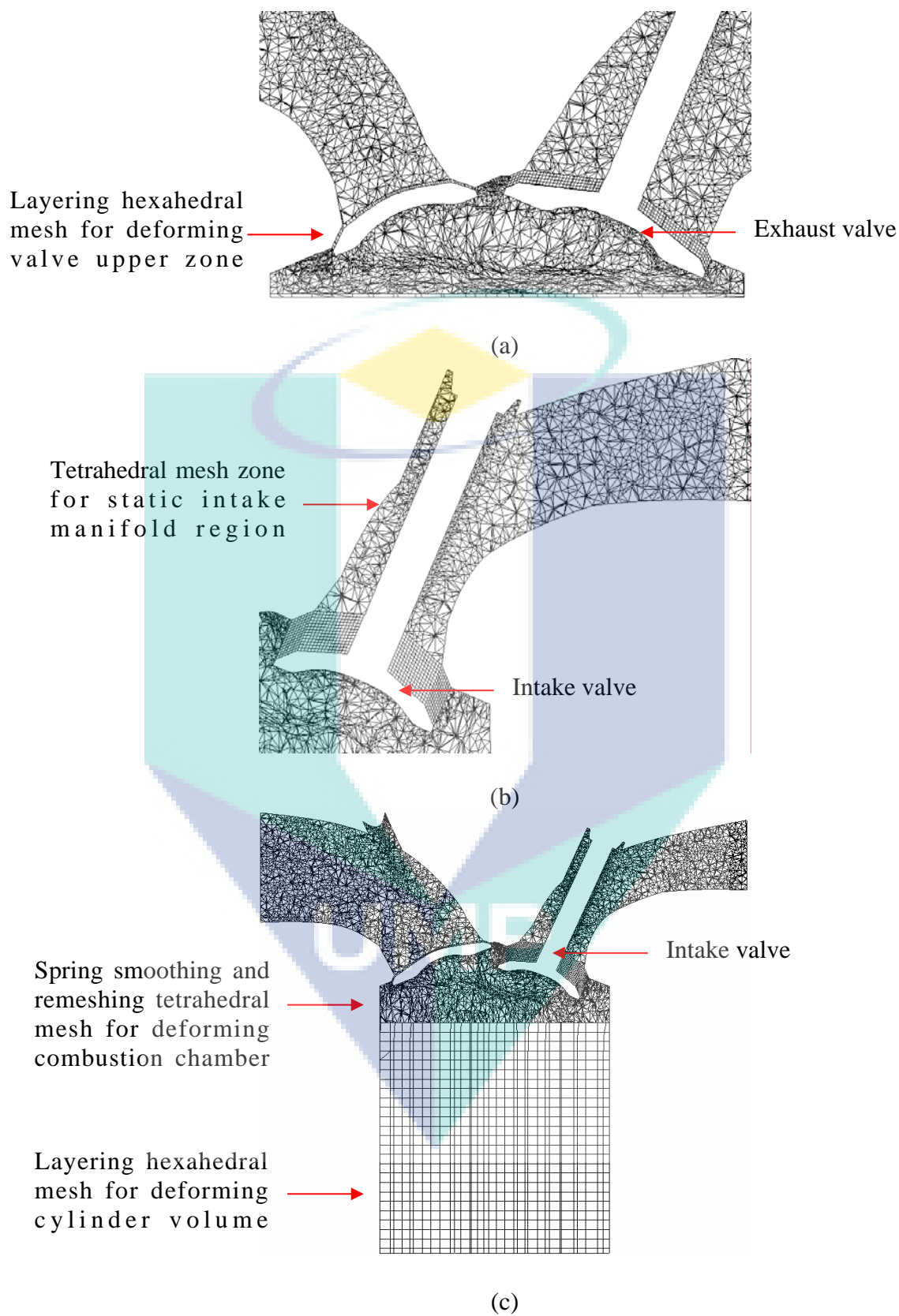


Figure 3.7: Cross sectional view of grid details (a) Exhaust valve closing in progress (b) Intake valve at maximum lift (c) Overview of mesh elements selection

therefore normally stretched without deteriorate the element aspect ratio and skewness. As the value of aspect ratio and skewness exceeding maximum value, these are remeshed to produce a new set of tetrahedral elements.

In the stationary parts such as the intake and exhaust manifold, the unstructured, tetrahedral mesh element was employed. In order to reduce the computing time, the flow in the stationary parts such as the intake and exhaust manifold volume only solved in the period of the intake and exhaust process only. In the period of compression, combustion and expansion, the cell volume is deactivated and not involved in calculation. Figure 3.7 presents all the grid generation in details.

In order to replicate the actual engine process, all the associated event occurred in the engine cylinder during a complete cycle of flow and combustion are modelled as well. The events simulated are started from -360° crank angle (CA) at TDC until the end of cycle at 360° CA. These include the intake, compression, ignition, combustion, expansion and exhaust stroke process. Table 3.2 provides all the defined events associated with the 4-stroke engine combustion process.

The coarse meshed model has been tested for full-cycle analysis of 720° crank angle without further refinement on the mesh size and the effect of convergence is ignored. The time-step size was set as equal to 1° crank angle while the iteration number was set as default, 20 iterations per time step. It was found out that the calculation time of the full cycle is too expensive. Due to the computing limitation, conclusion has been made to reduce the simulation period. This is possible by simulating only a short period of in-cylinder process, from the timing of ignition to the completion of combustion process for about 50° CA only. Hence, the initial condition that important at the start of combustion is based on measured results at the timing of ignition.

The simulated period is therefore reduced to include the simulation period only, from the timing of ignition until the completion of combustion, which required less than 50° crank angle. Thus, the computational domain finally includes the pent-roof and cylinder volume only as presented in Figure 3.8. Grid sensitivity results will be discuss in details in Chapter 4. According, to the grid sensitivity analysis, the grid has been

reduced for six times and the finest possible grid size has been chosen for the next analysis.

Table 3.2: Events definition from -360° to 360° CA

Crank angle	Events
-360°	Start of intake process (intake and exhaust valves already opened) at TDC
-347°	Intake process (Exhaust valve closed & exhaust manifold deactivation)
-180°	End of intake process/ Start of compression process
-117°	Compression process (intake valves closed & intake manifold deactivation)
-23°	Timing of ignition (for 2000 rpm)
0°	End on compression/ start of power stroke
123°	Power stroke (exhaust valves opened & exhaust manifold activation)
180°	End of power stroke/start of Exhaust stroke
345°	Exhaust stroke (intake valves opened & intake manifold activation)
360°	End of a single cycle

UMP

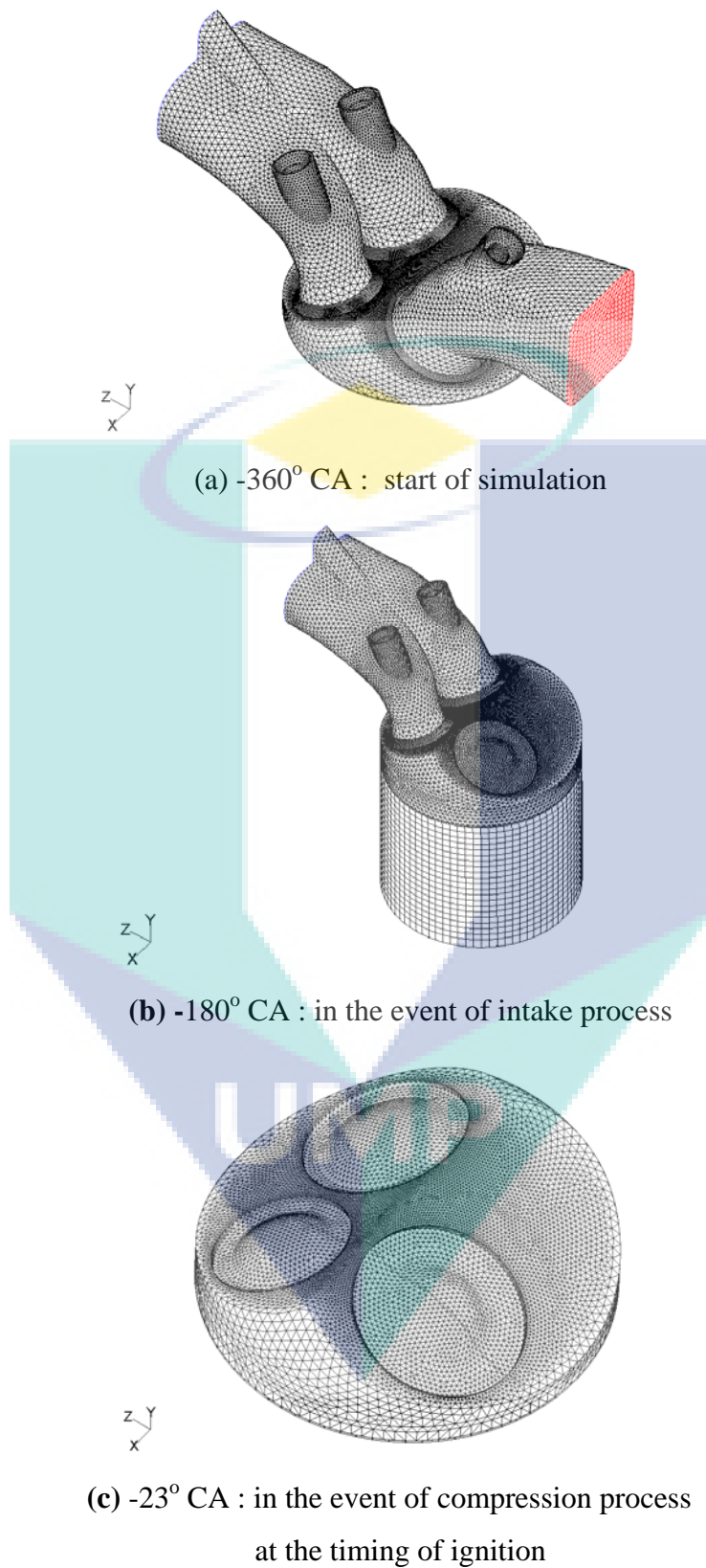


Figure 3.8: Computational domain associated with the event definition (a) during all valves opened (b) after exhaust valve closed and exhaust manifold deactivation and (c) during all valve closed

3.4.3 Governing Equations for CFD Modelling

The equations to be presented are the mathematical model that governed three-dimensional, unsteady, compressible, viscous, reactive fluid-flow for CFD modelling. These include the mass, momentum, energy and species conservation equations. The equations are given as density averaged, as it is more appropriate for problem with large density fluctuation (Kuo, 1986). The over bar signage denotes the density averaged quantity while the tilde denotes the time averaged quantity.

The mass-conservation equation is given in tensor notation as Eq. (3.1)

$$\frac{\partial \bar{\rho}}{\partial t} + \frac{\partial \bar{\rho} \tilde{u}_j}{\partial x_j} = 0 \quad (3.1)$$

where

$\bar{\rho}$: Averaged density
 $\bar{\rho} \tilde{u}_j$: Velocity components

The momentum-conservation equation is given in tensor notation as Eq. (3.2)

$$\frac{\partial \bar{\rho} \tilde{u}_i}{\partial t} + \frac{\partial \bar{\rho} \tilde{u}_j \tilde{u}_i}{\partial x_j} = \frac{\partial \bar{\rho} \tilde{u}_i'' u_j''}{\partial x_j} - \frac{\partial \bar{p}}{\partial x_i} + \frac{\partial \bar{\tau}_{ij}}{\partial x_j} + \bar{F}_i \quad (3.2)$$

where

$\bar{\rho} \tilde{u}_i'' u_j''$: Reynolds stress
 \bar{p} : Pressure forces
 $\bar{\tau}_{ij}$: Viscous stress tensor
 \bar{F}_i : Total body forces

The energy-conservation equation is given in tensor notation as Eq. (3.3):

$$\frac{\partial \bar{\rho} \tilde{h}_t}{\partial t} + \frac{\partial \bar{\rho} \tilde{u}_j \tilde{h}_t}{\partial x_j} = \frac{\partial \bar{\rho} \tilde{u}_j'' h_t''}{\partial x_j} + \frac{\partial \bar{p}}{\partial x_j} + \frac{\partial}{\partial x_j} (\bar{J}_j^h + \overline{u_i \tau_{ij}}) + \overline{u_j F_j} \quad (3.3)$$

where

$\bar{\rho} \tilde{h}_t$: Total enthalpy

$\bar{\rho} \tilde{u}_j'' h_t''$: Turbulent diffusion of enthalpy

\bar{J}_j^h : Laminar diffusion of enthalpy

The species-conservation equation is given in tensor notation as Eq. (3.4):

$$\frac{\partial \bar{\rho} \tilde{Y}_k}{\partial t} + \frac{\partial \bar{\rho} \tilde{u}_j \tilde{Y}_k}{\partial x_j} = - \frac{\partial \bar{\rho} \tilde{u}_j'' Y_k''}{\partial x_j} - \frac{\partial \bar{J}_j^k}{\partial x_j} + \bar{\dot{\omega}}_k \quad (3.4)$$

where

$\bar{\rho} \tilde{Y}_k$: Total amount of species k

$\bar{\rho} \tilde{u}_j'' Y_k''$: Turbulent diffusion of species k

\bar{J}_j^k : Laminar molecular diffusion of species k

$\bar{\dot{\omega}}_k$: Mass reaction rate of species k per unit volume

3.4.4 Turbulent $k-\epsilon$ Model

Two equations turbulent $k-\epsilon$ model with standard wall function are chosen to model turbulence effect. The $k-\epsilon$ model was first introduced by Jones and Launder for recirculation flow (Kuo, 1986). Since turbulent flow caused the production, transport and dissipation of flow energy, the conservation equations for turbulent kinetic energy, k and turbulent dissipation rate, ϵ is introduced.

The transport equation for the mean turbulent kinetic energy is given in tensor notation as Eq. (3.5):

$$\bar{\rho} \tilde{u}_j \frac{\partial k}{\partial x_j} = \frac{\partial}{\partial x_j} \left[\left(\frac{\mu_T}{\sigma_k} + \mu \right) \frac{\partial k}{\partial x_j} \right] - \bar{\rho} \tilde{u}_i'' u_j'' \frac{\partial \tilde{u}_i}{\partial x_j} + \frac{\mu_T}{\rho^2} \frac{\partial \bar{\rho}}{\partial x_i} \frac{\partial \bar{p}}{\partial x_i} - \bar{\rho} \epsilon \quad (3.5)$$

where

- μ_T : Turbulent or eddy viscosity
- σ_k : Turbulent Prandtl number for k
- μ_L : Laminar viscosity
- $\tilde{\rho} u_i'' u_j''$: Reynolds stresses

The transport equation for the turbulent dissipation rate is given in tensor notation as Eq. (3.6):

$$\bar{\rho} \tilde{u}_i \frac{\partial \epsilon}{\partial x_j} = \frac{\partial}{\partial x_j} \left[\left(\frac{\mu_T}{\sigma_k} + \mu \right) \frac{\partial \epsilon}{\partial x_j} \right] - C_{\epsilon 1} \frac{\epsilon}{k} \left(\tilde{\rho} u_i'' u_j'' \frac{\partial \tilde{u}_i}{\partial x_j} + \frac{\mu_t}{\rho^2} \frac{\partial \bar{\rho}}{\partial x_i} \frac{\partial \bar{p}}{\partial x_i} \right) - C_{\epsilon 2} \bar{\rho} \frac{\epsilon^2}{k} \quad (3.6)$$

where

$C_{\epsilon 1}$ and $C_{\epsilon 2}$ are models constants.

3.5 Zimont's TFSC Model

Descriptions of Turbulent Flame Speed Closure (TFSC) model enclose the explanation of (i) model equation and its assumptions (ii) turbulent flame speed model (iii) the mean reaction rate term (iv) model's approach for calculation of cylinder pressure (v) model's modification for SI engine application.

3.5.1 TFSC Model Equation

The model consists of conservation equation for the reactive progress variable. It predicts the instantaneous location of expanding turbulent flame brush, which is comparable to the geometrical flame structure of expanding spherical flames of engine cylinder (Lipatnikov et al., 1998). The density-averaged mean progress variable equation of the TFSC model as proposed by Zimont is given in tensor notation as Eq. (3.7)

$$\frac{\partial \bar{\rho} \tilde{c}}{\partial t} + \frac{\partial \bar{\rho} \tilde{u}_j \tilde{c}}{\partial x_j} = \frac{\partial}{\partial x_j} \left(\frac{\mu_T}{Sc_T} \frac{\partial \tilde{c}}{\partial x_j} \right) + \rho S_c \quad (3.7)$$

where

\tilde{c} : Reaction progress variable

Sc_T : Turbulent Schmidt number

S_c : Reaction rate source term

The reaction progress variable is usually defined as the ratio of mass fraction of product species, k to the equilibrium mass fraction of product species, k as given in Eq. (3.8):

$$\tilde{c} = \frac{\sum_{k=1}^n Y_k}{\sum_{k=1}^n Y_{k,eq}} \quad (3.8)$$

where

n : Total number of products

Y_k : Mass fraction of product species k

$Y_{k,eq}$: Equilibrium mass fraction of product species k

It follows that the value of $c = 0$ is corresponding to the unburned fuel mass fractions and the value of $c = 1$ is corresponding to the fully burned fuel mass fraction. The value of $0 < c < 1$ is therefore corresponding to the structure of reaction sheet flame that separates the unburned mixture to the fully burned mixture.

The mean reaction rate terms is therefore defined as product of unburned mixture density, turbulent flame speed and vector normal unit of progress variable and is given as Eq. (3.9):

$$\rho S_c = \rho_u S_T \left\{ \sum_{j=1}^3 \left(\frac{\partial \tilde{c}}{\partial x_j} \right)^2 \right\}^{\frac{1}{2}} \quad (3.9)$$

where

ρ_u : Unburned mixture density

S_T : Turbulent flame speed

The premixed combustion model is valid only for turbulent, subsonic flows. These types of flames are called deflagrations. The model assumed that the reaction occurred in thin reaction flame sheet which separating the unburned and burned mixture region. The propagation of turbulent flame brush thickness is assumed to be solely controlled by the turbulence flame speed, which in turn influenced by the laminar flame speed and flame front wrinkling and stretching by large eddies, and flame thickening by small eddies.

The model also assumed of equilibrium small-scale turbulence inside the laminar flame, resulting in a turbulent flame speed expression that is purely in terms of the large-scale turbulent parameters. The model is strictly applicable when the smallest turbulent eddies in the flow (the Kolmogorov scales) are smaller than the flame thickness, and penetrate into the flame zone. This is called the thin reaction zone region. The model is valid for premixed systems where the flame brush width increases in time, as occurs in most industrial combustors.

3.5.2 Turbulent Flame Speed Model

The closure for the reaction rate terms in TFSC is closed by the empirically derived turbulent flame speed model. The flame speed value represents the turbulent flame speed normal to the mean surface of the flame. The mathematical expression for the turbulent flame speed model is given as Eq. (3.10):

$$S_T = A(u')^3 S_L^{\frac{1}{2}} \alpha_L^{-\frac{1}{4}} l_T^{\frac{1}{4}}$$

$$= Au' \left(\frac{\tau_T}{\tau_c} \right)^{\frac{1}{4}} \quad (3.10)$$

where

- A : Model constant
- u' : Root mean square (RMS) velocity
- S_L : Laminar flame speed
- α_L : Laminar thermal diffusivity
- l_T : Turbulent length scale
- τ_T : Turbulent time scale where $\tau_T = l_T / u'$
- τ_c : Chemical time scale where $\tau_c = \alpha / S_L^2$

The turbulence parameter required for the model such as turbulent length scale, l_t , and turbulent time scale, τ_t are mostly calculated using the turbulent model.

3.5.3 Mean Reaction Rate Term

The mean reaction rate terms of Eq. (3.9) is further account the effect of the flame wrinkling and stretching due the turbulence and the effect of preferential diffusion due to the mixture inhomogeneity. To consider the effect of the wrinkling and stretching, a stretching factor G is introduced and is given by the error function as in Eq. (3.11):

$$G = \frac{1}{2} \operatorname{erfc} \left\{ -\sqrt{\frac{1}{2\sigma_\epsilon}} \left[\ln \left(\frac{\epsilon_{cr}}{\epsilon} \right) + \frac{\sigma}{2} \right] \right\} \quad (3.11)$$

where

ϵ_{cr} : Turbulence dissipation rate at critical rate of strain

ϵ : Turbulent dissipation rate

σ_ϵ : Standard deviation of distribution of ϵ

To consider the effect of the preferential diffusion, the concept of leading point in triple flame is introduced. The preferential diffusion effect is thus given by Eq. (3.12):

$$\lambda_{lp} = \left\{ \begin{array}{l} \frac{\lambda_0(1 + C_{st})d_{oxy/fuel} + d_{oxy/fuel} - 1}{d_{oxy/fuel} + C_{st}} \quad \lambda_{lp} \geq 1 \\ \frac{\lambda_0(C_{st} + d_{oxy/fuel})}{1 + \lambda_0 C_{st} + C_{st}(1 - \lambda_0 d_{oxy/fuel})} \quad \lambda_{lp} \leq 1 \end{array} \right\} \quad (3.12)$$

where

C_{st} : Mass- stoichiometric co-efficient

λ_0 : Stoichiometric ratio of unburned mixture composition

λ_{lp} : Stoichiometric ratio of leading point composition

$d_{oxy/fuel}$: Ratio of thermal diffusivities where $d_{oxy/fuel} = \sqrt{\frac{\alpha_{oxy}}{\alpha_{fuel}}}$

α_{oxy} : Molecular diffusivity of air

α_{fuel} : Molecular diffusivity of fuel

Therefore, the final reaction rate terms is completely given as Eq. (3.13) and Eq. (3.14):

$$\rho S_c = AG \rho_u I^{\frac{3}{4}} [S_L(\lambda_{lp})]^{\frac{1}{2}} [\alpha(\lambda_{lp})]^{-\frac{1}{4}} L_T^{\frac{1}{4}} |\nabla \tilde{c}| \quad (3.13)$$

$$= AG\rho_u I \left[\frac{\tau_t}{\tau_c (\lambda_{tp})} \right]^{\frac{1}{4}} |\nabla \tilde{c}| \quad (3.14)$$

where

I : Turbulent intensity

3.5.4 Model's Approach for Calculation of Cylinder Pressure

The ideal gas equation of state is coupled with the TFSC model to solve the cylinder pressure. The main important input for this model is the operating pressure and the effective molecular weight of the cylinder mixture. The mathematical expression used for pressure calculation is given as Eq. (3.15):

$$\rho = \frac{p_{op} + p}{\left(\frac{R}{MW} \right) T} \quad (3.15)$$

where

p : Local relative (or gauge) pressure

p_{op} : Specified operating pressure

R : Universal gas constant

MW : Specified mixture molecular weight

T : Instantaneous static temperature

3.5.5 Modification Suggested for SI Engine Combustion

In order to apply the TFSC model of Zimont for SI engine combustion problem, certain modifications are required. This modification includes (i) consideration on varying mixture equivalence ratio, (ii) consideration on elevated pressure and temperature and (iii) consideration on burning acceleration due to compressed.

Mixture Equivalence Ratio

Based on Lipatnikov et al. (1998), the laminar flame speed must consider the variation of the fuel-air equivalence ratio. The default laminar flame speed for most combustor has the value of 0.2 (Fluent, 2005) which is inappropriate for engine combustion. Therefore, a more accurate approach to calculate laminar flame speed using a curve-fitted polynomial, which is derived by Wallesten et al. (2002) and which is expressed as Eq. (3.16):

$$S_{L,0} = -4.4191\phi^6 + 28.4983\phi^5 - 71.5441\phi^4 + 88.4175\phi^3 - 56.8188\phi^2 + 18.8477\phi - 2.5763 \quad (3.16)$$

where

ϕ : Fuel–air equivalence ratio

This formulation is developed based on detail chemistry calculation of laminar flame propagation. The kinetic mechanism is based on isooctane combustion, which consists of 475 reactions and 100 species. The formulations suit for the equivalence ratio ranging from 0.5 to 1.8.

Elevated Pressure and Temperature

To consider the effect of pressure and temperature variation, an equation for pressure and temperature dependencies of laminar flame speed by Rotondi and Bella (2006) is employed. The calculated laminar flame speed from Eq. (3.16) was corrected using a power law function expressed as function of elevated pressure, temperature of unburned gases and is given as Eq. (3.17):

$$S_L = S_{L,0} \left(\frac{T_{unb}}{T_{ref}} \right)^\varphi \left(\frac{P}{P_{ref}} \right)^\beta \quad (3.17)$$

where

T_{unb} : Unburned gases temperature

For gasoline fuel, value of ϕ and β is given as Eq. (3.18) and Eq. (3.19):

$$\phi = 2.4 - 0.271\phi^{3.51} \quad (3.18)$$

$$\beta = -0.357 + 0.14\phi^{2.77} \quad (3.19)$$

Burning Acceleration Due to Compression

In the case of engine's combustion, the burning process is accelerated due to the compression of the cylinder mixture. This burning acceleration affects the chemical reaction time scale through the so-called laminar thermal diffusivity. In TFSC model of Zimont, the chemical time scale is defined as Eq. (3.20).

$$\tau_c = \frac{\alpha_L}{S_L^2} \quad (3.20)$$

The reference value of thermal diffusivity α_{ref} is given as Eq. (3.21):

$$\alpha_{ref} = k_{th} / \rho c_p \quad (3.21)$$

where

k_{th} : Laminar thermal conductivity

c_p : Mixture specific heat

Definition of the turbulence time scale and chemical time scale leads to the definition of the Damkohler number. The Damkohler number value measures the rate of the reaction and given as Eq. (3.22):

$$Da = \frac{\tau_t}{\tau_c} \quad (3.22)$$

Based on Lipatnikov et al. (1998), the value of the laminar thermal diffusivities must be priory modified to regard the burning acceleration. As suggested by Rotondi and Bella (2006) the correction factor for thermal diffusivities is given as Eq. (3.23):

$$\alpha_L = \alpha_{ref} \left(\frac{T_{unb}}{T_{ref}} \right)^{1.6} \left(\frac{P_{ref}}{P} \right) \quad (3.23)$$

3.6 Heat Transfer Model

The TFSC model originally solved only the heat convection process through the energy conservation. The energy equation is modified accordingly with the approach of TFSC model. The increase of enthalpy due to laminar diffusion is assumed small and negligible compared to turbulent diffusion. The effect of the body forces is also negligible. The current TFSC model of Zimont has included the contribution of enthalpy increased due to the reaction source term in the energy equation. Thus, final for the energy is then reduced to the following expression as in Eq. (3.24):

$$\frac{\partial \bar{\rho} \tilde{h}_t}{\partial t} + \frac{\partial \bar{\rho} \tilde{u}_j \tilde{h}_t}{\partial x_j} = \frac{\partial}{\partial x_j} \left(\left(\frac{k_{th} + k_T}{c_p} \right) \frac{\partial \tilde{h}}{\partial x_j} \right) + S_{h,chem} \quad (3.24)$$

where

$S_{h,chem}$: Heat gains due to chemical reaction

The heat gain due to the chemical reaction is given as in Eq. (3.25):

$$S_{h,chem} = \rho S_c H_{comb} Y_{fuel} \quad (3.25)$$

where

S_c : Normalized averaged rate of product formation

H_{comb} : Heat of combustion for burning 1 kg of fuel

Y_{fuel} : Unburned fuel mass fraction in mixture

3.7 Ignition Model

The TFSC model treats the ignition phase using the ignition model of Lipatnikov and Chomiak (2002). Consideration of the ignition process required modification on the conservation equation of the progress variable. Thus, the final conservation equation for the progress variable is given as Eq. (3.26):

$$\frac{\partial \bar{\rho} \tilde{c}}{\partial t} + \frac{\partial \tilde{u}_j \tilde{c}}{\partial x_j} = \frac{\partial}{\partial x_j} \left((\alpha_L + \alpha_T) \frac{\partial \tilde{c}}{\partial x_j} \right) + \rho_u S_T \left\{ \sum_{j=1}^3 \left(\frac{\partial \tilde{c}}{\partial x_j} \right)^2 \right\} \quad (3.26)$$

The expression for the turbulent diffusivity is also modified and is given as in Eq. (3.27):

$$\alpha_T = \begin{cases} \alpha_T \left(1 - \exp\left(-\frac{t_{td}}{\tau'}\right) \right) & \text{if } t_{td} \geq 0 \\ \alpha_T & \text{if } t_{td} < 0 \end{cases} \quad (3.27)$$

where

t_{td} : $t_{td} = t - t_{ig}$ in which t_{ig} is the timing for ignition, which is based on the experimental data

τ' : is the effective diffusion time

3.8 Input Data for Numerical Analysis

Appropriate usage of TFSC model of Zimont for turbulent premixed SI engine combustion requires a set of reasonable inputs. These include (i) definition of pre-

mixed mixture material properties, (ii) boundary condition and (iii) initial condition. The premixed mixture properties are the mixture specific heat, thermal conductivity, laminar viscosity, critical rate of strain, unburned fuel mass fraction, heat of combustion and mixture molecular weight.

3.8.1 Premixed Mixture Properties

Throughout the simulation, the premixed mixture is assumed as a mixture of isooctane (C_8H_{18}) and air (Peters et al., 2001). The equilibrium mixture specific heat and mixture molecular weight are calculated using third party Olikara and Borman routine of isooctane combustion for constant-volume adiabatic flame calculation based on specified fuel, equivalence ratio, and reactant properties (Turns, 2000). The code considers 12 species of combustion for C-H-O-N systems, invoking seven equilibrium reaction and four-atom conservation equation. This approach has produced successful results as demonstrated by Peters et al. (2001).

The value of mixture transport properties, such as mixture viscosity, and mixture thermal conductivity are estimated using the Kinetic Theory model and Sutherland's Law respectively (Fluent, 2005). Initially, the variation of the mixture viscosity and mixture thermal conductivity is calculated based on measured cylinder pressure and temperature for the period of combustion. Then, an average value for the whole period are calculated and utilised. The formulation for thermal conductivity calculation based on kinetic theory is given as in Eq. (3.28):

$$k_{th} = \frac{15}{4} \frac{R}{MW} \mu_L \left[\frac{4}{15} \frac{c_p MW}{R} + \frac{1}{3} \right] \quad (3.28)$$

While the formulation for mixture viscosity calculation based on Sutherland's Law is given as in Eq. (3.29):

$$\mu_L = \mu_{ref} \left(\frac{T}{T_{ref}} \right)^{\frac{3}{2}} \frac{T_{ref} + T_{eff}}{T + T_{eff}} \quad (3.29)$$

where

μ_{ref} : Mixture reference viscosity at standard pressure and temperature
(STP)

T_{ref} : Reference temperature (273.11 K)

T_{eff} : Effective temperature or Sutherland's constant (110.56 K)

The critical rate of strain, g_{cr} is calculated based on Flohr and Pitsch (2000). The formulation for critical rate of strain calculation is given as in Eq. (3.30):

$$g_{cr} = \frac{S_L^2}{\alpha_L} \quad (3.30)$$

The value of the heat of combustion was taken as 47.3 MJ/kg for isooctane fuel (Heywood, 1988). Moreover, the value of unburned fuel mass fraction is calculated based on the experimental data of air and fuel consumption. Based on the described approach for mixture properties calculation, a set of numerical input to the TFSC model of Zimont have been prepared. Table 3.3 listed the premixed mixture material properties.

Table 3.3: Input for pre-mixed mixture material properties at 2000 rpm

Properties	Value	Units
Specific heat	2040	J/kg.K
Thermal Conductivity	0.08207936	W/m.K
Laminar Viscosity	4.10317×10^{-5}	kg/m.s
Molecular Weight	27.4547	kg/kmol
Laminar Flame Speed	0.4762	m/s
Critical Rate of Strain	18563	s^{-1}
Unburned Fuel Mass Fraction	0.07643	-
Lower Heating Value	4.43×10^7	J/kg

3.8.2 Boundary and Initial Conditions

For the isolated domain, the imposed boundary condition is the wall temperature, which is based on typical wall temperature of spark-ignition gasoline

engine at wide-open throttle operation from (Pulkarabek, 1997). The wall temperatures are different in values depending on different wall region. All the temperature values are set as constant throughout the calculation, which are given in Table 3.4.

The initial conditions are the instantaneous condition of the cylinder gases prior to the timing of ignition. This condition is characterised by the instantaneous volume averaged (i) cylinder pressure, (ii) cylinder temperature, (iii) turbulent kinetic energy, (iv) turbulent dissipation rate, and (v) initial progress variable. For current study, the cylinder pressure and temperature is based on the experimental results. Table 3.5 present the associated initial conditions at 2000 rpm.

Table 3.4: Boundary conditions at 2000 rpm

Variables	Value	Units
Cylinder head Temperature	550	K
Piston face temperature	573	K
Intake region temperature	333	K
Exhaust region temperature	523	K
Cylinder wall temperature	458	K

Table 3.5: Initial conditions at 2000 rpm

Variables	Value	Units
Cylinder pressure	1150684	Pa
Cylinder temperature	605.1476	K
Turbulent kinetic energy	22.836	m^2/s^2
Turbulent dissipation rate	3396.147	m^2/s^3
Progress variable	0	-

The turbulence specification of kinetic energy and dissipation rate is calculated based on the velocity data from Delhaye and Duverger (1998). These data are measured using two-dimensional (two-point) Laser Doppler Velocimetry (LDV) on 4-valve pentroof engine running at 2000 rpm of engine speed at wide-open throttled condition. The engine configuration is comparable to the current engine as well as the measured data.

3.9 Simulated Problems

Based on Lipatnikov et. al. (1998) and Lipatnikov and Chomiak(2003), there are unresolved matters regarding the application of TFSC model for SI engine application. It can be listed as (i) the applicability of the model at high and low turbulence (ii) the model capability of predicting the flame-wall interaction. In addition, the model must able to predict details of the ignition process. Effect of the iteration number per time step has been chosen for detail analysis. The importance of current analysis lies on three most important reasons. (i) Correct procedure and approach of usage of TFSC model of Zimont for turbulent premixed SI engine combustion needed to be established at first before a more fundamental aspect related to the nature of the process is explored; Turbulent combustion modelling is associated with convergence difficulties problem due to the nature of turbulence and chemical reaction which is involved various length and time scales. In fact it is hard to be fully resolve all the scales using existing models and computing power; appropriate number of iteration must be determined for converged or nearly converged solution of SI engine combustion problem using TFSC model of Zimont thus enable the forecast of required calculation time and computing power suitable for such problem. Thus, it have been finalised that this study is concentrate on determining the effect of the number of iteration per time step onto the model's prediction of cylinder pressure data due to the number of iteration per time step will affect the convergence of model's prediction. All the associated convergences criterion and number of iteration for each simulated cases are presented in Table 3.6 and 3.7 respectively.

Table 3.6: Convergence limits for the solved equation

Residuals	Convergence criterion
Continuity	1×10^{-3}
x, y, z velocity	1×10^{-3}
Progress variable	1×10^{-3}
Energy	1×10^{-6}
Turbulence Kinetic Energy, k	1×10^{-3}
Turbulence Dissipation Rate, ε	1×10^{-3}

Table 3.7: Problems setup for the case study

Case study	Iteration/ time step
Case-1	20
Case-2	100
Case-3	500
Case-4	1000
Case-5	1500

3.9.1 Technical Specification of Workstation

The computing capability is affecting the total calculation time. In present study, a number of five personal computers have been used simultaneously to conduct the CFD analysis from the stage of model setup to the calculation process. The information about the machine's hardware specification is vital as it can be used to benchmark the resulted calculation time for this specific problem. Table 3.8 presents the technical specification of all the computers used for the numerical effort.

Table 3.8: Technical specification of computers used for numerical study

Parameter	Size and Feature
Operating System	Genuine Windows XP Professional SP3
Processor	Intel Core 2 Duo E6300 (C) DC 1.86 GHz
CPU FSB	1066 MHz
Standard L2 Cache	12MB shared cache
Chipset	P965
Serial ATA Hard Drives	80GB SATA 3G (3.0 Gb/sec) 7200 rpm (1 unit)
Memory	2GB (1GB x 2) DDR2 SDRAM
Memory Type Supported	DDR2 SDRAM PC2-5300 MB/sec
Memory Speed Supported	667MHz
Maximum Memory	8 GB
Graphics	GeForce 7300LE 64 MB DDR memory
Network Controller	Integrated 10/100 Base-T networking interface

3.10 Summary

This chapter has unveiled the underlying approaches of data collection and numerical model development procedure associated with the study. In the first part of the contents, (i) the engine test-rig for engine testing is presented and (ii) important parameters and associated measurement methods have been described. In the next part of the chapter, the approaches for CFD modelling of turbulent premixed combustion in SI engine are presented. The emphasis are given on (i) the definition of calculation domain and grid generation, (ii) the governing equations for CFD reactive flow problem, (iii) the TFSC model and its descriptions, (iv) required sub-model that idealizes the simulated problem, (v) detail inputs of the simulation and finally (vi) the description of the problems that have been studied. All descriptions include the schematic diagram and photographs of the hydraulic dynamometer engine test-rig, the calibration results of measurement methods, the underlying assumption and limitation of each model and its mathematical expression.

CHAPTER 4

RESULTS AND DISCUSSION

4.1 Introduction

This chapter is separated into two distinctive parts, which are experimental results and numerical results. Experimental test-rig results composed of measured engine torque, ignition timing, fuel-air equivalence ratio, cylinder pressure, mass fraction burned, and finally engine performance parameters. The numerical results composed of grid sensitivity analysis, cylinder pressure and mass fraction burned analysis at different iteration number, visualization of flame propagation and finally the influential factor that governed the overall results.

4.2 Experimental Test-Rig Results

Experiments were carried out at engine speed of 1500 rpm to 4000 rpm with speed interval of 500 rpm. The engine was run at wide-open throttle condition and maximum engine torque. Controlled variable is the throttle opening, independent variable is engine speed while torque and other parameters are set as dependent variables. Important experimental results are fuel-air equivalence ratio, ignition timing, and cylinder pressure as the three parameters are primarily used as input to the numerical engine model and as source of validation. Engine power, mean effective pressure, specific fuel consumption and engine efficiencies are subsequently evaluated for comparison in order to verify the trustworthiness.

4.2.1 Engine Torque

Maximum engine torque is imposed to ensure that the engine is operated at full power at each tested speed. Figure 4.1 presents the measured engine torque in the range of 1500-4000 rpm of engine speed. Typical trend of modern automobile engine produced a maxima curve torque and power against engine speeds in which its maximum engine torque value is achieved at lower engine speed than maximum power. The graph shows that the maximum torques for each engine speed fall in the range of 100-110 Nm. The highest engine torque is achieved at 2500 rpm with the value of 110 Nm.

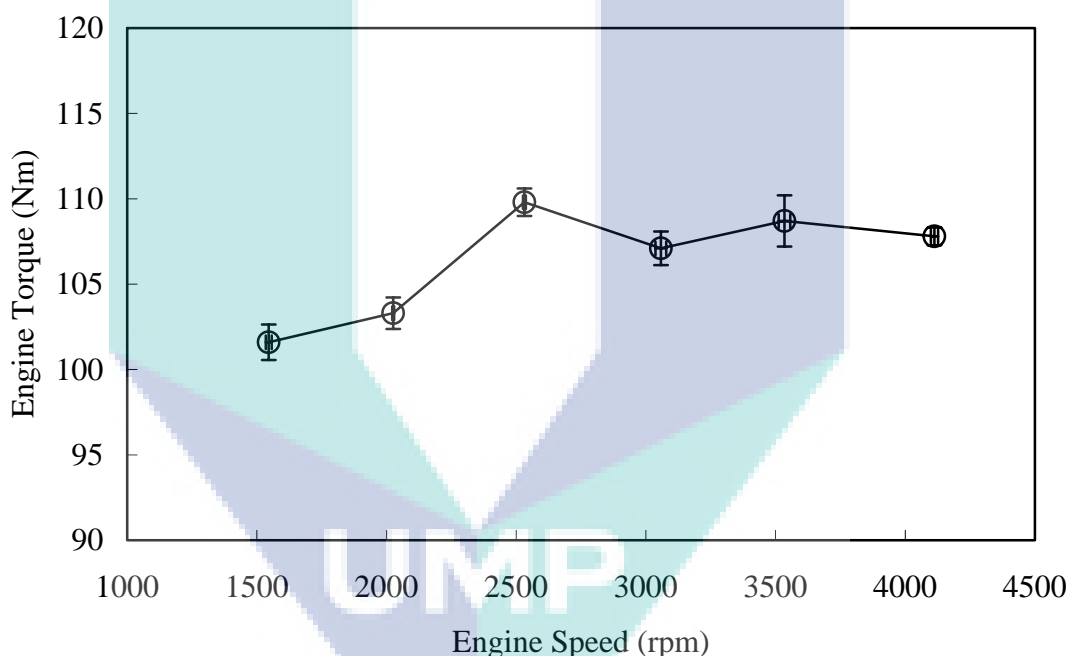


Figure 4.1: Measured engine torque at different engine speed for wide-open throttle condition

At high engine speed, the engine cannot withstand higher dynamometer load thus reduced the engine torque. This is due to the increased friction in engine components as the speed increased and become dominance (Pulkrabek, 1997). More work produced in the engine cylinder is used to overcome the increased friction. The highest engine torque is however smaller and achieved earlier than the rated torque as given by the manufacturer specification which has the value approximately about 126 Nm at 3000 rpm. This deviation is because the large interval of engine speed employed

for the study. Furthermore, the measured engine torque values have been subtracted with the inertia load imposed by the hydraulic dynamometer prior to the loading execution as stated in general testing procedure in Appendix E.

4.2.2 Fuel Air Equivalence Ratio and Ignition Timing

Fuel-air equivalence ratio and the ignition timing are important inputs to the CFD engine model. Both parameters influenced the resultant peak pressure and the timing for peak pressure and consequently engine performances (Heywood, 1988). The equivalence ratio is dependent of load and engine speed. For wide-open throttle condition, the airflow and fuel flow are increase as speed increase and maximize at each speed. Typically, the value of equivalence ratio is slightly rich and maintained at each speed in the range of 1.1-1.2 in order to maintain the highest engine power.

Figure 4.2 presents the measured equivalence ratio of the engine at each engine speed at wide-open throttle condition. According to the graph, the equivalence ratios are almost fall in the rich mixture region. The stoichiometric mixture ratio is corresponding to the equivalence ratio value of 1. Larger value indicates richer mixture and vice versa. Based on Figure 4.2, the leanest point is produced at engine speed of 3000 rpm with nearly stoichiometric equivalence ratio of 1.04 and the richest point is achieved at 3500 rpm with equivalence ratio of 1.28.

In current results, it is obvious that there is significant drop of equivalence ratio of engine speed of 3000 rpm. The trend is confirmed by the results of part open throttle test and results of exhaust gas analysis. The possibility of mechanical failure of carburettor system is small since it affects the overall results at each tested speed. On the other hand, the drop is only occurring at the speed of 3000 rpm only. The strongest reason for the trend is related with the vibration at natural frequency of the engine or the overall test-rig at that speed. This in turn affects the operation of carburettor's mechanical components as well as the fuel and air metering (Lenz, 1992). However, this requires further investigation and additional measurement made on the running engine.

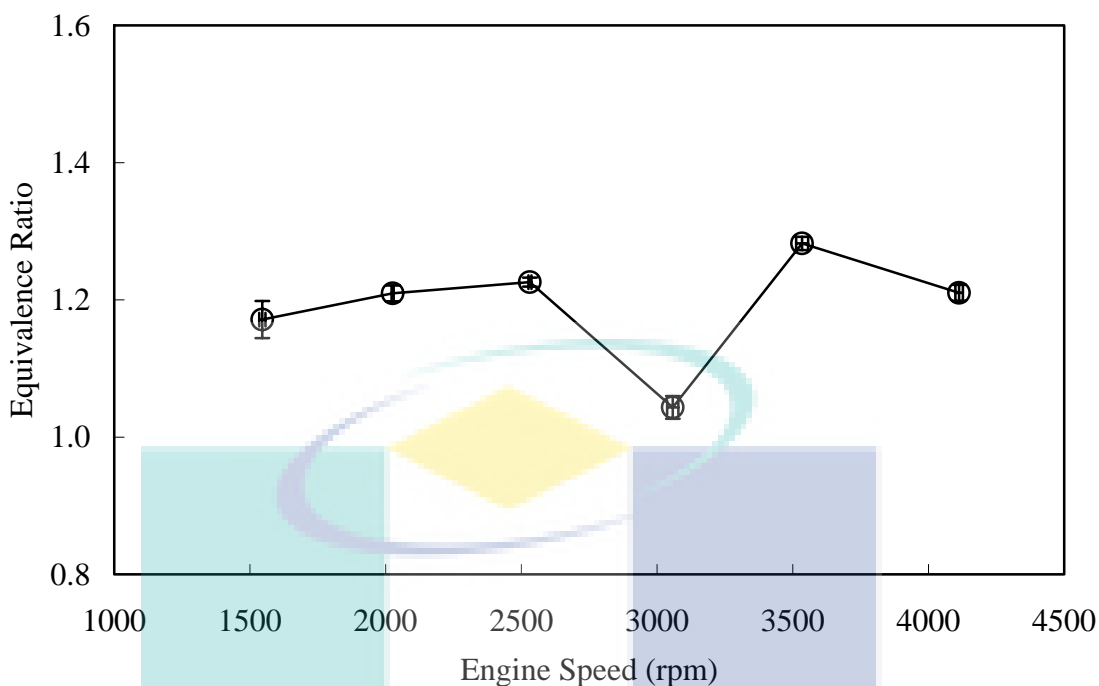


Figure 4.2: Equivalence ratio at different engine speed for wide-open throttle condition

Commonly, early spark timing promote early combustion. Nevertheless too early combustion results with extremely high peak pressure, large work transferred to the piston at the end of compression stroke, and consequently causing knock. If combustion starts too late, it results with extremely low peak pressure, low work transferred to the piston and consequently loss of power (Heywood, 1988). At the condition of wide-open throttle and increased engine speed, the spark is always advanced to maintain the maximum engine power at each tested speed.

Figure 4.3 presents the measured ignition timing at each engine speed. The plotted graph shows that the ignition timing is gradually increased as the speed increase. The measured ignition timing at wide-open throttle operation is varied in the range of 19-25 BTDC. The incremental of spark advance is almost constant except for the speed changes from 1500-2000 rpm where abrupt advanced is occurred. This is significantly due to the combination effect of increased engine speed and load since for the current engine; the advance timing is controlled by the centrifugal advance system and vacuum advance system, which in turn depend solely on the engine speed and load respectively.

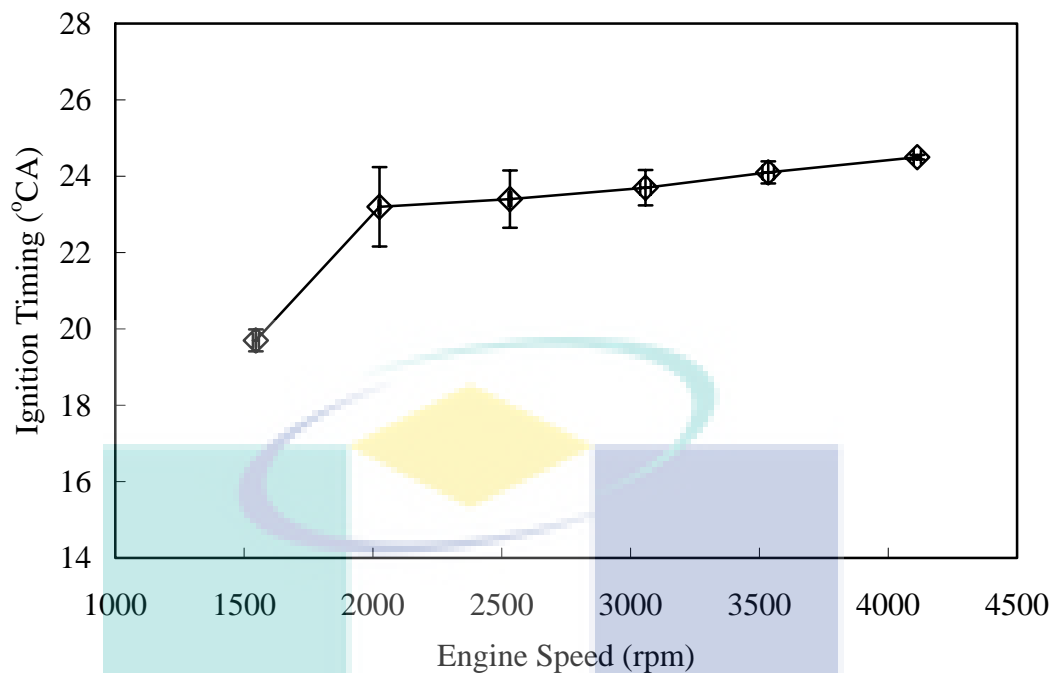


Figure 4.3: Spark ignition timing before top centre at different engine speed for wide-open throttle condition

4.2.3 Cylinder Pressure

Spark ignition engine combustion is evaluated mainly based on cylinder pressure. The cylinder pressure-crank angle diagram is characterized by using (i) cylinder peak pressure and (ii) timing for the peak pressure. In current study, instantaneous cylinder pressure is measured at each engine crank angle for a full 4-stroke cycle from -360° to 360° CA. To abide cycle-to-cycle variation, measured value is averaged over 200 consecutive cycles thus a smooth pressure profile is obtained. In addition, it is more reliable for validation of engine cycle simulation.

In current study, the resultant cylinder pressure is much influence by engine torque, speed, equivalence ratio, and ignition timing since all other engine-operating parameters such as compression ratio and throttle opening are kept constant. Typical trend shows that higher engine speed will results with more advanced ignition; consecutively faster peak pressure timing; and higher peak temperature and pressure. In addition, at higher engine torque will result with wider throttle opening, which

consequently increase air and fuel flow; producing richer mixture. This will also finally results with higher peak temperature and pressure (Heywood, 1988).

Figure 4.4 presents measured cylinder pressure plotted against crank angle degree. The corresponding value of peak pressure and timing of the peak pressure is presented in Table 4.1. Based on the figure and table, the maximum pressure exceeded the value of 57 ~ 66 bar in the range of measurement. The cylinder pressure profile exhibits typical characteristic of a natural aspirated SI engine where exhaust pressure is higher than the intake pressure. At each speed, nearly identical cylinder pressure profile is produced except for the peak pressure and its timing at each speed.

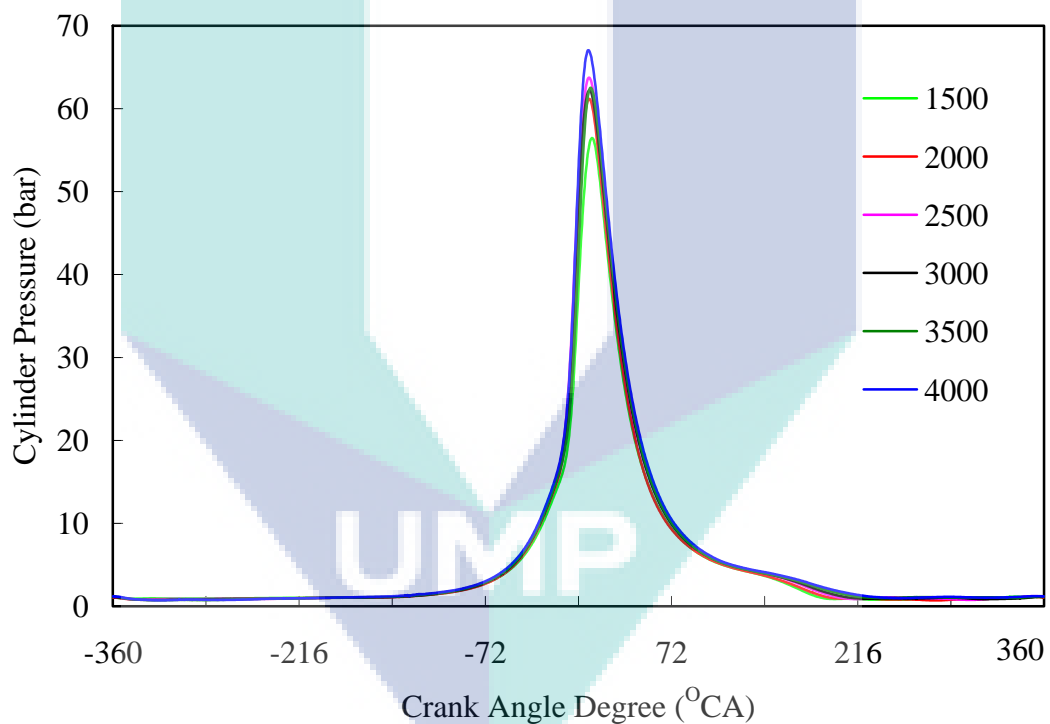


Figure 4.4: Measured cylinder pressure at different engine speed for wide-open throttle condition

Table 4.1: Measured maximum peak pressure and timing of the peak pressure at different engine speed for wide-open throttle condition

Engine speed (rpm)	Peak pressure (bar)	Timing of peak pressure (ATDC)
1500	56.46	10.40
2000	61.19	8.00
2500	63.74	8.00
3000	62.27	8.40
3500	62.54	9.20
4000	67.05	7.60

Principally, to obtain high peak pressure, the timing of peak pressure must occur as close as possible to the TDC point approximately in the range of 5-10° CA after TDC (Pulkrabek, 1997). Currently, all measured timing of peak pressure lies in the desired range, which give the best possible power. The lowest peak pressure is produced at 1500 rpm of engine speed. At 1500 rpm, the equivalence ratio is about 1.17; the ignition timing is about -19.7 °CA and the engine torque is about 101.6 Nm. Slightly leaner equivalence ratio resulted with low energy released. Late ignition timing resulted with late timing of peak pressure. Both factors reduced the cycle peak pressure as well as engine torque.

The highest peak pressure is produced at 4000 rpm of engine speed. At 4000 rpm, the equivalence ratio is about 1.21; the ignition timing is about -23 °CA, and the engine torque is about 107.8 Nm. Richer equivalence ratio produced more energy. The most advanced timing produced the most advanced peak pressure timing. Both factors results with the highest peak pressure. However, the torque is slightly low due to high friction at high engine speed.

4.2.4 Mass Fraction Burned

The mass fraction burned curve is derived based on the cylinder pressure diagram. In current study, this parameter is calculated using combustion analyzer, DEWE-CA 5000. Characterization of combustion process based on mass fraction burned introduced other important parameter such as the flame development angle, θ_d the rapid burning angle, θ_b and the overall burn rate angle, $\theta_d + \theta_b$. All the three

parameters have values that are equal to the number of units crank angle. Figure 4.5 presents the representative of all parameters (Heywood, 1988). These parameters are mostly used for distinguishing different stages of SI engine combustion process.

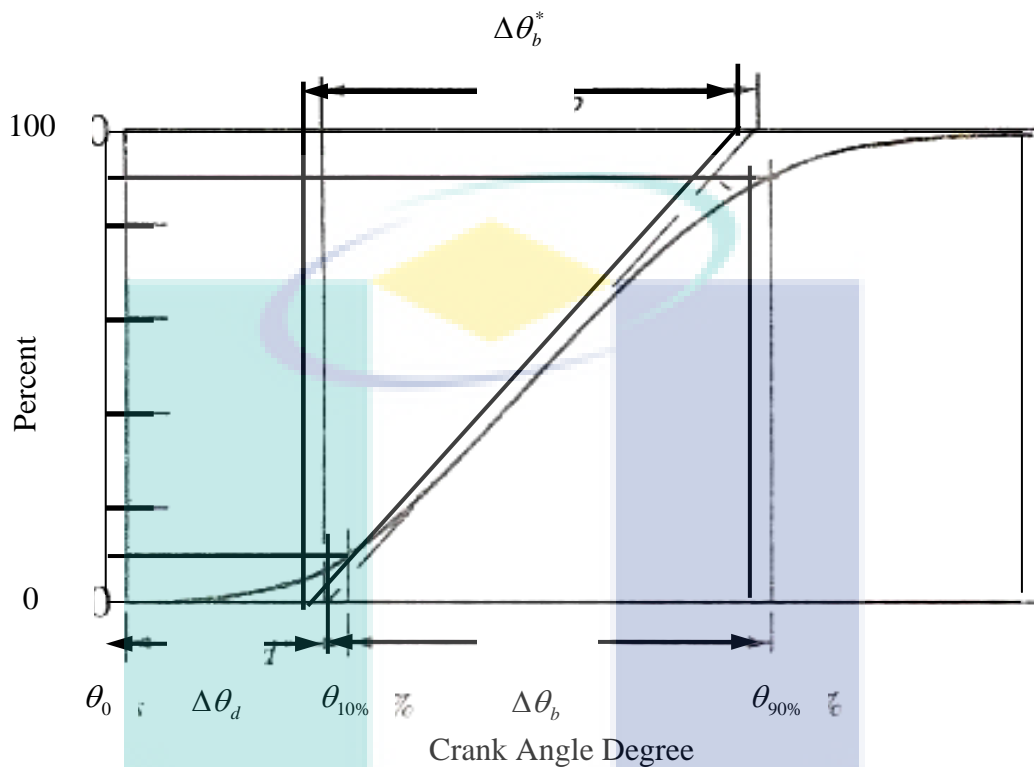


Figure 4.5: Characterization of combustion process based on mass fraction burned curve.

Source: Heywood, (1988)

Figure 4.6 present the mass fraction burned curve at different engine speed for wide-open throttle condition. The value of 0% is corresponding to the unburned mass fraction and value of 100% is corresponding to the value of fully burned mass fractions. In addition, Table 4.2 presents the measured value for the three parameters at different engine speed while Table 4.3 presents the corresponding timing of overall burn rate angle and the actual period of combustion. Generally, if the timing of completion is further advanced, the resultant peak pressure is higher because the instantaneous cylinder volume is smaller near TDC.

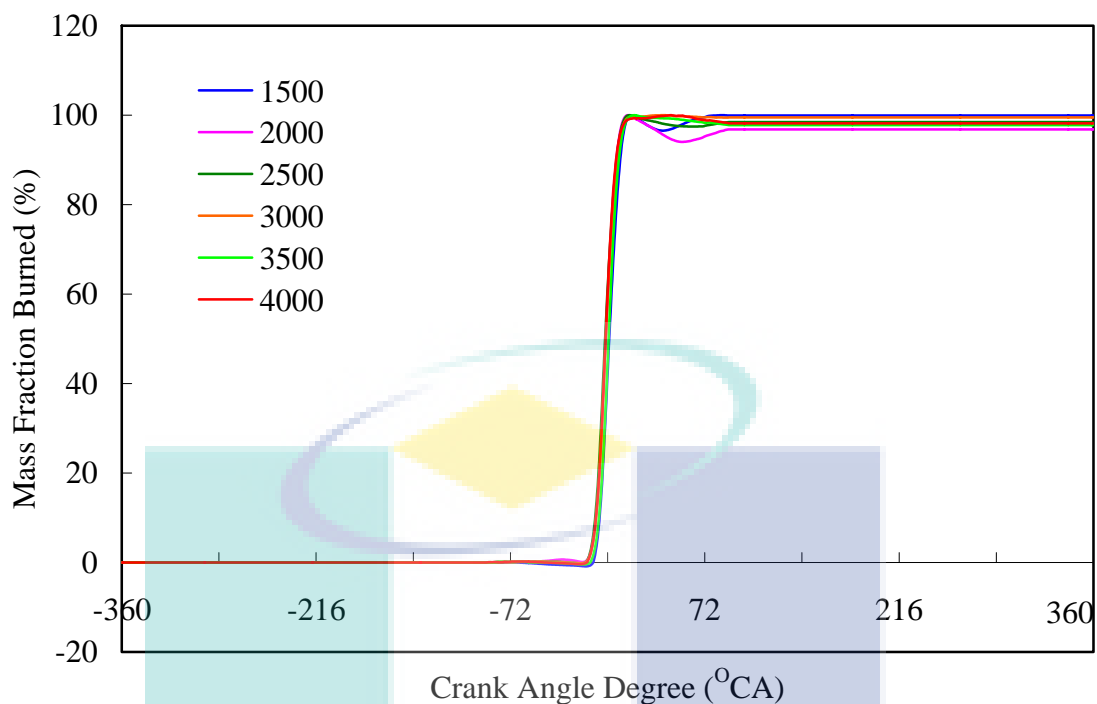


Figure 4.6: Mass fraction burned curve at different engine speed for wide-open throttle condition

Table 4.2: Measured flame development angle, rapid burning angle and overall burn rate angle at different engine speed

Engine speed (rpm)	θ_d	θ_b	$\theta_d + \theta_b$
1500	13.7	16.8	30.5
2000	14.4	16.8	31.2
2500	14.2	17.6	31.8
3000	15.3	18.4	33.7
3500	17.7	16.4	34.1
4000	15.7	17.2	32.9

Based on the plotted graph, the overall combustion process is completed in the period of not more than 35° crank angle. These kinds of processes are associated with rapid burning of cylinder mixture at wide-open throttle condition. This is evidence by large incline of the mass fraction burned at each tested speed. In terms of unit crank angle, the period of combustion is gradually increased as the speed increase from 30.5 °CA to 34.1 °CA because shorter time is available for combustion completion. Thus, combustion is completed in more units of crank angle as the speed increase. This excluded the speed of 4000 rpm where overall burn rate angle is reduced. This data also

suggested that the simulation period could be limited to the period of burning completion only. Nevertheless, the selected simulation period is 50° CA starts from the timing of ignition.

In terms of time scale, as the speed increased, the combustion period is gradually reduced as presented in Table 4.3. Thus, actually faster combustion is happen at higher engine speed even though it is completed in more units of crank angle. Overall results of the measured timing for burning completion are shown that the timing of burning completion has no specific trend. In addition, it cannot be well correlated with the value of peak pressure since the rate of reaction is also influenced by amount of residual gases, instantaneous pressure and temperature and the effect of compression. However, the fastest laminar flame speed recorded for hydrocarbon combustion occurred at equivalence ratio of ~1.1-1.2 (Heywood, 1994).

Table 4.3: Timing of overall burn rate angle and actual combustion period at different engine speed

Engine speed (rpm)	Timing for $\theta_d + \theta_b$ (ATDC)	Burning period (msec)
1500	11.2	3.38
2000	8.4	2.60
2500	8.8	2.12
3000	9.2	1.87
3500	10.4	1.62
4000	8.8	1.37

The timing of burning completion is found to be slightly late than the timing for peak pressure. Maximum difference is about 1.2 °CA for engine speed of 3500 and 4000 rpm. This is reasonable since the timing of burning completion is associated with the timing of equal or more than 95% cylinder mass burned. Additionally, it is noticeable that at an engine speed of 2000 rpm, there is slightly a drop of the mass fraction burned after the timing of peak pressure and overall burn rate angle are achieved. The noticeable drop is actually due to the inconsistency of pressure reduction after the peak value is achieved. The reduction inconsistency is due to the additional heat release late after TDC. This might be cause by the burning of end gases inside cylinder.

4.2.5 Engine Performance Parameters

In order to evaluate the trustworthiness of the measured results, the results must be compared in terms of more general and convenient parameters. These are enabled by deriving values for (i) engine power (ii) mean effective pressure (MEP) (iii) specific fuel consumption and (iv) engine efficiencies. This parameter is part of the parameters used for engine comparison (Heywood, 1988). Moreover, for current study, these parameters are compared against typical engine data for SI engine. Figure 4.7 presents the engine indicated and brake power at different engine speed for wide-open throttle condition.

Based on Figure 4.7, both indicated and brake power produced lies in the range of 16 kW at 1500 rpm to 52 kW at 4000 rpm. For the current baseline engine, the manufacturer specification gives the maximum brake power at engine speed of 6000 rpm with approximate value 66 kW. The manufacturer's value is unachievable because measurement is made up to 4000 rpm only. However, the current result of maximum brake power shows a comparable result of Kalam et al.(2005). They have measured about 42 kW brake power at engine speed of 4000 rpm while current measurement gives 40.67 kW. For engine power, both the indicated and brake quantity have shown a small discrepancy between others at low engine speed. As the speed is further increased, the differences between both quantities are larger as the friction is increased at higher speed.

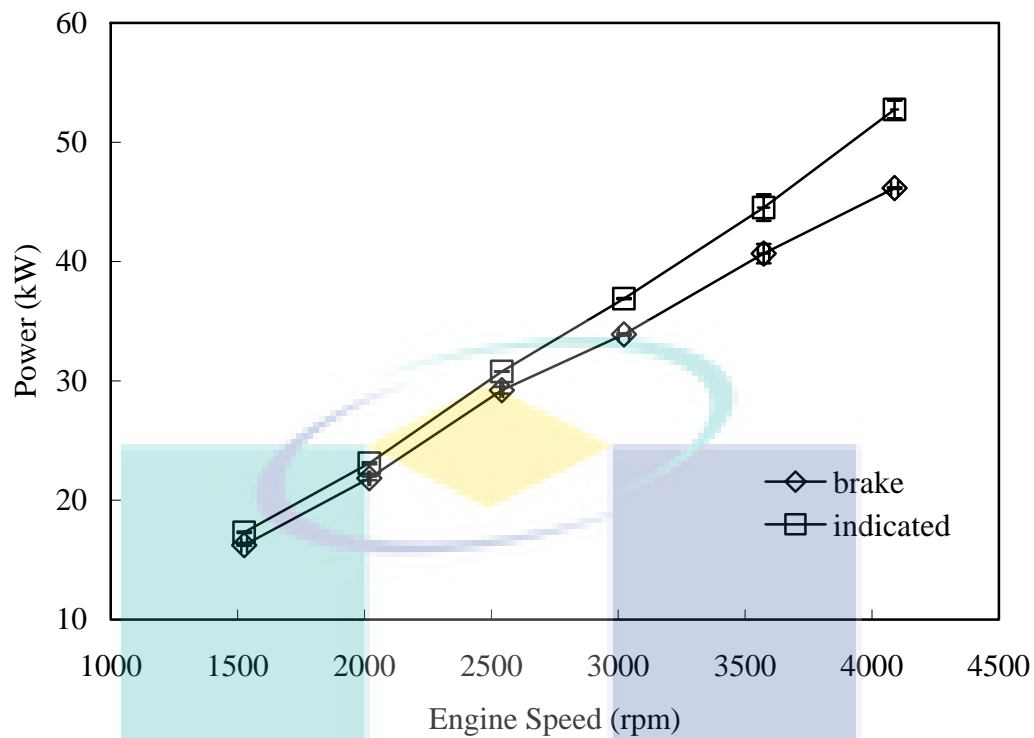


Figure 4.7: Indicated and brake power at different engine speed for wide-open throttle condition

Figure 4.8 presents the indicated and brake mean effective pressure at different engine speeds for wide-open throttle condition. Both the calculated indicated and brake mean effective pressure give values in the range of 870 kPa at 1500 rpm and 1010 kPa at 4000 rpm. Based on Heywood (1988), the typical values of BMEP for a natural aspirated medium size spark-ignition gasoline engine are in the range of 850 to 1050 kPa. Thus, these results are considered as acceptable for SI engine. For MEP, both the indicated and brake quantity have shown a small discrepancy between others at low engine speed. As the speed is further increased, the differences between both quantities are larger as the friction mean effective pressure (FMEP) is increased at higher speed.

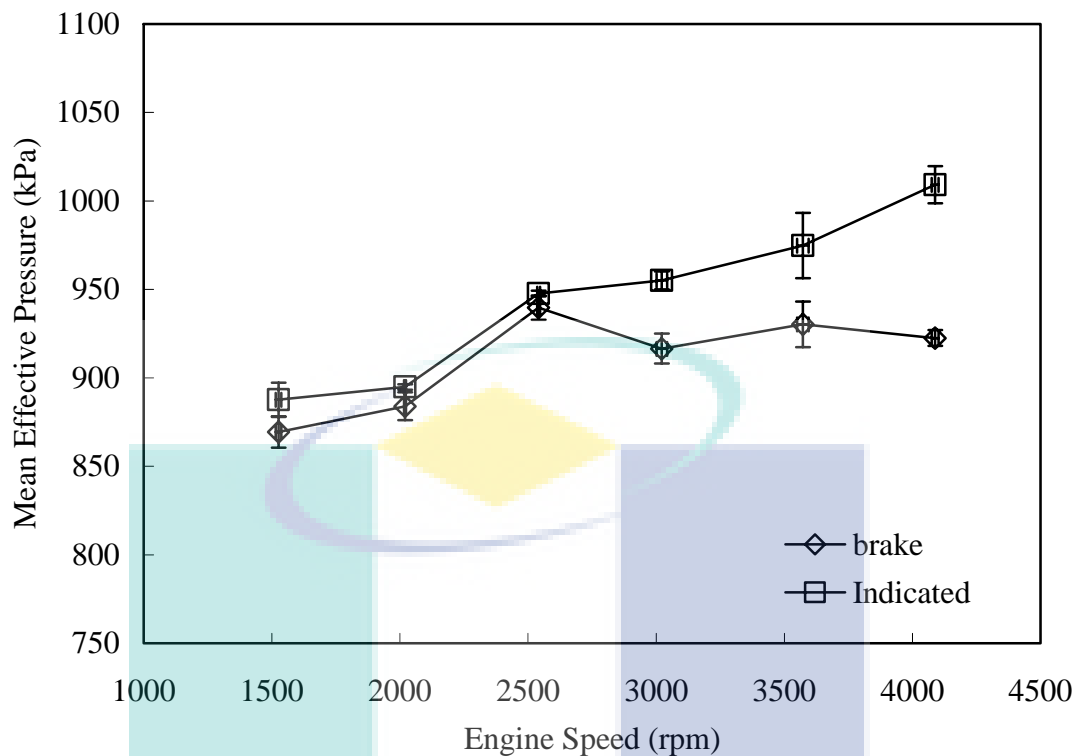


Figure 4.8: Indicated and brake mean effective pressure at different engine speed for wide-open throttle condition

Figure 4.9 presents the indicated and brake specific fuel consumption (BSFC) at different engine speed for wide-open throttle condition. The graph shows that the BSFC is varying in the range of 200 to 400 g/kW.h. The graph shows a minimal trend which agreed with typical plot of BSFC of conventional engine. Overall, the most optimum fuel utilisation is achieved at 3000 rpm of engine speed with the value of BSFC about 249.88 and 272 g/kW.h for the indicated and brake quantity respectively. The lowest BSFC point is coincide with the leanest equivalence point. However, these points are departing from the highest torque point by speed interval of 500 rpm. In actual practice, the optimum points of the three parameters are occurred at a nearly coincident speed. The departing is mostly due to the large interval of engine speed used for the measurement. By selecting a smaller interval of measurement point, exact results can be obtained and a finer curve is possible. Nevertheless, such an intensive measurement is beyond the purpose of current study.

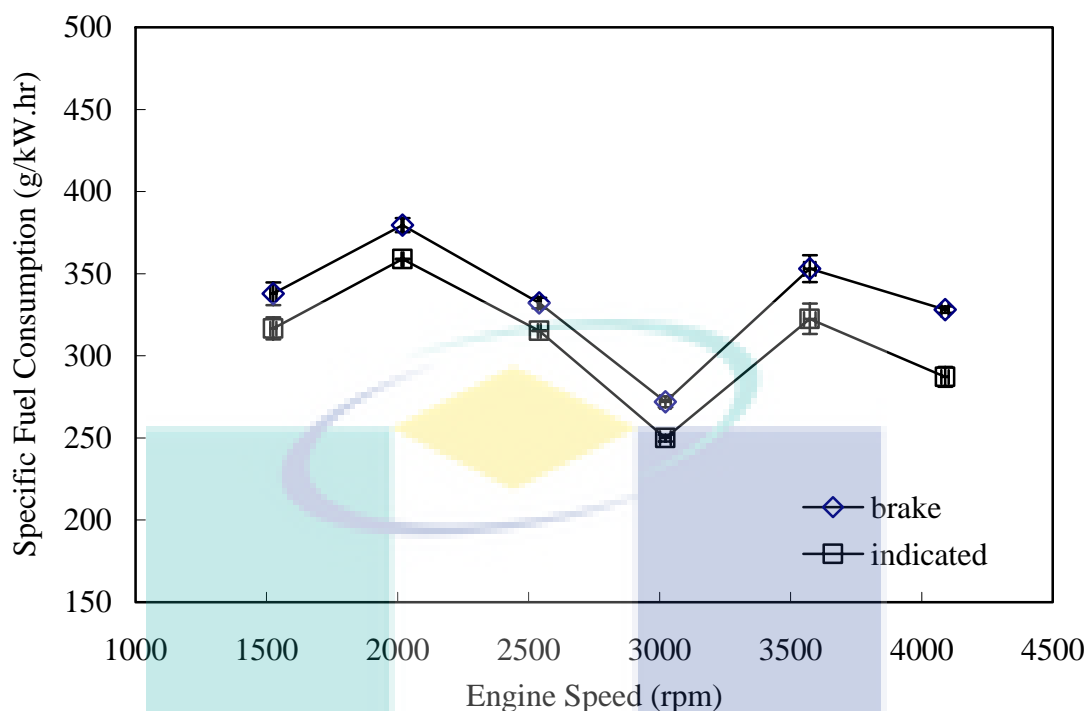


Figure 4.9: Indicated and brake specific fuel consumption at different engine speed for wide-open throttle condition

Figure 4.10 presents the measured mechanical efficiency at different engine speed for wide-open throttle condition. The measured mechanical efficiency values fall in the range of 91% to 98%. These values are still in typical range for natural aspirated SI engine where the value is about 90% at low speed and reduced to about 70% at high speed (Heywood, 1988). The graph shows that the efficiency value is reduced at higher engine speed due to the increase in mechanical friction. The value of the peak mechanical efficiency is about 98% at 2500 rpm. This point coincides with the highest torque point. It is expected that the mechanical efficiency will be further decreased at higher engine speed, approximating the value of 70%. However, current measurement is limited to the speed of 4000 rpm only, thus giving a moderate reduction of the efficiency.

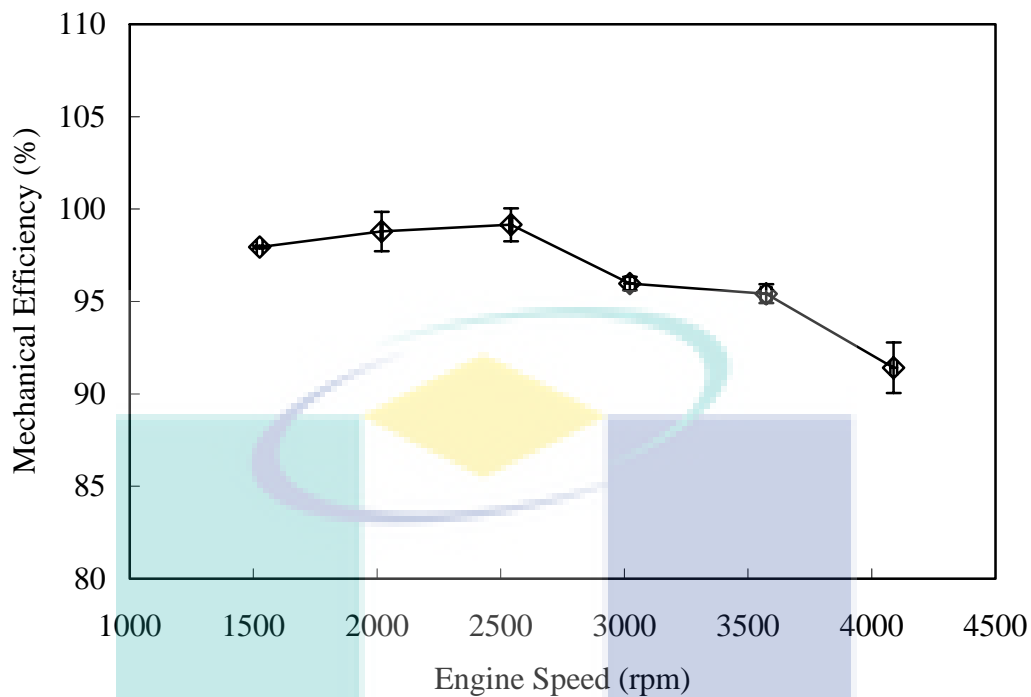


Figure 4.10: Mechanical efficiency at different engine speed for wide-open throttle condition.

Figure 4.11 presents the brake thermal efficiency (BTE) at different engine speed for wide-open throttle engine condition. The typical value of BTE for natural aspirated SI engine is in the range of 20 % to 35 % (Heywood, 1988) and shows a maxima trend. Based on Figure 4.11, the overall value of measured BTE falls in the range of 21.4% to 29.8 % thus gives a good agreement with the typical range. The highest BTE point is achieved at the leanest equivalence ratio and the lowest SFC point at 3000 rpm with the value of 29.8%.

Based on the overall results presented previously from Section 4.21 to 4.25, the optimum operating point of the engine at wide-open throttle condition is expected to occur in the range of engine speed 2500 to 3000 rpm. This is supported by the results of the highest engine torque, the leanest equivalence ratio, the lowest SFC and the highest BTE. However, the determination of the actual point is rather crucial and beyond the purpose of current study. With all presented results, it is found that the experimental engine data are sufficient to support the numerical study of turbulent premixed SI engine combustion. The presented results are essentially selected based on their

importance for the numerical study and not covering the whole data associated with the experimental test-rig measurement.

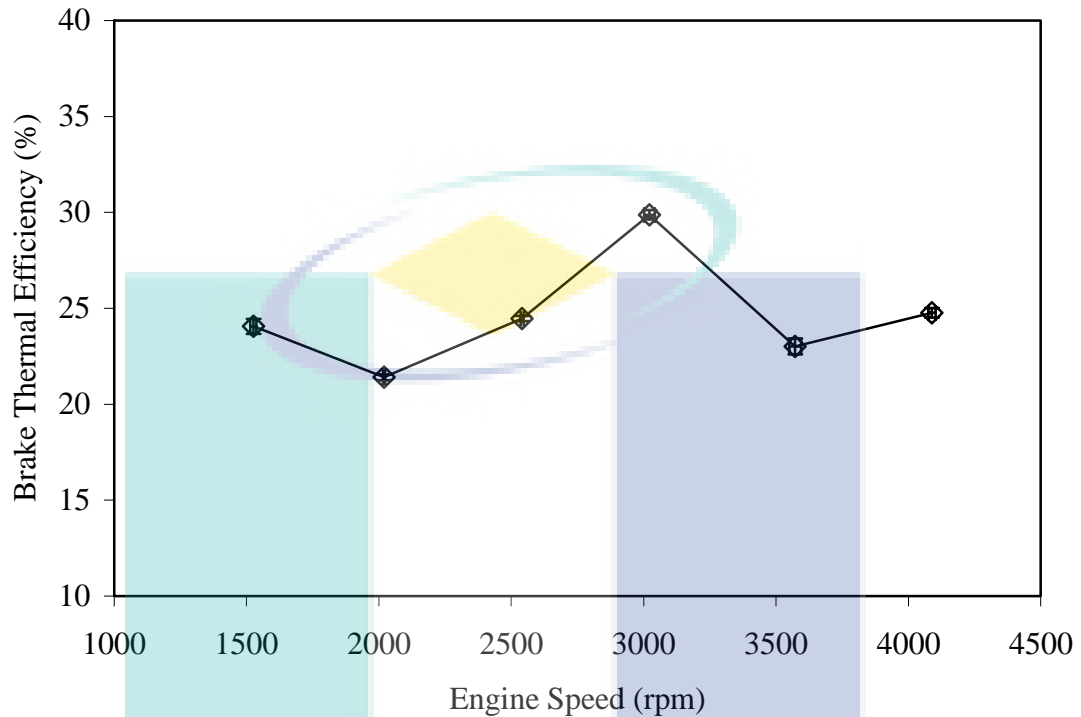


Figure 4.11: Brake thermal efficiency at different engine speed for wide-open throttle condition

4.3 Numerical Combustion Results

In the subsequent presentation, the numerical results are presented. The numerical results presented hereafter consist of the grid sensitivity analysis, the effect of iteration number study and its effect on cylinder pressure, mass fraction burned and flame visualization and finally influential factors and their effects on the numerical results.

4.3.1 Grid Sensitivity Analysis

The grid sensitivity analysis is carried out to eliminate the effect of grid dependency on the model's prediction. This procedure is carried out by reduced the grid element size. In present study, the grid element size is reduced from 0.3 to 0.1 cm. These values are corresponding to the increment of element density from 307.12

elements/ cm³ to 5840.77 elements/ cm³ respectively. Table 4.4 presents all the tested grid element sizes and their corresponding mesh element density per unit volume. The largest mesh size of 0.3 cm is restricted due to the existence of small clearance volume in the region between the valve faces and valve seats. While the smallest mesh size of 0.1 cm is limited by the available computing capability. The analysis is evaluated by comparing the calculated cylinder pressure for different mesh size at TDC.

Table 4.4: Grid element size and corresponding element density

Grid element size (cm)	Element Density (element/cm ³)
0.30	307.12
0.25	473.67
0.20	912.48
0.15	1752.47
0.125	3284.40
0.10	5840.77

Figure 4.12 presents the results of the effect of the mesh density on the calculated cylinder pressure at TDC. As the mesh element density is increased from 307.12 element/cm³ to 5840.77 element/cm³, the model prediction of cylinder pressure have reduced from the initial value of 18.22 bars to 16.61 bars. This gives maximum reduction of 8.84% from the initial prediction. The model with the finest mesh of 0.1 cm, which correspond to 5840.77 element/cm³ of element density predicted a nearly stabilized result and subsequently selected as the baseline mesh size for the reactive flow model.

The grid sensitivity analysis presented in this section has been carried out by simulated the engine firing condition at 2000 rpm with appropriate engine operating inputs from the measured data. The number of iteration per time step was set as 20 times and one time step is equal to one unit of crank angle degree. Thus, the predicted cylinder pressure of the selected baseline case is associated with non-converged solution because the number of iteration is insufficient. However, the overall results have provided a measurable means for the purpose of grid sensitivity study. Details evaluation of baseline model prediction is presented in section 4.3.2.

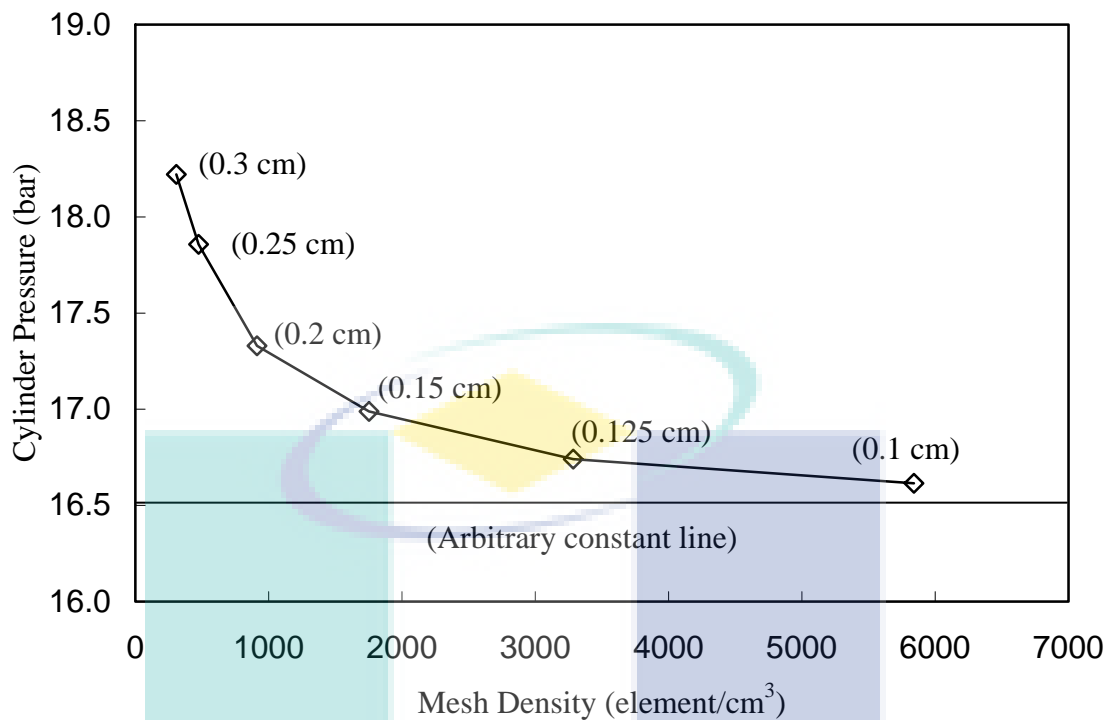


Figure 4.12: Effect of mesh density on simulated cylinder pressure at top dead centre

4.3.2 Preliminary Result of the Baseline Model

Figure 4.13 presents the comparison of experimental and numerical results of cylinder pressure of the baseline model. The result of cylinder pressure shows an increase in discrepancy between the experimental and numerical prediction as the combustion is initiated. The maximum value of deviation is produced at about 12 °CA after TDC with 74.51% of deviation. The peak pressure timing for calculated result is earlier than the measured peak pressure and occurred exactly at TDC. This indicates the predicted peak pressure is achieved due to the compression effect and not by the burning completion. Figure 4.14 presents the comparison between experimental and numerical results of mass fraction burned for the baseline model. The comparison further described the large discrepancy found previously in cylinder pressure plot. The burned mixture is never surpassed completion since at the end of simulation period, only 3.97% of the mixture is burned. As the fraction of the mixture burned is very small, excessively small amount of heat is released and consequently caused very low-

pressure raised. Based on the figure, the maximum deviation is produced at 6 °CA after TDC with 97.58% deviation.

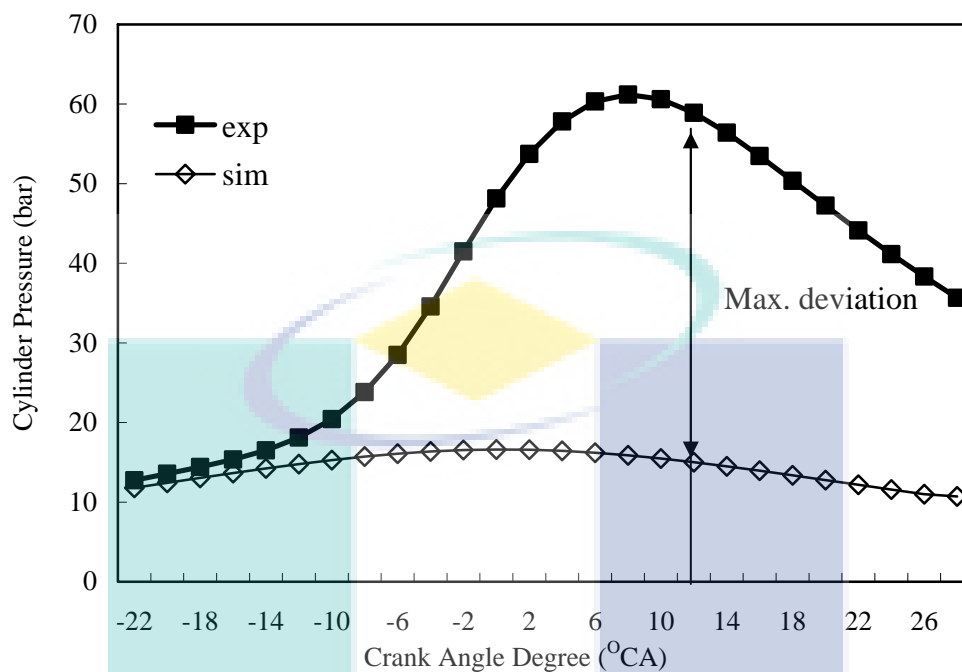


Figure 4.13: Comparison between measured and simulated cylinder pressure for the baseline model

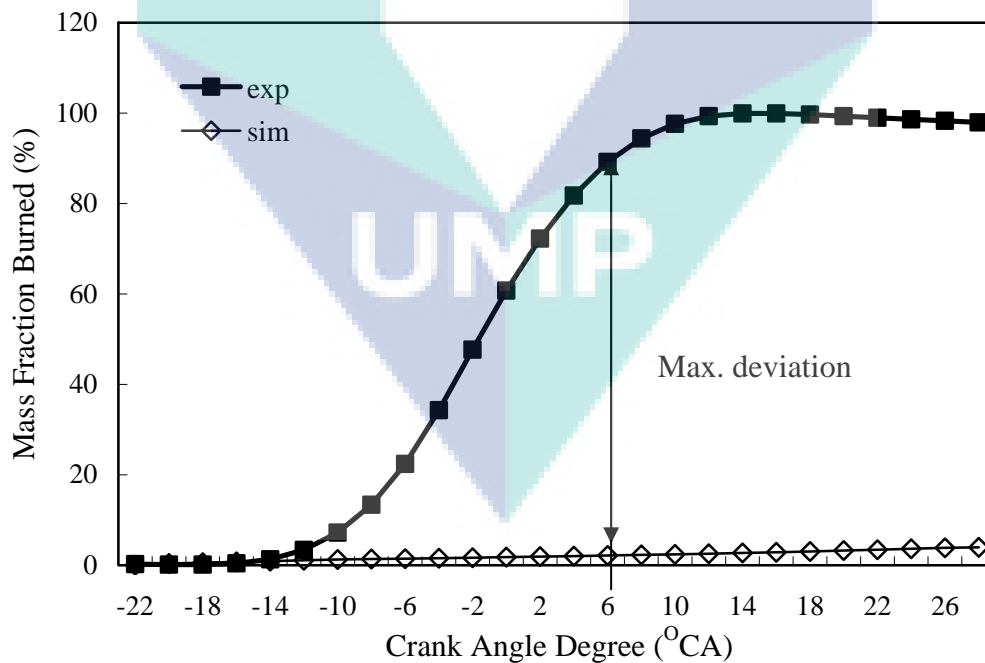


Figure 4.14: Comparison between measured and simulated mass fraction burned for the baseline model

The simulated value of turbulent flame speed has an average value of 9.089 m/s. Comparison of turbulent flame speed with a measured data from Matthews et al. (1996) shows that the turbulent flame speed prediction is reasonable where the measured values lies in the range of 2 m/s – 8 m/s. Thus, the rate of reaction is not considered as the major source of discrepancies. Turbulence flow with chemical reaction requires huge number of iterations to achieve convergences and the engine combustion process are considered as the most complex CFD problem (Gosman, 1999). Thus, the correct solution of the turbulence premixed SI engine combustion problem such in current study is greatly influence by the convergence as well as the number of iteration. Additionally, the effect of iteration number per time step is become crucial and significance as transient analysis is carried out.

4.3.3 Effect of Iteration Number Study

Simulation results explain the effect of iteration number per time step onto turbulent premixed SI engine combustion modelling using TFSC model of Zimont. The results consist of the validation, and analysis of simulated cylinder pressure, simulated mass fraction burned and flame propagation. Subsequently, appropriate factors that influence the discrepancies are given. The simulated cases are the baseline case or case 1, case 2, case 3, case 4 and case 5. These cases are corresponding to the number of iteration of 20, 100, 500, 1000 and 1500 respectively.

The maximum iteration number is limited to 1500 times per times step because the simulated cylinder pressure and mass fraction burned which are discussed afterwards have over predicted the measured results especially during the flame development stages. Total computing time is increased proportionally as the number of iteration per time step is increased. Table 4.5 presents the total calculation times for each simulated cases. These results are vital for the benchmarking of current computing capability and the resulted computing time.

Table 4.5: Effect of iteration number per time step on total computing time

Case Number	Number of iteration	Total computing time
Case 1	20	5 hours 6 min
Case 2	100	23 hours 45 min
Case 3	500	114 hours 44 min
Case 4	1000	192 hours 07 min
Case 5	1500	315 hours 44 min

Cylinder Pressure

The numerical results of turbulent premixed SI engine combustion modelling have been validated primarily based on cylinder pressure. Figure 4.15 presents the comparison of measured and simulated cylinder pressure for five different cases. The results of the cylinder pressure have been plotted from the start of combustion at -22°CA before TDC until a sufficient period for burning completion at 28°CA after TDC. Total simulation period is about 50 units crank angle. Further analyses have been carried out on measured and simulated cylinder pressure. The value of peak pressure and peak pressure timing are subtracted from Figure 4. 15 for cases 1 to 5. Tables 4.6 and 4.7 present peak pressure and peak pressure timing for each different case of 1 to 5 respectively.

Based on Figure 4.15, the experimental results of cylinder pressure at 2000 rpm shows a typical profile of cylinder pressure founded in SI engine. From -22°CA to -12°CA , there was only small raised of cylinder pressure corresponded to the burning of small fraction of cylinder mixture. This is associated with the flame development stage. From -12°CA to 6°CA , the cylinder pressure raised rapidly and achieved peak pressure value of 61.19 bar. The timing of peak pressure is about 8°CA ATDC. The high rate of pressure raised in this period is corresponded to the rapid burning of cylinder mixture. This is associated with turbulent propagating flame stage. As the peak cylinder pressure is achieved, the burning of overall cylinder mixture is nearly completed. The period after the burning completion is called the flame termination period where the flame front has reached and interacted with the cylinder wall.

From Figure 4.15, case 1 and case 2 are extremely under predicted cylinder pressure profile compared to the experimental result. There are no significant peak pressure have been achieved in both cases. The excessively low peak pressures demonstrated in both cases are resulted from the piston compression and are not because burning completion. The under predicted results in case 1 and case 2 are actually associated with inaccurate solution of instantaneous mass fraction burned value due to the number of iteration per time step are only 20 and 100 for case 1 and 2 respectively. The values of instantaneous mass fraction burned have been under predicted.

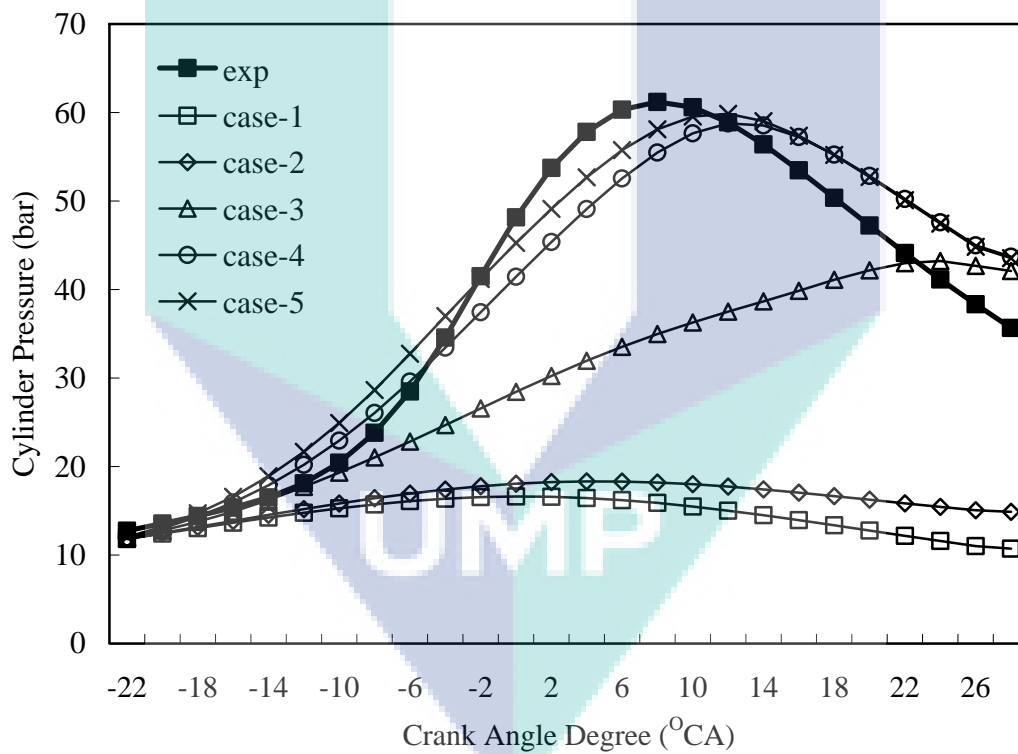


Figure 4.15: Comparison of measured and simulated cylinder pressure for each simulated cases

Table 4.6: Peak pressure predicted for cases 1 to 5

Case Number	Peak Pressure (bar)	Deviation from exp (%)
Exp.	61.19 bar	0 %
Case 1	16.62 bar	72.80 %
Case 2	18.32 bar	70.10 %
Case 3	43.23 bar	29.35%
Case 4	58.76 bar	3.97 %
Case 5	59.85 bar	2.19 %

Table 4.7: Peak pressure timing predicted for cases 1 to 5

Case Number	Timing ($^{\circ}$ CA ATDC)	Deviation from exp (%)
Exp.	8	0
Case 1	0	100%
Case 2	4	50 %
Case 3	24	200 %
Case 4	12	50 %
Case 5	10	25 %

Based on Tables 4.6 and 4.7, in case 1 and case 2, the peak pressure value is about 16.62 bar and 18.32 bar. These give deviations as much as 72.8% and 70.1% for both cases. The large deviations are shown to be unreasonable for a normal combustion process. On the other hand, the peak pressure timing for the case 1 and 2 are 0° CA and 4° CA respectively. These give about 100% and 50% deviation from measured value. However, the peak pressure timing is earlier than the measured value. This describes the invalidity of the peak pressure timing where it produced due to compression effect. Additionally, in actual condition the optimum peak-pressure timing for full power operation should lies in the range of $5-10^{\circ}$ CA after TDC.

In case 3, simulated combustion process is remained under predicted the cylinder pressure at each time steps. This mean that the TFSC model is still under predicted the instantaneous mass fraction burned value. Nevertheless, a significant peak pressure is still achieved late in the simulated combustion period as the number of iteration is increased to 500 times. However, the peak pressure value is quite low compared to the experimental results. The low peak pressure value is due to the late peak pressure timing. The burning completion must be completed as close as possible

to the TDC in order to obtain a high-pressure combustion. However, it was obvious that the case 3 have predict the closest cylinder pressure with the experimental results in the range of -22°CA to -12°CA . Thus, it is found that the cylinder pressure profile of case 3 has best fit the measured result in the flame development period.

The peak pressure for case 3 is about 43.23 bar which gives about 29.35% deviation from experimental results. While the peak pressure timing is about 24°CA after TDC. This gives a deviation of 200% compared to experimental results. At 24°CA after TDC, the cylinder volume has expanded as much as 46.14% compared to clearance volume. This proved that the late burning completion would result with late peak pressure timing and consequently low peak pressure value. Even though case 3 has a larger deviation of peak pressure timing compared to case 1 and 2, the timing is valid because it is produced due to burning completion. However, the timing is strictly not obtained in the optimum range thus causing power loss.

Finer predictions are obtained by case 4 and case 5. Reasonable cylinder pressure profiles of both cases are produced even though they cannot exactly fit the measured cylinder pressure profile. The peak pressure value and the peak pressure timing are closest to the measured value in both cases. As demonstrated in cases 4 and 5, the number of iteration per time steps in increased up to 1000 and 1500 times per time step; this has lead to a better prediction of instantaneous mass fraction burned and consequently improved cylinder pressure profiles. These results also show that a reasonable prediction can only be obtained when the iteration number is increased greater than 1000 iterations.

For case 4 and 5, the peak pressure value are 58.76 bar and 59.85 bar respectively. These give deviation of 3.97% and 2.19% compared to measured values. On the other hand, the peak pressure timing for both cases are 12°CA and 10°CA after TDC respectively. These give about 50% and 25% respectively. Even though both cases give a nearly similar cylinder pressure profile, case 5 predicts higher cylinder pressure compared to case 4. It is visible especially in the turbulent propagation flame period due to the higher iteration number for the case. In addition, only case 5 gives the peak pressure timing which lies in the optimum range. Furthermore, it gives the smallest

deviation of peak pressure and peak pressure timing of all cases. Thus, case 5 gives the best prediction of overall simulated cases.

The results of cylinder pressure for case 1 to 5 presented previously are strongly affected by the prediction of instantaneous mass fraction burned. The mass fraction burned represents the cumulative amount of burned mass fraction of cylinder mixture. This is true because as the cylinder mixture is burned, the process released amounts of heat or thermal energy. This heat will increase the cylinder temperature instantly. An increased in temperature will resulted with increased cylinder pressure. Thus, the overall process is a heat-driven process. In the circumstances of TFSC modelling, correct prediction of the mass fraction burned value is vital in order to obtain reasonable result of cylinder pressure.

Based on the finest prediction of case 5, current modelling approaches using TFSC model demonstrated one major drawback. The only left drawback is associated with the fitting of actual cylinder pressure profile. In the range of -22° CA to -12° CA, measured result has shown a slow rise of cylinder pressure within the stage. However, simulated result of case 5 is over predicted the rate pressure of pressure rise in that period. The case demonstrated an immediate increased of pressure as the spark ignited the mixture.

Current approaches also cannot exactly predict the turbulent flame propagation stage in the period of -12° CA to 6° CA. The rate of pressure rise in the case is lower than measured cylinder pressure. This is evidenced by a more sharper increased of cylinder pressure founded in measured results. Finally, current approaches cannot predict the flame termination periods, which occur after the burning completion in the range of 6° CA to 28° CA. Neither case 4 nor case 5 has predicted a correct value where both cases have over predicted the cylinder pressure. The rate of reduction of the simulated cylinder pressure is slower than the measured result. This is related with improper wall's thermal boundary employed for the study. In actual condition, the wall's temperature as well as the heat flux is highly fluctuate where as constant values are used in current study. This drawback is also related to the known disadvantage of

the model since it did not consider the flame termination stage or the flame-wall interaction process explicitly in the model equation.

The fitting problem presented previously is associated with the prediction of instantaneous mass fraction burned. Thus, in order for exactly fit the measured cylinder pressure profile, the simulated models at first must approximate exact values of the instantaneous mass fraction burned at each time steps. In TFSC model formulation, prediction of the instantaneous mass fraction burned value is governed by the conservation equation of the progress variable. Hence, the model assumed that the instantaneous mass fraction burned is equivalent to the instantaneous progress variable value. Next, results of the mass fraction burned are discussed in details.

Mass Fraction Burned and Flame Propagation

In order to understand the variation of cylinder pressure, the results of mass fraction burned has been study. The mass fraction burned value is equivalent to the instantaneous progress variable, calculated by TFSC model. Figure 4.16 presents the comparison of measured and simulated mass fraction burned for five different cases. The results of mass fraction burned have been plotted from the start of combustion at -22° CA BTDC until a sufficient period for burning completion at 28° CA ATDC. Total simulated period is 50 units crank angle degree. Further analyses have been carried out on mass fraction burned results. The value of flame development angle, θ_d the rapid burning angle, θ_b and the overall burn rate angle, $\theta_d + \theta_b$. have been subtracted from Figure 4.16 for case 1 to 5. All the values are presented by Tables 4.8 and 4.9.

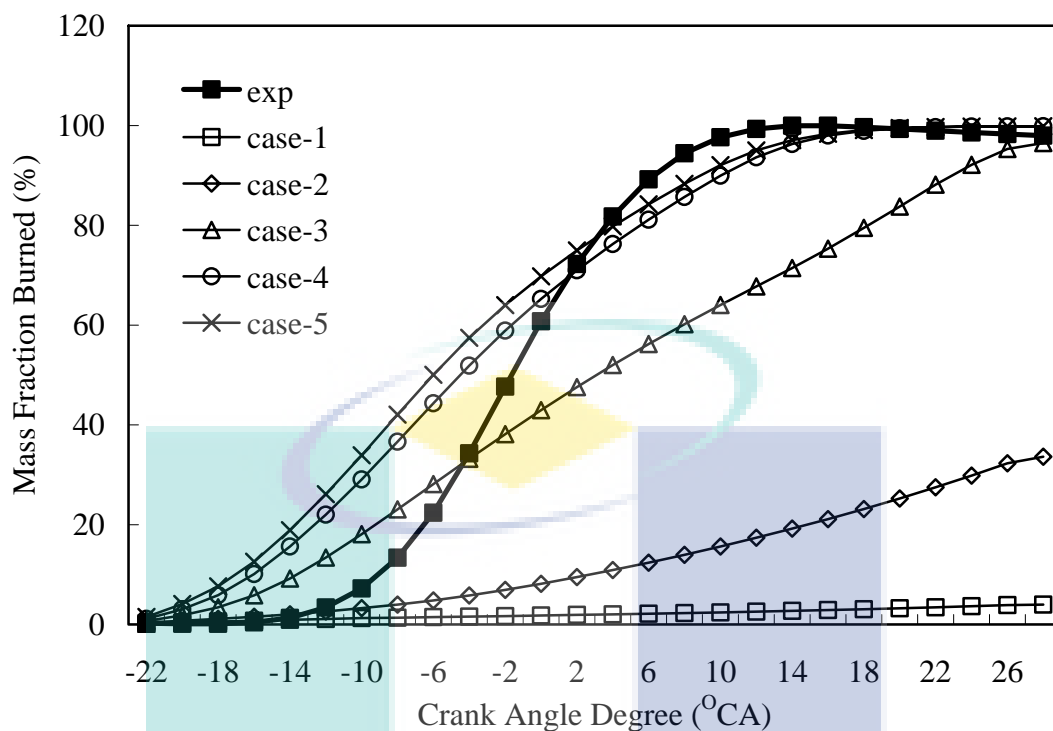


Figure 4.16: Comparison of the measured and simulated mass fraction burned for each simulated cases

Table 4.8: Burn rate angle predicted for cases 1 to 5

Case Number	θ_a (CA)	θ_b (CA)	$\theta_a + \theta_b$ (CA)	Deviation from exp (%)
Exp.	14.4	16.8	31.2	0
Case 1	nil	nil	nil	nil
Case 2	27	nil	nil	nil
Case 3	8	40	48	53.85 %
Case 4	6	30	36	15.38 %
Case 5	6	28	34	8.97 %

Table 4.9: Timing of overall burn-rate angle predicted for cases 1 to 5

Case Number	Timing (°CA ATDC)	Deviation from exp (%)
Exp.	10	0
Case 1	nil	nil
Case 2	nil	nil
Case 3	26	160 %
Case 4	14	40 %
Case 5	12	20 %

Based on Figure 4.16, the experimental result of mass fraction burned at 2000 rpm shows a typical profile of mass fraction burned found in conventional SI engine. In the range of 22° CA to -12° CA, a very small fraction of cylinder mixture is burned causing a very low heat release and consequently small rise of cylinder pressure. This is associated with the flame development stage. This gives a flame development angle, θ_d equal to 14.4 units crank angle. In the range of -12° CA to 6° CA, the rate of mixture consumption is high thus gives a large amount of mass fraction burned and heat release. As result, the cylinder pressure is highly raised. This period is associated with the turbulent propagating flame. The associated rapid burning angle, θ_b equal to 16.8 units crank angle. Finally, both parameters give an overall burn rate angle, $(\theta_d + \theta_b)$ equal to 31.2 units crank angle.

The profile of the simulated mass fraction burned for case 1 to 5 demonstrated the effect of iteration number on the TFSC model prediction. For case 1 and 2, the simulated profile of the mass fraction burned curve clearly exhibit a different trend compared to the measured results. The profiles show gradual increase from the start of ignition until the end of simulation period. There are no significant points of burning completion. At the end of the simulation period at 28° CA after TDC, only 3.97% and 33.60% of the cylinder mixture were burned for case 1 and 2 respectively. However, Figure 4.16 shows that the case 1 and 2 have predicted the closest mass fraction burned value in the range of -22° CA to -12° CA which associated with the flame development stage.

Based on Table 4.8, the simulated model of case 1 is unable to predict the flame development angle, θ_d and the rapid burning angle, θ_b . Where as for case 2, the model over predicted the value of flame development angle, θ_d by the value of 27 units crank angle whilst the rapid burning angle, θ_b is never attained. Following of the results, case 1 and case 2 provide immeasurable timing of burning completion. Thus, case 1 and case 2 are extremely under-predicted the process. Case 1 and 2 are seems to have an incomplete combustion process. However, the truth is that both cases have under estimated the instantaneous progress variable due to the small iteration numbers per

time step. This has resulted with under estimation of the instantaneous mass fraction burned and cylinder pressure.

For case 3, the mass fraction burned profile exhibits an equivalent trend as case 1 and 2. It shows a gradual increment of instantaneous mass fraction burned value from the start of ignition to the end of simulation period. However, the point of burning completion is achieved late in the simulation period. At 28° CA ATDC, the calculated value of mass fraction burned is 96.50%. Since the burning completion is achieved late from TDC, the cycle produced a low peak pressure. This agreed with typical case found in actual practice. For case 3, the flame development angle, θ_d is about 8 unit crank angle and the rapid burning angle, θ_b is about 40 unit crank angle. These give an overall burn rate angle, $(\theta_d + \theta_b)$ of 48-unit crank angle that deviates for about 53.85% from the measured result. While the timing for the overall burn-rate angle achieved is about 26° ATDC, which has a deviation about 160% from the measured result. Thus, the model is still under predicted the value of instantaneous progress variable. However, the result is improved as the iteration number is increased to 500 per time step.

In case 4 and 5, the simulated mass fraction burned profile are further improved as the number of iteration number per time step is increase to 1000 and 1500 iteration per time step respectively. The simulated profiles for both cases nearly resemble the measured mass fraction burned profile. At the end of simulation period at 28° CA ATDC, the calculated mass fractions burned are 99.85% and 99.85% respectively. By comparing both cases, even though the values of mass fraction burned are equal at the end of simulation, the burning completion in case 5 is achieved earlier thus promoted a higher peak pressure. In case 4, the flame development angle, θ_d is about 6 unit crank angle and the rapid burning angle, θ_b is about 30 unit crank angle. These give an overall burn rate angle, $(\theta_d + \theta_b)$ of 36 unit crank angle that deviates for about 15.38% from the measured result. Whilst the timing of overall burn rate angle is about 14° CA ATDC. These give a deviation about 40% from the measured timing. Where as for the case 5, the flame development angle, θ_d is about 6 unit crank angle and the rapid burning angle, θ_b is about 28 unit crank angle. These give an overall burn rate angle, $(\theta_d + \theta_b)$

of 34 unit crank angle that is deviates for about 8.97% from the measured result. Whilst the timing of overall burn rate angle is about 12° CA ATDC. These give a deviation about 20% from the measured timing. Both profiles of case 4 and 5 proved that the number of iteration has greatly affected the prediction of the mass fraction burned.

Based on Figure 4.16, case 4 and 5 however are not fitted the profile of measured mass fraction burned. During the ignition and flame development period of -22° CA to -12° CA, it is clearly evidence that there were abrupt burning of cylinder mixture as the sparks were ignited. This abrupt burning of large percent of cylinder mass during the flame development period and prolonged into rapid burning period deliberated huge amount of heats; and consequently increased the cylinder pressure abruptly. As a result, the finest prediction of mass fraction burned of case 4 and 5 have still over predicted the mass fraction burned and cylinder pressure results especially in the flame development period, in the range of -22° CA to -12° CA. Since the instantaneous mass fraction burned value is equivalent to the mean progress variable of the TFSC model, it can also be said that current approach of modelling are still showing poor performance in the prediction of progress variable at each crank angle or time steps.

Figure 4.17 presents simple description of flame propagation in term of progress variable contour while Figure 4.18 presents the results of flame propagation of each case at -14° CA BTDC and 0° CA at TDC. Qualitative examination on instantaneous flame propagation at both timing have support the results of section 4.4.1 and 4.4.2. Based on Figure 4.17, case 1 and case 2 are extremely under predicted the flame propagation especially at 0° CA or TDC where the flame radius is expanded at a very small size for the selected period after the ignition. In case 2, the flame radius is larger than case 1 as the number of iteration per time step is increased. Small iteration number in both cases have resulted with under prediction of flame propagation, which consequently resulted with low mass fraction burned, low heat release and finally low cylinder pressure. However, both cases 1 and 2 give the most reliable prediction of flame propagation at -14° CA BTDC since they give the closest prediction of mass fraction burned compared to the measured result as presented in Figure 4.16.

Case 3, 4 and 5 have predicted more reliable predictions of expanding spherical flame front in the whole simulation especially at 0° CA or TDC. All the predictions have shown an increase in the flame radius as the number of iteration is increased. Deterioration of the spherical flame is visible in case 3 due to the restriction of exhaust valve faces on propagating flame front. However, the three cases have over predicted the flame propagation at -14° CA BTDC since they give over prediction of mass fraction burned compared to the measured result as presented in Figure 4.16. This qualitative examination is parallel with the results of previous finding of the cylinder pressure and mass fraction burned.

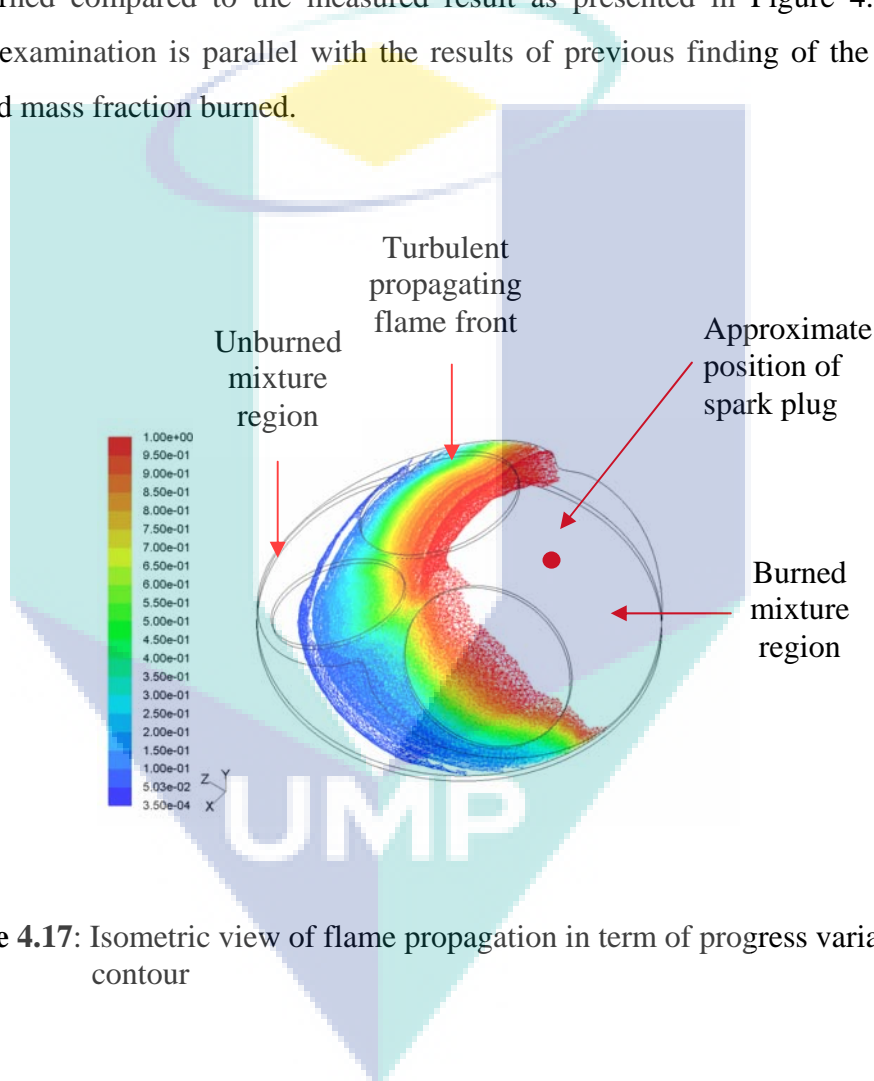


Figure 4.17: Isometric view of flame propagation in term of progress variable contour

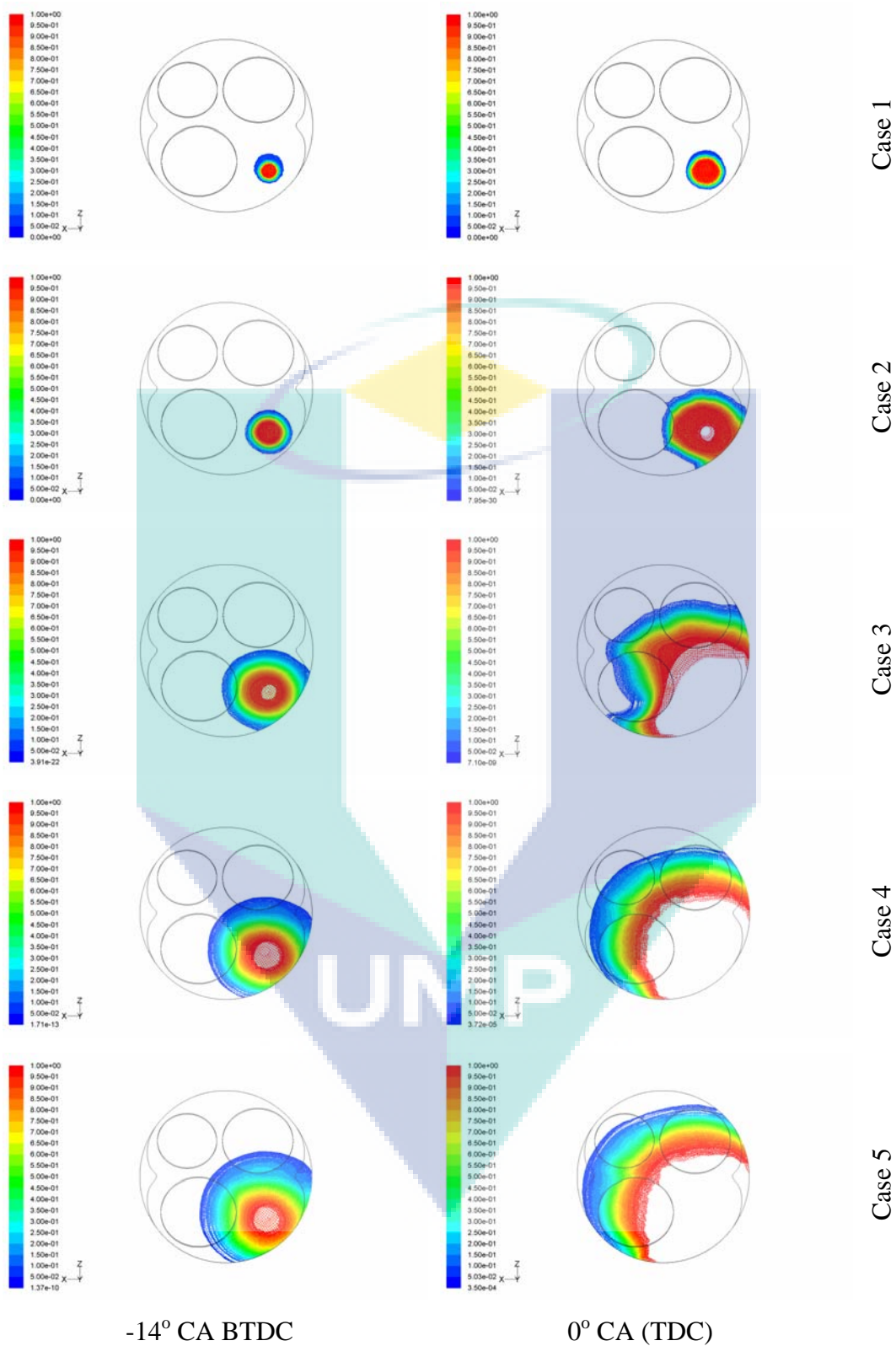


Figure 4.18: Visualization of instantaneous flame propagation in term of progress variable contour of each simulated cases at two different timing after the ignition

As a summary, based on overall results of the cylinder pressure, mass fraction burned and visualization of flame propagation, the following points can be used to summarize a few important findings that are crucial for the study. First, the iteration number greatly influences the simulated profile results. The trend shows that the discrepancies between measured and simulated results are greatly reduced as the number of iterations per time step is increased from case 1 to case 5 due to improved convergence. However, this will proportionally increase computing time. Second, the best possible result for numerical prediction using TFSC model can be obtained if the iteration number per time step is increased equal to or larger than 1500 times as demonstrated in case 5. Finally, the only left drawback is that the simulated results cannot exactly fit the measured profile. This is associated with the stages of SI engine combustion process. The major reason for the discrepancy is that the current approach of modelling is unsuccessful in predicting accurate reaction rate at every stage of SI engine combustion hence resulted with inaccurate prediction of mass fraction burned and consequently cylinder pressure. In TFSC model formulation, the model assumed that the instantaneous mass fraction burned is equivalent to the instantaneous progress variable value. Furthermore, the prediction of the instantaneous progress variable value is mostly controlled by the mean reaction terms ρS_c , which in turn is highly affected by the so-called turbulence burning speed S_T .

The turbulent flame speed S_T is the core parameter that governs the reaction rate at each stage of SI engine combustion. Thus, prediction of the turbulent flame speed variation through the simulated combustion process is vital for the establishment of accurate mass fraction burned and cylinder pressure profile. The mean reaction rate term is introduced in the conservation equation of progress variable of Eq. (3.7) and detail definition is given by the equation of mean reaction rate of Eq. (3.9). On the other hand, detail definition of the turbulent flame speed S_T is given by the equation of Zimont's turbulent flame speed model of Eq. (3.10). Even though the mean reaction rate is also influenced by the effect of the flame wrinkling and stretching term (Eq. 3.11) and the preferential diffusion term (Eq. 3.12), the effect of the first term is minimally studied and the effect of second term is minimized by the assumption of equal

distribution of equivalence ratio throughout the cylinder mixture. Thus, it is regarded that S_T has the utmost influential effect on the current outcome.

Based on Eq. (3.10) of Zimont's turbulent flame speed model, the value of S_T is influenced by the root mean square (RMS) velocity u' , laminar flame speed S_L , laminar thermal diffusivity α_L , turbulent length and time scale (l_T, τ_T) and chemical time scale τ_c . For current study, the RMS velocity is computed by the solver based on the prescribed boundary and initial condition. The value of laminar flame speed is set by the user. The value of chemical time scale is computed based on the value of laminar thermal diffusivity and laminar flame speed of Eq (3.20). Laminar thermal diffusivity is priority computed by using laminar thermal conductivity and specific heat of Eq (3.21). Where as the turbulence associated parameters are computed using the turbulence model. Hence, the calculated value of S_T is almost influenced by the mixture properties set by the user.

Most of all thermo-chemical properties such as the specific heat, laminar thermal conductivity, laminar flame speed, laminar fluid viscosity were set constant. In actual practice, this is not exactly true since most of them are varies as a function of pressure and temperature especially in a chemical reaction process which included heat generation. Constant laminar flame speed S_L is directly affecting the instantaneous turbulent flame speed prediction. Constant specific heat c_p and laminar thermal conductivity k_{th} affected the instantaneous thermal diffusivity α_L prediction. The calculated values of thermal diffusivity is become nearly constant or less effected by the by the variation of cylinder pressure and temperature which in turn affect the instantaneous chemical time scale τ_c prediction. Then, the chemical time scale value is directly affecting the instantaneous turbulent flame speed prediction.

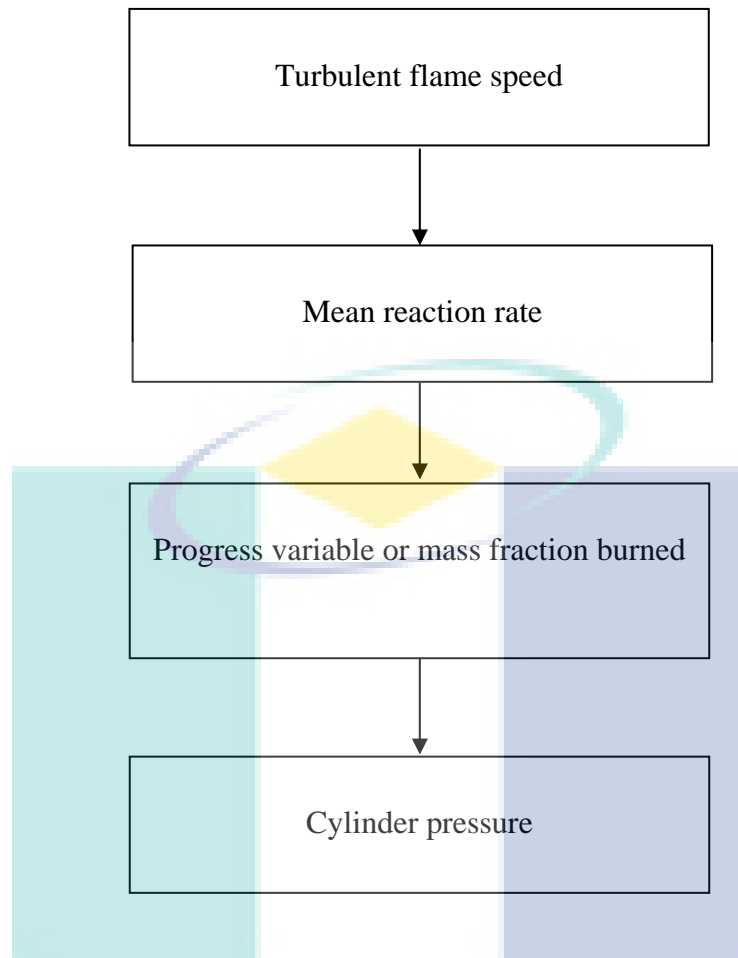


Figure 4.19: Relationship between turbulent flame speed and cylinder pressure

The modelling approaches presented so far will affect S_T and consequently the mean reaction rate ρS_c . Incorrect prediction of mean reaction rate will consequently affected the instantaneous value of progress variable at each SI combustion stages hence produced non-fitted profile of mass fraction burned and finally cylinder pressure. Figure 4.19 presents the cause-effect relationship between the turbulent flame speed and cylinder pressure. The most promising way of getting better results is by updating all the thermo-chemical properties at each time step before proceed with further calculation. This can be executed by setting the properties as a function of temperature or pressure.

In order to justify the reasoning of inaccurate prediction of the mean reaction rate that is strongly influenced by turbulent flame speed, variations of simulated turbulent flame speed are examined. Figure 4.19 presents the prediction of turbulent

flame speed S_T variation throughout the simulation period for case 1 to 5. Measured turbulent flame speed shows a significant variation. In most cases, S_T plotted show a maxima trend. The maximum flame speed is largely obtained near TDC or 50% mass fraction burned (Borman and Ragland, 1998). During the ignition and flame development period, turbulent flame speed should have small values. As the flame changing to turbulent and rapidly propagates across the chamber, turbulent flame speed is increased as well. When the flame approaching the wall, the flame speed reduced and terminated at the instance the flame front reaching the wall.

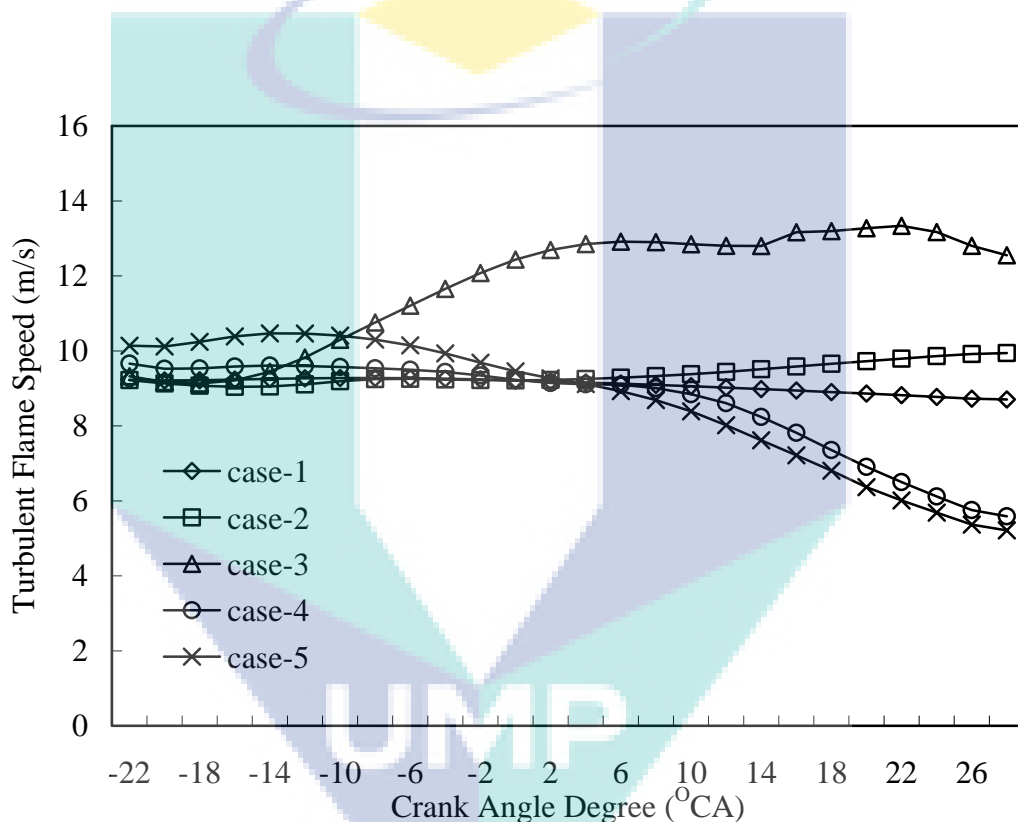


Figure 4.20: Turbulent flame speed prediction of cases 1 to 5

Based on Figure 4.20, the overall predicted turbulent flame speed falls in the range of 4 to 14 m/s in the range of simulated period. Based on the simulated profile, no case has shown a significant maxima trend as in actual case. In addition, all cases predict a high value of S_T at the start of the combustion process where the value lies in the range of 9.220 m/s to 10.14 m/s. Based on Borman and Ragland (1998), the initial value of S_T at the start of combustion is only about 0 to 5 m/s. This answers why at the start of combustion, there are abrupt burning an amount of mass fraction of cylinder

mixture thus caused abrupt increase in cylinder pressure. These are all resulted from the aforementioned constant mixture properties setup. Moreover, the values are all calculated based on the maximum temperature and pressure.

By examined each cases, it was found out that case 1 and 2 show the least variation among of all cases. The predicted flame speed varies in the range of 8-10 m/s only. Case 1 has an averaged turbulent flame speed of 9.09 m/s while case 2 has an averaged turbulent flame speed of 9.38 m/s. These are all resulted from the aforementioned constant mixture properties setup. In addition, cases 1 and 2 are associated with low number of iteration per time step thus resisting efficient update of the flow variables. Important point than can be drawn from the results is that the nearly unaffected turbulent flame speed in both cases of 1 and 2 are significantly differ from the actual trend and contributed to the under prediction of the overall result of case 1 and 2. Case 3 shows a quite different profile compared to the other cases. Turbulent flame speed profile shows a quite significant variation. However, the simulated trend still differs from the measured trend. In the range of -22°CA to -12°CA , turbulence flame speed shows less variation. Instead of relatively high turbulence flame speed predicted in the range, the value is still managed to become higher in the next stages of combustion. However, the flame speed value tends to become constant as the burning is in progress. Only at the end of simulation period, the value is gradually decreased.

In cases 4 and 5, nearly comparable turbulent flame speed profile are produced for both cases. Relatively high flame speed value is predicted at the start of combustion process, in the range of -22°CA to -12°CA . This provide a strong reason for condition at start of combustion where there are abrupt burning an amount of mass fraction of cylinder mixture thus caused abrupt increase in cylinder pressure in both cases. However, as the combustion processes are continued, predicted turbulent flame speed profile in both cases show decrease in value. These significantly support previous finding of slower rate of consumption of cylinder mixture in terms of simulated mass fractions burned than measured results in both cases. The result of turbulent flame speed presented previously is used primarily to justify the results of cylinder pressure and mass fraction burned. This is because turbulent flame speed is the most dominant factor that influenced the mean reaction rate at each time step or simulated crank angle.

Moreover, it was discussed that the prediction of the turbulent flame speed is influenced by the setup of the mixture properties.

Other Influential Factor

Other important factor that affects the model's predictions is boundary condition. The crucial boundary is the wall's thermal boundary. Wall thermal boundary is used to determine the wall heat transfer. Wall heat transfer has direct connection with the predicted cylinder pressure. A low heat transfer through the wall usually linked to high cylinder pressure and high efficiency. An excessive heat transfer through the wall usually resulted with low cylinder pressure thus reduce engine power. The wall thermal boundary can be specified as wall temperature or wall heat flux. In current study, constant typical wall temperatures at full load condition are used as wall thermal boundary. These affect the overall heat transfer process through the wall. Because, in actual practice, neither temperature nor heat flux has a constant value throughout the SI engine combustion process. Both quantities are significantly fluctuates with the crank angle where the highest value is produced approximately during the burning completion point. This has contributed for the slow reduction of cylinder pressure after the peak value is achieved. The slow reductions of cylinder pressure are evidenced in Case 4 and 5.

Other important factor that connected to the TFSC model of Zimont is the input of critical rate of strain, which is used to consider the effect of flame wrinkling and stretching as well as the preferential diffusion, which is used to consider the effect of non-uniform distribution of equivalence ratio. Both phenomena affect the rate of combustion process and both parameters have not been studied in details. In addition, both parameters are approximated as constant throughout the simulation. The value of critical rate of strain is calculated by using expression derived for general premixed combustion of gas turbine. The usage of the expressions for the IC engine combustion is not guaranteed.

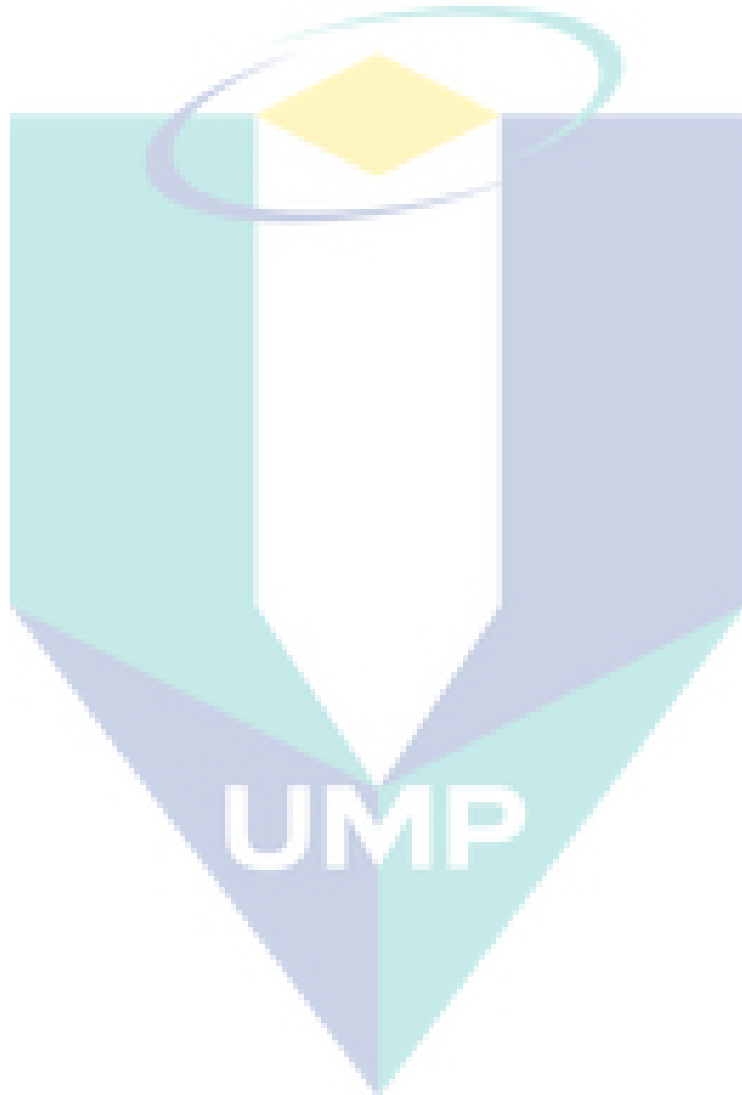
Another factor that affects the simulation results is associated with the ignition model. The TFSC model is developed principally for propagating turbulence flame and ignored the flame initiation process. The inclusion of the general ignition model as in current study did assist the treatment of ignition phase but still require detail study on its effect on overall combustion process. On the other hand, in the period of flame quenching process, where the flame has reached the wall, the TFSC model provides no treatment for the flame-wall interaction. Thus, the effect of flame quenching is not well predicted and has contributes to the slow reduction of cylinder pressure just after the burning completion.

Transient solution of in-cylinder combustion process requires that the overall process started from the ignition to burning completion being discretized into a finite number of time steps of time advancement where convergence should be achieved at every time step (Fluent, 2005). Smaller time step size usually gives better prediction of the combustion in progress since it predicts at smaller time interval. However, the time step size in current study is set equal to a crank angle size in order to reduce computing time.

4.4 Summary

This chapter has presented the experimental data of engine test-rig and prediction of combustion simulation of 4-stroke SI engine. The experimental data consist of the engine torque, fuel-air equivalence ratio and ignition timing, cylinder pressure; mass fraction burned, and engine performance parameters. The measured data have been discussed and compared to the typical engine performance data. The simulated results have discussed and validated against the previous experimental data. The main parameter of interest for analysis and validation is the cylinder pressure. The discussions are then supported by the results of mass fraction burned, the flame propagation and the turbulent flame speed. This approach is vital because these parameters are the controlling parameters that govern the engine cylinder pressure. However, for current study, only the events at 2000-rpm of engine speed are simulated. It requires that all the associated sources of discrepancies within this initial work are

identified and proper solutions are known at first before continuing to the other engine condition.



CHAPTER 5

CONCLUSION AND RECOMMENDATIONS

5.1 Conclusion

The overall study has demonstrated the feasibility of the TFSC model of Zimont for simulating a realistic turbulent premixed SI engine combustion process based on Mitsubishi Magma (4G15) engine. Based on preliminary results of combustion simulation, it was identified that the iteration number per time step has the highest possible influence on the resultant combustion process; thus lead further to the effect of iteration number study of cases 1 to 5. Comparison of simulated and measured result primarily based on cylinder pressure has confirmed that the iteration number was greatly influenced the TFSC model prediction. Analysis of cylinder peak-pressure and timing of peak pressure shows that the model's prediction of case 5 has only 2.19% and 25% deviation from the measured result results respectively. These are obtained as the number of iteration is increased up to 1500 iteration per time step. However, the finest prediction of cylinder pressure is still illustrated some discrepancy especially in fitting the measured cylinder pressure profile at each stage of SI engine combustion. This is due to the inaccurate prediction of mass fraction burned. The inaccurate prediction of mass fraction burned indicates an inaccurate prediction of the mean reaction rate at each stage of SI engine combustion. Subsequently, the mean reaction rate is highly controlled by the prediction of turbulent flame speed. Turbulent flame speed is one of the most important parameter that influenced the actual SI engine combustion process as well as the prediction of Zimont combustion model. In TFSC model formulation, turbulence flame-speed calculation is influenced by the prescribed mixture material properties. Crucial mixture material properties are laminar flame speed, laminar thermal diffusivity, laminar thermal conductivity and specific heats. Hence, the approach of setting the

properties as constants throughout the combustion simulation has become the major cause for inaccurate prediction of turbulent flame speed at each stage of SI engine combustion and subsequently affect the overall results. As conclusion, the TFSC model of Zimont has demonstrated its capability and promisingly applied for solving SI engine combustion. Factors that influence the model prediction are identified and crucially need refinement in future works.

5.2 Recommendations for Future Work

Vast knowledge and experiences gathered from the study have suggested the following recommendations for further improve the TFSC model's prediction. Importance mixture properties are essentially needed to be set as function of instantaneous pressure and temperature. Varying wall heat flux is vital for a more realistic modelling of flame-wall interaction. In order to solve accurately the ignition and flame development phase, the general ignition model and all its related parameter must be tested thoroughly and studied in details. Finally, it is suggested that the time step size is further reduce with the intention that the progress of combustion is well capture. The aforementioned refinements are suggested to be carrying out by using the same model of 2000 rpm. The discrepancy associated with the current results should be reduced at first before further testing the TFSC model of Zimont at a wider engine condition or particularly higher engine speed. Additional works required to justify the universalities of the model are by testing the TFSC model at higher engine speed of 4000 rpm that associated with highly turbulence. From the aspect of computing power, it is highly suggested that further studies should be conduct on a more suitable machine such as supercomputer or parallel node computers as the computing time is highly increased as the number of iteration per time step is increased in order to assure convergence.

REFERENCES

- Amann, C.A. 1985. Classical combustion diagnostics for engine research. In: Engine combustion analysis: new approaches. Warrendale: *SAE Technical Paper*. Paper no. 850395.
- Amstrong, N.W.H. and Bray, K.N.C. 1992. Premixed turbulent combustion flow field measurements using piv and lsv and their application to flamelet modelling of engine combustion. *SAE Technical Paper*. Paper no. 922322.
- Borman, G.L. and Ragland, K.W. 1998. *Combustion engineering*. Singapore: McGraw Hill International Edition Series.
- Bradley, D., Haq, M.Z., Hicks, R.A., Kitagawa, T., Lawes, M., Sheppard, C.G.W. and Woolley, R. 2003. Turbulent burning velocity, burned gas distribution, and associated flame surface definition. *Proceedings of the Combustion Institute*. 133: 415-430.
- Cengel Y.A. and Cimbala, J.M. 2006. *Fluid mechanics: fundamental and application*. Singapore: McGraw Hill International Edition Series.
- Delhaye, B. and Cousyn, B. 1996. Computation of flow and combustion in spark ignition engine and comparison with experiment. *SAE Technical Paper*. Paper no. 961960.
- Delhaye B. and Duverger T. 1998. Modelling of internal flow and combustion in a four valve lean burn SI engine. *The 4th International Symposium of Combustion Diagnostics and Modelling of Reciprocating Engine (COMODIA)*. Japan: Japan Society of Automotive Engineer.
- Douglas, R., Kee, R.J. and Carberry, B.P. 1997. Analysis of cylinder pressure data in two stroke engine. *SAE Technical Paper*. Paper no. 972792.
- Drake, M.C. and Haworth, D.C. 2007. Advanced gasoline engine development using optical diagnostics and numerical modelling. *Proceedings of the Combustion Institute*. 31(1): 99-124.
- Duclos, J.M. and Colin, O. 2001. Arc and kernel tracking ignition model for 3d spark ignition engine calculations. *The 5th International Symposium of Combustion Modeling and Diagnostics in Reciprocating Engine (COMODIA)*. Japan: Japan Society of Automotive Engineer.
- Ewalds, J. and Peters, N. 2007. On unsteady premixed turbulent burning velocity prediction in internal combustion engine. *Proceedings of the Combustion Institute*. 31, 3051-3058.
- Ferziger, J.H. and Peric, M. 2002. *Computational methods for fluid dynamic, 3rd Edition*. Germany: Springer Verlag.

- Flohr, P. and Pitsch, H. 2000. A turbulent flame speed closure model for les of industrial burner flow. *In: Proceeding of the Summer Program. Stanford: Center for Turbulent Research.*
- Fluent Inc. 2005. *Fluent 6.2 user's guide.* New Hampshire, United States.
- Gosman, A.D., Johns, R.J.R. and Watkins, A.P. 1980. *Development of prediction methods for in-cylinder processes in reciprocating engine.* In: Mattavi, J.N. and Amann, C.A. *Combustion modelling in reciprocating engine.* New York: Plenum Press.
- Gosman A.D. 1985. Computer modelling of flow and heat transfer in engines: progress and prospect. *The 1st International Symposium of Combustion Modelling and Diagnostics in Reciprocating Engine (COMODIA).* Japan: Japan Society of Automotive Engineer.
- Gosman, A.D. 1999. State of art of multi dimensional modelling of engine reacting flows. *Oil and Gas Science Technology.* 54(2): 149-159.
- Heywood, J.B. 1980. *Engine combustion modeling- An overview.* In: Mattavi, J. N. and Amann, C. A. *Combustion modelling in reciprocating engine.* New York: Plenum Press.
- Heywood, J.B. 1988. *Internal combustion engine fundamental,* Singapore: McGraw Hill.
- Heywood, J.B. 1994. Combustion and its modelling in spark ignition engines. *The 3rd International Symposium of Combustion Modelling and Diagnostics in Reciprocating Engine.* Japan: Japan Society of Automotive Engineer.
- Kalam, M.A., Masjuki, H.H., Maleque, M.A. and Amalina, M.A., 2005. Power improvement of a modified natural gas engine. *The 1st Asia Pacific Natural Gas Vehicle Association Conference and Exhibition.* Kuala Lumpur: Asia Pacific Natural Gas Vehicle Association.
- Kuo, K. K. 1986. *Principles of combustion.* United States of America: John Wiley and Sons Inc.
- Lenz, H. P. 1992. *Mixture formation in spark ignition engine.* United States of America: Society of Automotive Engineer.
- Lipatnikov, A., Wallesten, J. and Nisbet, J. 1998. Testing of a model for multidimensional computations of turbulent combustion in spark ignition engines. *The 4th International Symposium Of Combustion Modelling And Diagnostics In Reciprocating Engine.* Japan: Japan Society of Automotive Engineer.

- Lipatnikov, A., and Chomiak, J. 2000. Modelling of pressure and non-stationary effects in spark ignition engine combustion: A comparison of different approaches. *SAE Technical Paper*. Paper No. 2000-01-2034.
- Lipatnikov A. and Chomiak, J. 2002. Turbulent flame speed and thickness: Phenomenology, evaluation, and application in multi-dimensional simulations. *Progress in Energy and Combustion Science*. 28,1-74.
- Lipatnikov, A. and Chomiak, J. 2003. *Premixed turbulent flame theory and simulations of combustion in si engines: connections, discrepancies, and practical solutions*. Chalmers Combustion Engine Research Centre, Chalmers University of Technology, Goteborg.
- Matthews, R.D., Hall, M.J., Dai, W. and Davis, G.C. 1996. Combustion modelling in SI engines with a peninsula-fractal combustion model. *SAE Technical Paper*. Paper no.960072.
- Merker, G.P., Schwarz, C., Stiesch, G. and Otto, F. 2006. *Simulating combustion: Simulation of combustion and pollutant formation for engine development*. Germany: Springer-Verlag.
- Mugele, M., Tribulowski, J., Peters, H., Spicher, U. and Roskamp, H. 2001. Numerical analysis of gas exchange and combustion process in a small two stroke gasoline engine. *SAE Technical Paper*. Paper no. 2001-01-3602.
- Nishiwaki, K. 1985. Prediction of 3-dimensional fluid motion during intake process and swirl ratio in four cycle engine. *The 1st International Symposium of Combustion Modelling and Diagnostics in Reciprocating Engine*. Japan: Japan Society of Automotive Engineer.
- Peters, H., Worret, R. and Spicer, U. 2001. Numerical analyses of the combustion process in spark ignition engine. *The 5th International Symposium of Combustion Modelling and Diagnostics in Reciprocating Engine*. Japan: Japan Society of Automotive Engineer.
- Pinchon, P. 1990. Modelling of fluid dynamics and combustion in piston engine. *The 1st International Symposium of Combustion Modelling and Diagnostics in Reciprocating Engine*. Japan: Japan Society of Automotive Engineer.
- Plint, M and Martyr, A. 1999. *Engine testing, theory and practice*, Warrendale: Society of Automotive Engineers.
- Pulkrabek, W.W. 1997. *Engineering fundamental of the internal combustion engine*. United States of America: Prentice Hall International.
- Randolph, A.L. 1994. Cylinder pressure-based combustion analysis in race engines. *SAE Technical Paper*. Paper no.942487.

- Richard, S., Colin, O., Vermorel, O., Benkkena, A., Algelberger, C. and Veynante, D. 2007. Towards large eddy simulation of combustion in spark ignition engine. *Proceeding of the Combustion Institute*. 31, 3051-3058.
- Roth, K.J., Sobiesiak, A., Robertson, L. and Yates, S. 2002. In-cylinder pressure measurements with optical fibre and piezoelectric pressure transducers. *SAE Technical Paper*. Paper no.2002-01-0745.
- Rotondi, R. and Bella, G. 2006. Gasoline direct injection spray simulation. *International Journal of Thermal Sciences*. 45,168–179.
- Tatschl, R., Wieser, K. and Reitbauer, R. 1994. Multidimensional simulation of flow evolution, mixture preparation and combustion in a 4-valve si engine, *The 3rd International Symposium of Combustion Modelling and Diagnostics in Reciprocating Engine*. Japan: Japan Society of Automotive Engineer.
- Turns, S.R. 2000. *An introduction to combustion: concept and applications*. 2nd Edition. Singapore: Mc-Graw Hill.
- Versteeg, H.K. and Malalasekera, W. 1995. *An introduction to computational fluid dynamic: the finite volume method*. England: Longman Scientific and Technical.
- Veynante, D. and Vervisch, L. 2002. Turbulence combustion modelling. *Progress in Energy and Combustion Science*. 28, 193-266.
- Wallesten, J., Lipatnikov, A. and Nisbet, J. 1998. Turbulent flame speed closure model: further development and implementation for 3-d simulation of combustion in si engine. *SAE Technical Paper*. Paper no. 982613.
- Wallesten, J., Lipatnikov, A. and Chomiak, J. 2002. Simulations of fuel-air mixing, combustion and pollutant formation in a direct injection gasoline engine. *SAE Technical Paper*. Paper no. 2002-01-0835.
- Walter, T., Brechbühl, S., Gossweiler, C., Schnepf, M. and Wolfer, P. 2004. *Pressure indicating with measuring spark plugs on a DI-gasoline engine – state of technology*. Switzerland: Kistler Instrumente AG. Special Publication.
- Yasar, O. 2001. A new ignition model for spark ignited engine simulations. *Journal of Parallel Computing*. 27, 179-200.
- Zhao, X., Matthews, R. D. and Elizzey, J. L. 1993. Three-dimensional numerical simulation of flame propagation in spark ignition engines. *SAE Technical Paper*. Paper no.932713.

APPENDIX A

ATE-60 HYDRAULIC DYNAMOMETER SPECIFICATION AND PERFORMANCE CURVE FROM MANUFACTURER DATA SHEET

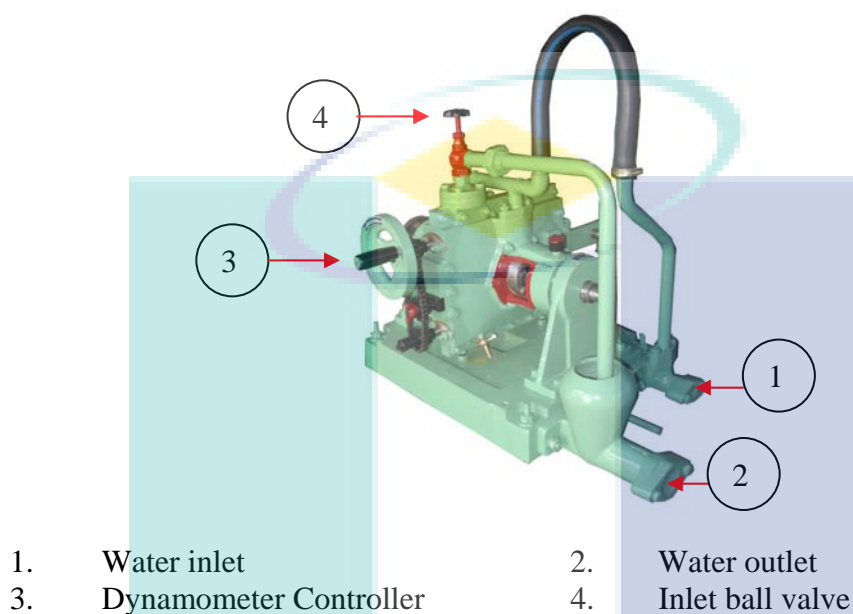


Figure A.1: ATE-60 hydraulic dynamometer

Table A.1: ATE-60 hydraulic dynamometer specifications

Description	Specifications
Manufacturer	M/S. Hytech Educational Equipments Pvt. Ltd,
Model	ATE-60
Serial no.	6077
Weighing mechanism	Load cell
Load cell capacity	0-150 kg (0-450 Nm)
Calibration arm length	358.1 mm
Dynamometer arm length	305.8 mm
Ratio of calibration	1 kg:3.513 Nm
Maximum torque	300 N.m
Maximum speed	7000 rpm
Maximum power	170 BHP

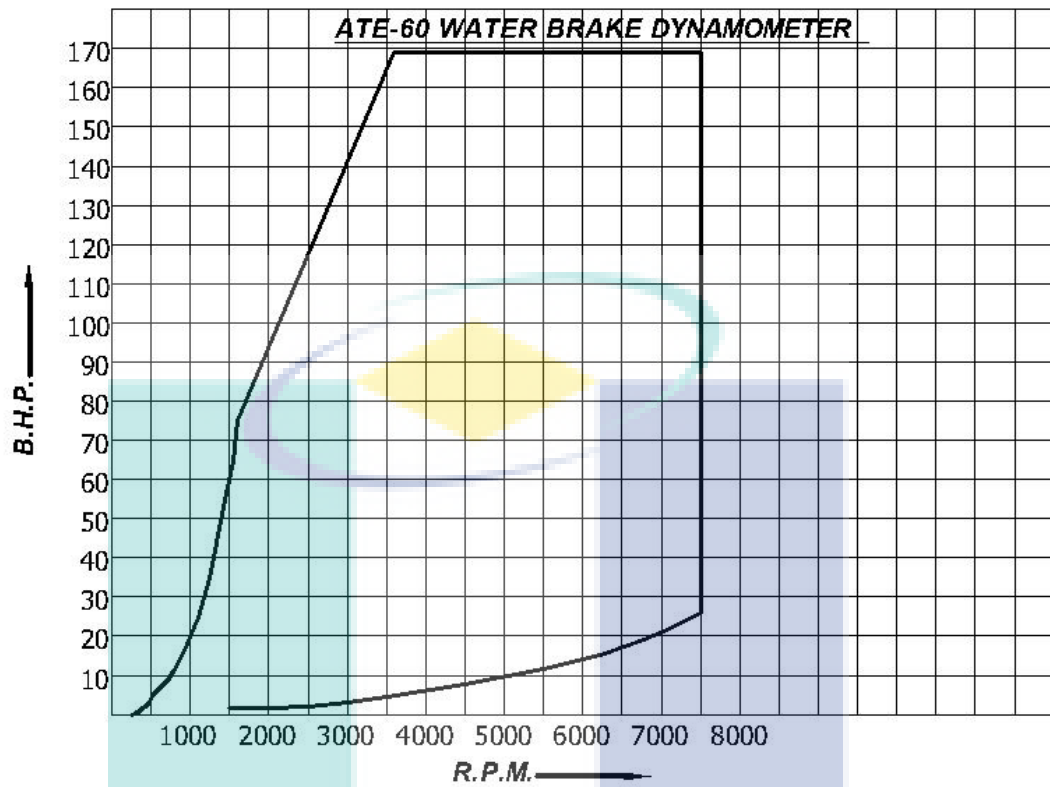


Figure A.2: Performance curve shows the operating region for the ATE-60 Hydraulic dynamometer

APPENDIX B

**SPECIFICATION AND TECHNICAL DATA OF SPARK PLUG TYPE
PRESSURE TRANSDUCER (TYPE 6117 B)**

Table B.1: Technical specification of spark plug type pressure transducer


Range (bar)	0-200 bar
Calibrated Partial Range (bar)	0-50 bar
Overload (bar)	250 bar
Sensitivity at 200°C (pC/bar)	~ -15
Natural Frequency of Spark Plug with Integrated Sensor (kHz)	~ 130 kHz
Linearity % FSO	≤ ± 0.6
Acceleration Sensitivity	
Axial (bar/g)	<0.005 bar/g
Radial (bar/g)	<0.005 bar/g
Operating Temperature Range (°C)	≤ 350 °C
Sensitivity Shift (200 ± 50°C) (%)	≤ ± 1.5%
Thermal Shock	
At 1500 min -1,9 bar imep	
Δp (short time drift) (bar)	≤ ± 0.8 bar
Δimep (%)	≤ ± 4%
ΔP max (%)	≤ ± 2%
Insulation resistance of sensor	
At 20°C (Ω)	>10 ¹³
At 200°C (Ω)	>10 ¹¹
Insulation resistance of spark plug	
At ambient temperature	
Between central electrode and spark plug body at 1000 V (MΩ)	>100 MΩ
Electrical final test of spark PLUG	
Spark discharge for (bar/kW)	7 bar/20 kW
Break through resistance (kV)	<35 kV
Tightening Torque of sensor (Nm)	1.2-1.3Nm
Tightening torque of spark plug (Nm)	20-25 Nm
Capacitance for sensor	
(with 1 m cable) (pF)	110 pF
Weight (with protection cartridge) (g)	130 g

Manufacturer: Kistler Instrument AG, PO BOX, Eulachstrasse 22, CH-8408,
Wintherthur, Schweiz,

Tel: +41 52-224 1111, Fax: +41 52-2241414

Email: info@kistler.com, webpage: www.kistler.com

Figure B.1: Calibration certificate of pressure transducer



KISTLER
measure. analyze. innovate.

Kalibrierschein DRUCK Calibration Certificate PRESSURE

Type 6117BCD15 Serial No. 1336442

Kalibriert durch Calibrated by	Datum Date
G. Ratano	06.01.2006

Referenzgeräte Reference Equipment	Typ Type	Serien-Nr. Serial No.
Gebrauchsnorm Working Standard	Kistler 6961A250	992713
Ladungsverstärker Charge Amplifier	Kistler 5011B	602394
Ladungskalibrator Charge Calibrator	Kistler 5395A0	605251

Umgebungstemperatur Ambient Temperature °C	Relative Feuchte Relative Humidity %
23	38

Messergebnisse Results of Measurement

Kalibrierter Bereich Calibrated Range bar	Empfindlichkeit Sensitivity pC / bar	Linearität Linearity ≤ ±% FSO
0 ... 200 (23°C)	-15,36	0,2
0 ... 50 (23°C)	-15,22	0,1
0 ... 150 (200°C)	-15,69	0,1
0 ... 50 (200°C)	-15,62	0,2

UMP

Bestätigung Confirmation

Wir bestätigen, dass das oben identifizierte Gerät nach den vorgeschriebenen Verfahren geprüft wurde. Alle Messmittel sind auf nationale Normale rückverfolgbar. Kistler betreibt die SCS (Swiss Calibration Service) Kalibrierstelle Nr. 049, akkreditiert nach ISO 17025. Das Kistler Qualitätsmanagement System ist nach ISO 9001 zertifiziert.

We confirm that the device identified above was tested by the prescribed procedures. All measuring devices are traceable to national standards, the SCS (Swiss Calibration Service) Calibration Laboratory No. 049 is operated by Kistler and accredited per ISO 17025. The Kistler Quality Management System is certified per ISO 9001.

Kistler Instrumente AG Eulachstrasse 22 PO Box CH-8408 Winterthur	Tel. +41 52 224 11 11 Fax +41 52 224 14 14 info@kistler.com	ZKB Winterthur BC 732 Swift: ZKBKCHZZ80A Account: 1132-0374.628 Seite page 1/1
IBAN: CH67 0070 0113 2003 7462 8 VAT: 229 713 ISO 9001 certified	www.kistler.com	

APPENDIX C

MEASUREMENT SYSTEM FOR DETERMINATION OF ENGINE SPEED

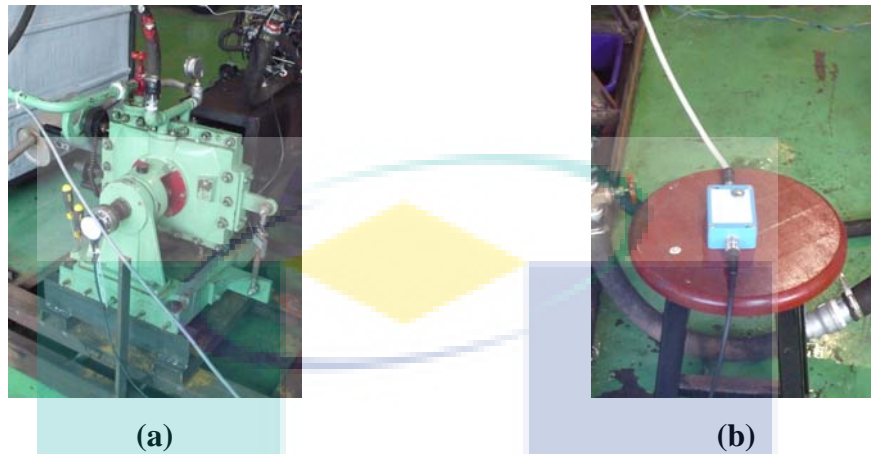


Figure C.1: (a) Crank angle encoder at the end of the dynamometer's shaft (b) Signal conditioner which connected the crank angle encoder to the DEWE-CA system

Table C.1: Crank Angle Encoder (Type 2613B) Specification

Specification	Units	Range
TTL crank angle signal		0.1-6
Resolution	° (degree)	
Dynamic accuracy at 10 000 1/min (signal delay)	° (degree)	+0.02
TTL trigger signal (TRG)		
Resolution	° (degree)	0.1-6
Speed range	1/min	1-20 000
Operating temperature range		
Encoder and amplifier	°C	-30-60
Connection flange	°C	-30-100
Power supply with stabilized voltage	VDC	5 ± 0.25
Current consumption with unstabilized voltage	mA	200
Current consumption	VDC	6...24
Mounting diameter of encoder	mm	200...400
Encoder weight	g	69
Amplifier dimensions	mm	460
Amplifier weight	g	98x64x37
		300

APPENDIX D

LOAD MEASUREMENT SYSTEM AND DETAILS SPECIFICATION OF THE
LOAD CELL

Figure D.1: Load cell used to measure engine torque on the right side of the dynamometer

Table D.1: Load cell (type 60001) specifications

PARAMETER	VALUE				UNIT
Rated capacity-R.C. (E_{max})	25, 50, 75, 100, 150, 200, 250, 300, 500, 750, 1K, 1.5K, 2K, 2.5K, 3K, 5K, 10K, 15K, 20K 50kg, 100kg, 250kg, 500kg, 1t, 2.5t, 5t, 10t*				lbs kg/metric tons
NTEP/OIML Accuracy class	NTEP III	NTEP IIIIL	Standard	OIML R60	
Maximum no. of intervals (n)	5000 single	10000 single		3000*	
$Y = E_{max}/V_{min}$	NTEP Cert. No 86-043A1			6667	Maximum available
Rated output-R.O. lbs	3.0				mV/V
Rated output tolerance lbs	25 - 3K: +25 / -10 5K - 20K: ± 0.25				%
Rated output-R.O. kg	3.0				mV/V
Rated output tolerance kg	50kg -1t: +25 / -10 2.5t - 3t: ± 0.25				%
Zero balance	1.0				\pm % FSO
Combined error	0.02	0.02	0.03	0.02	\pm % FSO
Non-repeatability	0.01				\pm % FSO
Creep error (30 minutes)	0.03	0.025	0.03	0.017	\pm % FSO
Temperature effect on zero	0.0010	0.0010	0.0015	0.0010	\pm % FSO/ $^{\circ}$ F
Temperature effect on output	0.0008	0.0008	0.0008	0.0007	\pm % of load/ $^{\circ}$ F
Compensated temperature range	14 to 104 (-10 to 40)				$^{\circ}$ F ($^{\circ}$ C)
Operating temperature range	0 to 150 (-18 to 65)				$^{\circ}$ F ($^{\circ}$ C)
Storage temperature range	-60 to 185 (-50 to 85)				$^{\circ}$ F ($^{\circ}$ C)
Safe sideload	30				% of R.C.
Maximum safe central overload	150				% of R.C.
Ultimate central overload	300				% of R.C.
Excitation, recommended	10				Vdc or Vac rms
Excitation, maximum	15				Vdc or Vac rms
Input impedance	343 - 450				Ω
Output impedance	349 - 355				Ω
Insulation resistance at 50VDC	>1000				M Ω
Material	Nickel plated alloy tool steel**				
Environmental protection	IP67				

Note: * OIML approval 100-5Klbs & 50-2500kg only

NTEP approval from 25-20Klbs only

** Stainless steel available - model number 60050

FSO - Full Scale Output

All specifications subject to change without notice.

Manufacturer Calibration Data

ATE/04-05/CAL/010

11-01-2005

Sr. No.	Particulars	
1	Name Of Dynamometer User	M/S. Hytech Educational Equipments Pvt. Ltd, Laygude Industrial Estate, Lagad Mala, Vadgaon Dhayari, Sinhgad Road, Near Sanas High School, Pune
2	Dynamometer Model	ATE – 60 'LC'
3	Dynamometer Sr. No.	60077
4	Type Of Weighing Mechanism	Load Cell
5	Capacity Of Load Cell	0 to 150 Kg. (0 to 450 N-m)
6	Calibration Arm Length	358.1 mm
7	Dynamometer Lever Arm Length	305.8 mm
8	Ratio Of Calibration	1 Kg : 3.513 N-m
9	Full Torque of Dyno.	300 N-m

CALIBRATION REPORT

Observations:

Sr. No.	Weight Applied In Kg.	Torque Indicated In N-m		Error In N-m.	% Error W.R.T. Full Scale Torque
		Required	Actual		
1	0.000	0.0	0.0	0	0
2	1.000	3.5	3.5	0	0
3	2.000	7.0	7.0	0	0
4	3.000	10.5	10.7	0.2	+0.07
5	4.000	14.0	14.0	0	0
6	5.000	17.6	17.8	0.2	+0.07
7	6.000	21.1	21.2	0.2	+0.07
8	7.000	24.6	24.6	0	0
9	8.000	28.1	27.9	-0.2	-0.07
10	9.000	31.6	31.3	-0.3	-0.1
11	10.000	35.1	35.1	0	0
12	15.000	52.7	52.9	0.3	0.1
13	20.000	70.3	70.3	0	0
14	25.000	87.8	88.1	0.3	+0.1
15	30.000	105.4	105.6	0.2	+0.07
16	35.000	123.0	123.2	0.2	+0.07
17	40.000	140.5	140.8	0.3	+0.1
18	45.000	158	158.2	0.2	+0.07
19	50.000	175.6	175.6	0.0	0

Remarks

- 1) Calibration of the Dynamometer is within the Limit of $\pm 0.25\%$ with respect to Full Scale Deflection
- 2) Sensitivity of the Dynamometer is 0.3 N-m.

Checked By –

For Accurate Test Equipments & Engineers

V.P. Ghatge

(Engineer – Production)

APPENDIX E

GENERAL PROCEDURE OF ENGINE TESTING

This appendix presents the general procedure for engine testing and importance steps in experimental data collection. The steps include (i) basic safety instructions (ii) general inspection and (iii) engine starting and (iv) position-speed mode test for wide open throttle (WOT) condition.

1.1 Basic Safety Instructions

- 1.1.1 Electrical supply must be shut off when the system is not in used or repair is in progress.
- 1.1.2 Avoid from touching any wiring connection when the engine is in running condition.
- 1.1.3 Secure all wires and cables properly by not leaving any of them dangling and exposed to contact with engine moving parts.
- 1.1.4 Avoid from touching any moving parts of the test-rig system and do not standing beside of rotating parts.
- 1.1.5 Exhaust manifold and tail-pipe are extremely hot; strictly do not touch it even after the engine is shut down for certain period.

1.2 General Inspection:

The following items need to be check before starting the engine and test. They must be in appropriate level and condition in order to allow the engine operated at its best performance.

- 1.2.1 Gasoline fuel level and fuel line connection
- 1.2.2 Engine lubricating oil level
- 1.2.3 Engine cooling water level
- 1.2.4 Dynamometer water supply level
- 1.2.5 Dynamometer arm must be in horizontal condition

1.2.6 Engine-dynamometer coupling bolts and nuts

1.2.7 Battery condition

1.3 Engine starting:

1.3.1 Switch on the engine (only after all relevant steps in 1.1 and 1.2 are carefully taken).

1.3.2 Carefully check and ensure that all the instruments and control systems are working properly.

1.3.3 Let the engine stabilized at this condition (idling) for a few minutes until the normal operating condition is achieved (by checking the coolant outlet temperature~80°C-90°C and the engine speed, in which it reduced to the desired engine speed at idle).

1.3.4 Carefully check out the initial load produce by the hydraulic dynamometer and ensure the dynamometer load is reset to zero.

1.3.5 Check out all the instruments reading as the engine idling and make sure all the reading give acceptable values for idle conditions.

1.4 Position and Speed Mode Test: Wide Open Throttle (100% opening)

1.4.1 Start the test with the engine speed of 1500 RPM. Increase the throttle opening until the engine overshoot up to 1500-2000 RPM.

1.4.2 At that instantaneous engine speed, increase the brake load until the speed reduced to 1500 RPM, and let the engine stabilized before applying any load or throttle opening. Make sure do not overload the engine as the speed will reduced lower than 1500 RPM.

1.4.3 As the engine stabilized, again, increase the throttle opening until the engine overshoot up to 1500-2000 RPM again and increase the brake load to reduce the engine speed down to the engine speed of 1500 rpm. And Let the engine stabilized.

(As the throttle opening is become wider at, the engine speeds will increase. Therefore, the load will need to be applied to maintain the engine speed at that certain RPM.)

- 1.4.4 Repeat the steps from (1.4.1 to 1.4.3) until the throttle opening achieved the 100% opening at 1500 RPM. As the 100% opening is achieved, do not apply any more loads on the engine.
- 1.4.5 Let the engine stabilize, and then start to take the reading. (This is the reading for 100% throttle opening at 1500 RPM. In this method, the brake load is a dependent variable where as the engine speed is dependent variable and the throttle opening is the controlled variable).
- 1.4.6 After the readings are taken, reduce the throttle opening and unload the engine gradually until the engine return to the idle state.
- 1.4.7 Repeat all the steps above with an increase in engine speed to 2000 RPM, 2500 RPM, 3000 RPM, 3500 RPM, 4000 RPM, 4500 RPM and finally 5000 RPM.

The logo for UMP (Universiti Malaysia Perlis) is a large, downward-pointing arrow shape. It is composed of several overlapping geometric shapes in shades of teal, light blue, and yellow. The letters 'UMP' are written in a bold, white, sans-serif font across the bottom of the arrow.

UMP

APPENDIX F

LIST OF FORMULA FOR ENGINE PERFORMANCE CALCULATION

1. Indicated Power Per Cylinder, $IP_{i,c}$

$$IP = \frac{(IMEP_{i,c} \times V_d \times N)}{n_R \times 60} \text{ (kW)} \quad (\text{F.1})$$

or

$$IP = \frac{(W_{i,c})N}{n_R \times 60} \text{ (kW)} \quad (\text{F.2})$$

where

$IMEP_{i,c}$: Indicated mean effective pressure per cylinder (kPa)

$W_{i,c}$: Indicated work per cylinder (kJ)

n_R : Number of crank revolution for each power stroke per cylinder
(2 for 4-stroke)

V_d : Displacement volume (m^3)

N : Engine revolution (rpm)

Note : Total engine power can be obtain by multiply IP with number of cylinder

2. Indicated Mean Effective Pressure, $IMEP_{i,c}$

$$IMEP_{i,c} = IMEP_{ref.cyl} \text{ (kPa)} \quad (\text{F.3})$$

where

Note : $IMEP_{ref.cyl}$ is taken from the DEWE-CA measurement for reference cylinder (cylinder No.1)

3. Total Brake Power, BP

$$BP = \frac{2\pi NT_e}{60000} \quad (\text{kW}) \quad (\text{F.4})$$

where

T_e : Engine Torque (Nm)

Note : Brake power per cylinder can be obtain by dividing BP by the number of cylinder

4. Total Brake Mean Effective Pressure, $BMEP$

$$BMEP = \frac{60BP}{LA_p N} \quad (\text{kPa}) \quad (\text{F.5})$$

where

L : Length of stroke (m)

A_p : Piston face area (m²)

Note : $BMEP$ per cylinder can be obtain by dividing the total $BMEP$ by the number of cylinder

5. Rate of Fuel Consumption, \dot{m}_f

$$\dot{m}_f = \frac{\left(\frac{50 \times 10^{-3}}{1000}\right) \times \rho_{fuel}}{t} \quad (\text{kg/s}) \quad (\text{F.6})$$

where t : Consumption time for 50 ml of fuel (sec)

ρ_{fuel} : Fuel density (kg/m³)

6. Brake Specific Fuel Consumption, BSFC

$$BSFC = \frac{\dot{m}_f \times 3600}{BP} \text{ (kg/kW.hour)} \quad (\text{F.7})$$

7. Rate of Air Consumption, \dot{m}_a

Pressure Drop across orifice, Δp

$$\Delta p = \rho g \Delta h \text{ (Pa)} \quad (\text{F.8})$$

where

Δh = height difference of manometer (m)

Flow velocity, V

$$V = \sqrt{\frac{2\Delta p}{\rho_{air}}} \text{ (m/s)} \quad (\text{F.9})$$

Volumetric Flow rate, Q

$$Q = C_d \pi \frac{d^2}{4} \sqrt{\frac{2\Delta p}{\rho_{air}}} \text{ (m}^3\text{/s)} \quad (\text{F.10})$$

Mass flow rate, \dot{m}

$$\dot{m}_a = \rho_{air} \times Q \text{ (kg/s)} \quad (\text{F.11})$$

where

$$\rho_{air} : \text{Air density in kg/m} = \frac{P_{atm}}{RT_{atm}}$$

$$P_{atm} : \text{Atmospheric pressure} = 101.325 \text{ kPa}$$

$$R : \text{Gas constant} = 0.287 \text{ (kJ/kgK)}$$

$$T_{atm} : \text{Atmospheric temperature in K}$$

$$: (273 + T) \text{ } ^\circ\text{C}$$

8. Air Fuel Ratio, (A/F)

$$(A/F) = \frac{\dot{m}_a}{\dot{m}_f} \quad (\text{F.12})$$

9. Fuel-Air Equivalence Ratio, ϕ

$$\phi = \frac{(F/A)_{actual}}{(F/A)_{stoic}} \quad (\text{F.13})$$

where

$(F/A)_{stoic}$: is the stoichiometric fuel air ratio

10. Brake Thermal Efficiency, η_{bth}

$$\eta_{bth} = \frac{BP}{\dot{m}_f \times LCV} \times 100 (\%) \quad (\text{F.14})$$

where

LCV : Lower calorific value of the fuel (kJ/kg)

11. Mechanical Efficiency, η_m

$$\eta_m = \frac{BP}{IP} \times 100 (\%) \quad (\text{F.15})$$